

QA: QA

MDL-NBS-HS-000011 REV 03

June 2007

Saturated Zone Site-Scale Flow Model

**NOTICE OF OPEN CHANGE DOCUMENTS - THIS DOCUMENT IS IMPACTED BY
THE LISTED CHANGE DOCUMENTS AND CANNOT BE USED WITHOUT THEM.**

1) ACN-001, DATED 10/01/2007



Prepared for:
U.S. Department of Energy
Office of Civilian Radioactive Waste Management
Office of Repository Development
1551 Hillshire Drive
Las Vegas, Nevada 89134-6321

Prepared by:
Sandia National Laboratories
OCRWM Lead Laboratory for Repository Systems
1180 Town Center Drive
Las Vegas, Nevada 89144

Under Contract Number
DE-AC04-94AL85000

DISCLAIMER

This report was prepared as an account of work sponsored by an agency of the United States Government. Neither the United States Government nor any agency thereof, nor any of their employees, nor any of their contractors, subcontractors or their employees, makes any warranty, express or implied, or assumes any legal liability or responsibility for the accuracy, completeness, or any third party's use or the results of such use of any information, apparatus, product, or process disclosed, or represents that its use would not infringe privately owned rights. Reference herein to any specific commercial product, process, or service by trade name, trademark, manufacturer, or otherwise, does not necessarily constitute or imply its endorsement, recommendation, or favoring by the United States Government or any agency thereof or its contractors or subcontractors. The views and opinions of authors expressed herein do not necessarily state or reflect those of the United States Government or any agency thereof.

QA: QA

Saturated Zone Site-Scale Flow Model

MDL-NBS-HS-000011 REV 03

June 2007

ACKNOWLEDGEMENTS

This work relied on the expertise and hard work of dedicated scientists and support staff too numerous to list here. The primary contributors including their areas of responsibility are:

| | |
|----------------------------|--|
| Scott James (SNL) | Lead author, project integrator, and team lead |
| Bill Arnold (SNL) | General scientific consultant and water-table rise analyst |
| Al-Aziz Eddebbbarh (LANL) | Co-lead author |
| June Fabryka-Martin (LANL) | Geochemist largely responsible for Appendices A, B, and F |
| Terry Miller (LANL) | Generation of HFM input files for FEHM and Appendix G |
| Bob Roback (LANL) | Chief geochemist responsible for Appendices A and B |
| Dave Rudeen (RHYM) | Data qualification and model validation and Appendices C and D |
| Tim Vogt (ISSI) | HFM development and potentiometric surface in Appendix E |

INTENTIONALLY LEFT BLANK



Model Signature Page/Change History

Complete only applicable items.

1. Total Pages: 636

638 ^{2/2/07} 6/21/07

2. Type of Mathematical Model:

- Process Model
 Abstraction Model
 System Model

Describe Intended Use of Model

The purpose of the saturated zone site-scale flow model is to describe the spatial distribution of groundwater as it moves from the water table below the repository, through the saturated zone, and to the point of uptake by the receptor of interest.

3. Title

Saturated Zone Site-Scale Flow Model

4. DI (including Revision No. and Addendum No.):

MDL-NBS-HS-000011 REV 03

| | Printed Name | Signature | Date |
|-----------------------------------|--------------|-----------------------------|-----------|
| 5. Originator | S.C. James | <i>Scott James</i> | 6/19/2007 |
| 6. Independent Technical Reviewer | M. Zhu | <i>M. Zhu</i> | 6/19/07 |
| 7. Checker | C.L. Axness | <i>Paul Axness</i> | 6/19/07 |
| 8. QCS/Lead Lab QA Reviewer | R.E. Spencer | <i>Robert Spencer</i> | 6/20/07 |
| 9. Responsible Manager/Lead | B.W. Arnold | for <i>Kenneth Rehfeldt</i> | 6/20/07 |
| 10. Responsible Manager | S.P. Kuzio | <i>S.P. Kuzio</i> | 6/20/07 |

11. Remarks

Change History

| 12. Revision No. and Addendum No. | 13. Description of Change |
|-----------------------------------|---|
| REV 00 | Initial Issue. |
| REV 00, ICN 01 | Change bars were used in REV 00, ICN 01, to indicate corrections to the original document. |
| REV 01 | Change bars are not used in REV 01 because there were extensive changes to the original document. |
| REV 01 ERRATA 1 | Response to CR 2234. |

| | |
|--------|---|
| REV 02 | <p>Description and presentation of alternative model. The alternate models are developed to evaluate the impact of new data and analyses on the saturated zone site-scale model predictions. The new data include a revised and reinterpreted hydrogeologic framework model conceptual model, boundary fluxes and recharge derived from the 2001 regional flow model and the 2004 UZ flow model, and the latest Nye County water-level data. The alternative models also include the incorporation of different conceptualization of site-scale features including the large hydraulic gradient, Solitario canyon fault, anisotropy etc. The revision also contains as Appendix A the analysis titled “Geochemical and Isotopic Constraints on Groundwater Flow.”</p> <p>This report addresses CR-1873D resulting from BSC Surveillance No. BQA-SI-04-002:</p> <p>This report addresses comments from the Regulatory Integration Team. The entire model documentation was revised, because the changes were too extensive to indicate individual changes.</p> |
| REV 03 | <p>Change bars were not used because this revision presents a completely new flow model. This major change updates the SZ flow model with the new hydrogeologic framework model, new Nye County Early Warning Drilling Program data through Phase IV and information from the recent USGS update to the Death Valley regional groundwater flow system model (Belcher 2004 [DIRS 173179]). The entire model documentation was revised. Changes were too extensive to show changes with change bars. The work scope of this report addresses actions related to (often through complete reformulation of the report) the following CRs: 4734, 6012, 6493, 6767, 6842, 7089, 7182, and 8337.</p> |

CONTENTS

| | Page |
|---|-------------|
| ACKNOWLEDGEMENTS..... | iii |
| ACRONYMS AND ABBREVIATIONS..... | xxi |
| 1. PURPOSE..... | 1-1 |
| 2. QUALITY ASSURANCE..... | 2-1 |
| 3. USE OF SOFTWARE..... | 3-1 |
| 3.1 SOFTWARE TRACKED BY CONFIGURATION MANAGEMENT..... | 3-1 |
| 3.1.1 Parameter Optimization..... | 3-3 |
| 3.1.2 Flow Modeling..... | 3-3 |
| 3.1.3 Particle Tracking..... | 3-3 |
| 3.1.4 Grid Generation..... | 3-3 |
| 3.2 EXEMPT SOFTWARE..... | 3-3 |
| 3.3 PROTOTYPE SOFTWARE..... | 3-4 |
| 4. INPUTS..... | 4-1 |
| 4.1 DIRECT INPUT..... | 4-1 |
| 4.2 CRITERIA..... | 4-2 |
| 4.3 CODES, STANDARDS, AND REGULATIONS..... | 4-4 |
| 5. ASSUMPTIONS..... | 5-1 |
| 6. MODEL DISCUSSION..... | 6-1 |
| 6.1 MODELING OBJECTIVES..... | 6-1 |
| 6.2 FEATURES, EVENTS, AND PROCESSES CONSIDERED IN THE MODEL..... | 6-1 |
| 6.3 THE CONCEPTUAL MODEL..... | 6-3 |
| 6.3.1 Key Features..... | 6-5 |
| 6.3.1.1 Groundwater Flow..... | 6-7 |
| 6.3.1.2 Hydrologic Features..... | 6-9 |
| 6.3.1.3 Flow Field..... | 6-10 |
| 6.3.1.4 Large, Moderate, and Small Hydraulic Gradients..... | 6-12 |
| 6.3.1.5 Vertical Gradients..... | 6-14 |
| 6.3.1.6 Lateral Boundary Conditions..... | 6-16 |
| 6.3.1.7 Recharge..... | 6-17 |
| 6.3.1.8 Discharge..... | 6-18 |
| 6.3.1.9 Heterogeneity..... | 6-18 |
| 6.3.1.10 Role of Faults..... | 6-21 |
| 6.3.1.11 Altered Northern Region..... | 6-21 |
| 6.3.2 Groundwater Flow Processes..... | 6-22 |
| 6.4 FORMULATION OF THE CONCEPTUAL MODEL..... | 6-24 |
| 6.4.1 Mathematical Description of the Conceptual Model..... | 6-24 |
| 6.4.2 Computational Model..... | 6-26 |

CONTENTS (Continued)

| | Page |
|----------|---|
| 6.4.3 | SZ Site-Scale Flow Model Inputs 6-28 |
| 6.4.3.1 | Hydrogeologic Framework Model (HFM) Overview..... 6-28 |
| 6.4.3.2 | Grid Generation 6-31 |
| 6.4.3.3 | Hydrogeologic Properties 6-39 |
| 6.4.3.4 | Evaluation of Hydrogeology represented in the SZ Computational Grid 6-39 |
| 6.4.3.5 | Hydrogeology at the Water Table..... 6-42 |
| 6.4.3.6 | Uncertainty..... 6-45 |
| 6.4.3.7 | Features 6-46 |
| 6.4.3.8 | Boundary and Initial Conditions..... 6-52 |
| 6.4.3.9 | Recharge 6-52 |
| 6.4.3.10 | Nodal Hydrogeologic Properties..... 6-54 |
| 6.4.3.11 | Vertical Anisotropy..... 6-55 |
| 6.5 | SZ SITE-SCALE FLOW MODEL RESULTS 6-56 |
| 6.5.1 | Model Calibration 6-56 |
| 6.5.1.1 | Calibration Criteria 6-56 |
| 6.5.1.2 | Parameter Optimization Procedure..... 6-56 |
| 6.5.1.3 | Calibration Parameters..... 6-65 |
| 6.5.2 | Calibration Results..... 6-69 |
| 6.5.2.1 | Water Levels..... 6-69 |
| 6.5.2.2 | Comparing Volumetric/Mass Flow Rates from the Regional-Scale Model with Volumetric/Mass Flow Rates from the Calibrated Site-Scale Model..... 6-73 |
| 6.5.2.3 | Simulated Flow Paths 6-74 |
| 6.5.2.4 | Specific Discharge 6-75 |
| 6.6 | CONSIDERATION OF ALTERNATIVE CONCEPTUAL MODELS..... 6-77 |
| 6.6.1 | Removal of Vertical Anisotropy 6-78 |
| 6.6.2 | Removal of Horizontal Anisotropy..... 6-80 |
| 6.6.3 | Removal of LHG and Change to the Solitario Canyon Fault Anisotropy..... 6-82 |
| 6.6.4 | Water Table Rise..... 6-82 |
| 6.6.4.1 | Water Table Rise below Repository 6-82 |
| 6.6.4.2 | Incorporation of Water-Table Rise into the SZ Flow and Transport Models 6-84 |
| 6.7 | UNCERTAINTY..... 6-93 |
| 6.7.1 | Uncertainty in Specific Discharge 6-96 |
| 6.7.2 | Nonlinear Analysis..... 6-98 |
| 6.7.3 | Discussion of the Effect of Hydrogeologic Contact Uncertainty on Specific Discharge 6-99 |
| 6.7.4 | Site Data..... 6-100 |
| 6.7.5 | Remaining Uncertainties in Specific Discharge Estimates..... 6-101 |
| 6.7.6 | Effect of Perched Water on Flow Paths and Specific Discharge..... 6-101 |
| 6.7.7 | Representing Faults with Reduced Permeability Grid Blocks..... 6-102 |
| 6.7.8 | Scaling Issues..... 6-102 |

CONTENTS (Continued)

| | Page |
|--|-------------|
| 6.7.9 Flowpath Uncertainty..... | 6-103 |
| 6.8 DESCRIPTION OF BARRIER CAPABILITY..... | 6-103 |
| 7. VALIDATION..... | 7-1 |
| 7.1 VALIDATION CRITERIA..... | 7-1 |
| 7.1.1 Confidence Building During Model Development to Establish Scientific Basis and Accuracy for Intended Use..... | 7-2 |
| 7.1.2 Hydraulic Gradient Comparison to Build Model Confidence During Development..... | 7-4 |
| 7.1.3 Confidence Building After Model Development to Support the Scientific Basis of the Model..... | 7-7 |
| 7.2 VALIDATION RESULTS..... | 7-7 |
| 7.2.1 Comparison of Observed and Predicted Nye County Water Levels..... | 7-8 |
| 7.2.2 Comparison of Calibrated Effective Permeabilities to Field Test Results..... | 7-12 |
| 7.2.2.1 General Permeability Data..... | 7-12 |
| 7.2.2.2 Implications of Permeability Data..... | 7-17 |
| 7.2.2.3 Permeability Data from the Yucca Mountain Area..... | 7-18 |
| 7.2.2.4 Permeability Data from the Nevada Test Site..... | 7-21 |
| 7.2.2.5 Inferences About Permeability from Regional Observations.... | 7-27 |
| 7.2.2.6 Comparing Permeability Data to Calibrated Permeability Values..... | 7-30 |
| 7.2.3 Specific Discharge..... | 7-32 |
| 7.2.4 Comparison of Hydrochemical Data Trends with Calculated Particle Pathways..... | 7-34 |
| 7.3 VALIDATION SUMMARY..... | 7-36 |
| 8. CONCLUSIONS..... | 8-1 |
| 8.1 SUMMARY OF MODELING ACTIVITIES..... | 8-2 |
| 8.1.1 Saturated Zone Flow Characterization..... | 8-2 |
| 8.1.2 Conceptual Model of SZ Site-Scale Flow..... | 8-3 |
| 8.1.3 Mathematical Model and Numerical Approach..... | 8-4 |
| 8.1.4 Model Validation and Confidence Building..... | 8-4 |
| 8.2 OUTPUTS..... | 8-4 |
| 8.3 OUTPUT UNCERTAINTY..... | 8-5 |
| 8.3.1 Specific Discharge Uncertainty Range..... | 8-5 |
| 8.3.2 Flowpaths Uncertainty..... | 8-6 |
| 8.4 HOW THE APPLICABLE ACCEPTANCE CRITERIA ARE ADDRESSED..... | 8-7 |
| 9. INPUTS AND REFERENCES..... | 9-1 |
| 9.1 DOCUMENTS CITED..... | 9-1 |
| 9.2 CODES, STANDARDS, REGULATIONS, AND PROCEDURES..... | 9-21 |
| 9.3 SOURCE DATA, LISTED BY DATA TRACKING NUMBER..... | 9-22 |
| 9.4 OUTPUT DATA, LISTED BY DATA TRACKING NUMBER..... | 9-33 |
| 9.5 SOFTWARE CODES..... | 9-34 |

CONTENTS (Continued)

| | Page |
|--|-------------|
| APPENDIX A – GEOCHEMICAL AND ISOTOPIC CONSTRAINTS ON GROUNDWATER FLOW | A-1 |
| APPENDIX B – REEVALUATION OF CONSTRAINTS ON GROUNDWATER FLOW USING GEOCHEMICAL AND ISOTOPIC DATA FROM NYE COUNTY EARLY WARNING DRILLING PROGRAM WELLS | B-1 |
| APPENDIX C – DATA SUITABILITY EVALUATION – THE 2004 DEATH VALLEY REGIONAL GROUNDWATER FLOW SYSTEM MODEL..... | C-1 |
| APPENDIX D – DATA SUITABILITY EVALUATION – NYE COUNTY EARLY WARNING DRILLING PROGRAM (NC-EWDP) WELL DATA..... | D-1 |
| APPENDIX E – POTENTIOMETRIC SURFACE FOR THE SATURATED ZONE SITE-SCALE FLOW MODEL..... | E-1 |
| APPENDIX F – CONVERSION OF SURVEY COORDINATES FOR SELECTED NYE COUNTY EARLY WARNING DRILLING PROGRAM BOREHOLES, THROUGH PHASE IV..... | F-1 |
| APPENDIX G – DISTRIBUTION AND ELEVATIONS OF HYDROGEOLOGIC UNITS IN THE SZ COMPUTATIONAL GRID | G-1 |
| APPENDIX H – REGULARIZED INVERSION AS A BASIS FOR MODEL CALIBRATION AND PREDICTIVE UNCERTAINTY ANALYSIS: AN EXPLANATION..... | H-1 |
| APPENDIX I – PREDICTIVE ERROR ANALYSIS THROUGH CONSTRAINED PREDICTION MAXIMIZATION/MINIMIZATION | I-1 |

FIGURES

| | | Page |
|-------|---|-------------|
| 1-1. | Generalized Flow of Information among Reports Pertaining to Flow and Transport in the SZ | 1-2 |
| 6-1. | Important Physiographic Features Near Yucca Mountain Including Some of Those Explicitly Included the SZ Site-Scale Flow Model | 6-4 |
| 6-2. | Potentiometric Surface Map and Gradient Areas Developed Using Water-Level Data from 1993 | 6-6 |
| 6-3. | Location of Faults in the Yucca Mountain Region..... | 6-10 |
| 6-4. | Potentiometric Surface and Inferred Flow Directions | 6-11 |
| 6-5. | Top of the 250-m SZ Site-Scale Computational Grid | 6-33 |
| 6-6. | Close-Up View of Computational Grid (3× Vertical Exaggeration) Showing Cut Away at UTM Easting = 549,000 m and UTM Northing = 4,078,000 m Through the Yucca Mountain Repository | 6-37 |
| 6-7. | View of the 250-m Computational Grid (2× Vertical Exaggeration) Showing Node Points Colored by Hydrogeologic Units Values from HFM2006..... | 6-38 |
| 6-8. | Hydrogeologic Units Present at North-South Cross Section in the SZ Computational Grid at UTM Easting = 552,500 m | 6-41 |
| 6-9. | Hydrogeologic Units Present at West-East Cross Section in the SZ Computational Grid at UTM Northing = 4,064,000 m..... | 6-41 |
| 6-10. | Hydrogeologic Grid Nodes and Spacing at West-East Cross Section in the SZ Computational Grid at UTM Northing = 4,064,000 m..... | 6-42 |
| 6-11. | Hydrogeologic Units Present at the Water-Table Surface in the SZ Computational Grid | 6-44 |
| 6-12. | Geologic Features Included in the SZ Site-Scale Flow Model..... | 6-48 |
| 6-13. | The Altered Northern Region and Well Locations..... | 6-49 |
| 6-14. | Recharge Applied to the SZ Site-Scale Flow Model..... | 6-54 |
| 6-15. | Contour Plot of Potentiometric Surface (Left Panel) and Simulated Water-Level Data with Residual Heads (Right Panel) | 6-71 |
| 6-16. | Well Locations and Head Residuals between Measured Water-Level Data and the Potentiometric Surface Used to Construct Model Boundary Conditions | 6-72 |
| 6-17. | Flow Paths for Particles Released (uniformly but randomly distributed) below the Repository Area | 6-76 |
| 6-18. | Particle Tracks for a Model without Vertical Anisotropy | 6-79 |
| 6-19. | Particle Tracks for Isotropic Yucca Mountain Volcanic Units..... | 6-81 |
| 6-20. | Estimated Water Table Elevations for Future Glacial-Transition Climatic Conditions..... | 6-86 |
| 6-21. | Estimated Depth to the Water Table for Future Glacial-Transition Climatic Conditions..... | 6-88 |
| 6-22. | Hydrogeologic Framework Model Units at the Water Table for Present-Day Conditions..... | 6-90 |
| 6-23. | Hydrogeologic Framework Model Units at the Water Table for Estimated Future Glacial-Transition Climatic Conditions | 6-91 |
| 6-24. | Simulated Potentiometric Surface After a Rise in the Water-Table..... | 6-92 |

FIGURES (Continued)

| | Page |
|---|-------------|
| 6-25. Conceptual Representation of the Resolution Matrix Illustrating How Estimated Model Parameters Are “Contaminated” During the Modeling Process | 6-95 |
| 6-26. Uncalibrated and Calibrated Model Parameter Impact on Normalized Uncertainty in Specific Discharge | 6-97 |
| 6-27. Value of Observation Group to Reducing Uncertainty in Specific Discharge | 6-98 |
| 7-1a. Location of wells for Measured and Simulated Head Along Flowpath | 7-5 |
| 7-1b. Measured and Simulated Head Along Flowpath | 7-6 |
| 7-2. Locations of NC-EWDP Wells..... | 7-11 |
| 7-3. Comparison of Single-Hole Air and Water Permeabilities | 7-17 |
| 7-4. Logarithms of Effective Permeabilities Estimated During Model Calibration Compared to Logarithms of Permeability Determined from Pump-Test Data..... | 7-31 |
| 7-5. Transport Pathways Deduced from Hydrochemistry Data Compared to Particle Pathways Calculated for the SZ Site-Scale Transport Model..... | 7-35 |
| A6-1. Important Physiographic Features near Yucca Mountain..... | A-57 |
| A6-2. Selected Geologic and Hydrogeologic Units for the Saturated Zone at Yucca Mountain..... | A-58 |
| A6-3. Potentiometric Surface and Inferred Flow Directions (light blue arrows) for Yucca Mountain and Vicinity..... | A-59 |
| A6-4. Effects of Different Processes on Delta Deuterium and Delta Oxygen-18 Composition of Subsurface Water | A-86 |
| A6-5. Locations of Boreholes in the Vicinity of Yucca Mountain and the Northern Amargosa Desert..... | A-91 |
| A6-6. Trilinear and Scatter Plots for Samples that Surround Yucca Mountain But Are Generally North of the Amargosa Valley | A-93 |
| A6-7. Trilinear and Scatter Plots for Samples from the Yucca Mountain Area | A-94 |
| A6-8. Trilinear and Scatter Plots for Samples from Groupings in the Amargosa Desert Region..... | A-95 |
| A6-9. Plots of Selected Hydrochemical Constituents for the Different Depth Intervals of Boreholes NC-EWDP-19D and -19P | A-97 |
| A6-10. Plots of Selected Hydrochemical Constituents for the Different Depth Intervals of Borehole NC-EWDP-9SX..... | A-98 |
| A6-11. Plots of Selected Hydrochemical Constituents for the Different Depth Intervals of Boreholes NC-EWDP-1S and -1DX | A-99 |
| A6-12. Plots of Selected Hydrochemical Constituents for the Different Depth Intervals of Boreholes NC-EWDP-3S and -3D | A-100 |
| A6-13. Plots of Selected Hydrochemical Constituents for the Different Depth Intervals of Boreholes NC-EWDP-12PA, -12PB and -12PC | A-101 |
| A6-14. Areal Distribution of pH in Groundwater..... | A-103 |
| A6-15. Areal Distribution of Chloride in Groundwater..... | A-104 |
| A6-16. Areal Distribution of Sulfate in Groundwater | A-106 |
| A6-17. Areal Distribution of Bicarbonate in Groundwater | A-107 |
| A6-18. Areal Distribution of Fluoride in Groundwater | A-108 |

FIGURES (Continued)

| | Page |
|--|-------|
| A6-19. Areal Distribution of Silica in Groundwater..... | A-109 |
| A6-20. Areal Distribution of Calcium in Groundwater | A-110 |
| A6-21. Areal Distribution of Magnesium in Groundwater..... | A-112 |
| A6-22. Areal Distribution of Sodium in Groundwater | A-114 |
| A6-23. Areal Distribution of Potassium in Groundwater | A-115 |
| A6-24. Areal Distribution of Delta Deuterium in Groundwater..... | A-116 |
| A6-25. Areal Distribution of $\delta^{18}\text{O}$ in Groundwater | A-117 |
| A6-26. Areal Distribution of $\delta^{34}\text{S}$ in Groundwater..... | A-119 |
| A6-27. Areal Distribution of $\delta^{13}\text{C}$ in Groundwater | A-120 |
| A6-28. Areal Distribution of ^{14}C in Groundwater | A-122 |
| A6-29. Areal Distribution of Uranium in Groundwater | A-123 |
| A6-30. Areal Distribution of $^{234}\text{U}/^{238}\text{U}$ Activity Ratios in Groundwater | A-124 |
| A6-31. Areal Distribution of Strontium in Groundwater..... | A-126 |
| A6-32. Areal Distribution of $\delta^{87}\text{Sr}$ in Groundwater | A-127 |
| A6-33. Comparison between Measured Dissolved Aluminum Concentrations and Dissolved Aluminum Concentrations Calculated by PHREEQC Assuming Equilibrium with Kaolinite | A-141 |
| A6-34. Areal Distribution of Ionic Strength in Groundwater..... | A-142 |
| A6-35. Areal Distribution of Dissolved Inorganic Carbon in Groundwater..... | A-143 |
| A6-36. Areal Distribution of Dissolved Carbon-Dioxide Partial Pressure in Groundwater | A-145 |
| A6-37. Areal Distribution of Calcite Saturation Index in Groundwater..... | A-146 |
| A6-38. Areal Distribution of Smectite Saturation Index in Groundwater | A-147 |
| A6-39. Areal Distribution of Calcium Clinoptilolite Saturation Index in Groundwater | A-148 |
| A6-40. Areal Distribution of K-Feldspar Saturation Index in Groundwater | A-149 |
| A6-41. Uranium Isotopic Compositions and Schematic Evolutionary Trends at Yucca Mountain..... | A-155 |
| A6-42. Scatter Plot Comparing Sulfate and Chloride Compositions of Perched Waters and Saturated Zone Groundwaters..... | A-157 |
| A6-43. Scatter Plot Comparing Delta Carbon-13 and Dissolved Inorganic Carbon Compositions of Perched Waters and Saturated Zone Groundwaters..... | A-158 |
| A6-44. Scatter Plot Comparing Delta Deuterium and Delta Oxygen-18 Data for Perched Water and Groundwater near Yucca Mountain | A-159 |
| A6-45. ^{14}C Activity versus Delta ^{13}C of Perched Water and Groundwater near Yucca Mountain..... | A-160 |
| A6-46. Scatter Plot Comparing Calcium and Sodium Compositions of Perched Waters and Saturated Zone Groundwaters..... | A-161 |
| A6-47. Chloride Mass-Balance Method for Estimating Infiltration..... | A-166 |
| A6-48. Delta Deuterium and Delta ^{18}O Data for Borehole UZ-14 Unsaturated Zone Pore Water, Perched Water, and Groundwater near Yucca Mountain | A-170 |
| A6-49. Scatter Plots Showing Mixing in Southern Yucca Mountain..... | A-178 |
| A6-50. Cross Correlation Plot of Sulfate versus Chloride for Samples in the Amargosa Desert Region | A-179 |

FIGURES (Continued)

| | Page |
|--|-------------|
| A6-51. Scatter Plot of Delta 34S versus Inverse Sulfate for Samples in the Amargosa Desert Region | A-181 |
| A6-52. Geologic Units Defined in the Saturated Zone Flow Model | A-196 |
| A6-53. Steady-State Distribution of the Percentage of Yucca Mountain Recharge in Downgradient Groundwater Calculated Using the Saturated Zone Flow Model.... | A-197 |
| A6-54. Map View of Steady-State Distribution of the Percentage of Inflow through the Pre-Tertiary Units of Northwest Crater Flat Groundwater Calculated Using the Saturated Zone Flow Model | A-199 |
| A6-55. Cross Sectional View of Steady-State Distribution of the Percentage of Inflow through the Pre-Tertiary Units of Northwest Crater Flat Groundwater Calculated Using the Saturated Zone Flow Model..... | A-200 |
| A6-56. Steady-State Distribution of the Percentage of Inflow through the Tertiary Units of Northwest Crater Flat Groundwater Calculated Using the Saturated Zone Flow Model..... | A-201 |
| A6-57. Steady-State Distribution of the Percentage of Shallow Timber Mountain Area Groundwater through the Tertiary Units Calculated Using the Saturated Zone Flow Model..... | A-202 |
| A6-58. Map View of Steady-State Distribution of the Percentage of Shallow Upper Fortymile Wash Area Groundwater through the Pre-Tertiary Units Calculated Using the Saturated Zone Flow Model..... | A-204 |
| A6-59. Cross Sectional View of Steady-State Distribution of the Percentage of Shallow Upper Fortymile Wash Area Groundwater through the Pre-Tertiary Units Calculated Using the Saturated Zone Flow Model..... | A-205 |
| A6-60. Steady-State Distribution of the Percentage of Shallow Upper Fortymile Wash Area Groundwater through the Tertiary Units Calculated Using the Saturated Zone Flow Model..... | A-206 |
| A6-61. Steady-State Distribution of the Percentage of Pre-Tertiary Rocks of the Skeleton Hills Area Groundwater Calculated Using the Saturated Zone Flow Model..... | A-207 |
| A6-62. Regional Flow Paths Inferred from Hydrochemical and Isotopic Data..... | A-212 |
| | |
| B6-1. Map Showing Locations of New Nye County Boreholes in the Vicinity of the Northern Amargosa Desert | B-23 |
| B6-2. Trilinear and Scatter plots for New Nye County Boreholes and Zones | B-26 |
| B6-3. Map Showing Assignment of New Nye County Boreholes to Hydrochemical Groupings..... | B-27 |
| B6-4. Areal Distribution of Chloride in Groundwater..... | B-29 |
| B6-5. Areal Distribution of Sulfate in Groundwater | B-31 |
| B6-6. Areal Distribution of Bicarbonate in Groundwater | B-32 |
| B6-7. Areal Distribution of Calcium in Groundwater | B-33 |
| B6-8. Areal Distribution of Sodium in Groundwater | B-34 |
| B6-9. Areal Distribution of Delta ¹³ C in Groundwater..... | B-35 |
| B6-10. Areal Distribution of ¹⁴ C in Groundwater | B-36 |
| B6-11. Scatter Plots Showing Mixing in Southern Yucca Mountain | B-38 |

FIGURES (Continued)

| | Page |
|--|-------------|
| B6-12. Cross Correlation Plot of Sulfate versus Chloride for Groundwaters within the Boundaries of the Site Model, and South and East of Yucca Mountain | B-40 |
| B6-13. Scatter Plot of $\delta^{34}\text{S}$ versus Inverse Sulfur for Samples in the Vicinity of Yucca Mountain and the Amargosa Desert Region..... | B-41 |
| B6-14. Comparison of Radiocarbon Measurements of Inorganic and Organic Dissolved ^{14}C in Groundwater Samples from the Yucca Mountain Vicinity | B-43 |
| B6-15. Regional Flow Paths Inferred from Hydrochemical and Isotopic Data..... | B-45 |
| D-1. Snapshot of Index Nye County QAP | D-5 |
| F-1. Screen Shot of the Validation Test Case for CORPSCON Version 5.11.08 | F-7 |
| G-1. Distribution and Elevations of ICU, Intrusive Confining Unit (2)..... | G-2 |
| G-2. Distribution and Elevations of XCU, Crystalline-Rock Confining Unit (3) | G-3 |
| G-3. Distribution and Elevations of LCCU, Lower Clastic-Rock Confining Unit (4) | G-4 |
| G-4. Distribution and Elevations of LCA, Lower Carbonate-Rock Aquifer (5) | G-5 |
| G-5. Distribution and Elevations of UCCU, Upper Clastic-Rock Confining Unit (6) | G-6 |
| G-6. Distribution and Elevations of UCA, Upper Carbonate-Rock Aquifer (7) | G-7 |
| G-7. Distribution and Elevations of LCCU-T1, Lower Clastic Confining Unit – Thrust (8) | G-8 |
| G-8. Distribution and Elevations of LCA-T1, Lower Carbonate Aquifer – Thrust (9)..... | G-9 |
| G-9. Distribution and Elevations of VSU-Lower, Lower Volcanic and Sedimentary Units (11)..... | G-10 |
| G-10. Distribution and Elevations of OVU, Older Volcanic Units (12)..... | G-11 |
| G-11. Distribution and Elevations of CFATA, Crater Flat Tram Aquifer (14)..... | G-12 |
| G-12. Distribution and Elevations of CFBCU, Crater Flat Bullfrog Confining Unit (15)..... | G-13 |
| G-13. Distribution and Elevations of CFPPA, Crater Flat Prow Pass Aquifer (16)..... | G-14 |
| G-14. Distribution and Elevations of WVU, Wahmonie Volcanic Unit (17)..... | G-15 |
| G-15. Distribution and Elevations of CHVU, Calico Hills Volcanic Unit (18) | G-16 |
| G-16. Distribution and Elevations PVA, Paintbrush Volcanic Aquifer (19)..... | G-17 |
| G-17. Distribution and Elevations of TMVA, Timber Mountain Volcanic Aquifer (20) ... | G-18 |
| G-18. Distribution and Elevation of VSU, Volcanic and Sedimentary Unit (Upper) (21) | G-19 |
| G-19. Distribution and Elevations of LFU, Lava Flow Unit (23)..... | G-20 |
| G-20. Distribution and Elevations of LA, Limestone Aquifer (24)..... | G-21 |
| G-21. Distribution and Elevations of OAA, Older Alluvial Aquifer (26) | G-22 |
| G-22. Distribution and Elevations of YACU, Young Alluvial Confining Unit (27)..... | G-23 |
| G-23. Distribution and Elevations of YAA, Young Alluvial Aquifer (28) | G-24 |
| I-1. Points in Parameter Space Corresponding to Maximum/Minimum Values of a Prediction at a Certain Confidence Level..... | I-1 |

INTENTIONALLY LEFT BLANK

TABLES

| | Page |
|---|-------------|
| 3-1. Computer Codes Used in the SZ Site-Scale Flow Model..... | 3-1 |
| 4-1. Direct Input Data Sources..... | 4-1 |
| 4-2. Intermediary Direct Input Data Sources (see also Table 8-1) | 4-1 |
| 5-1. Assumptions | 5-1 |
| 6-1. Features, Events, and Processes Included in TSPA-LA and Relevant to this Model Report | 6-2 |
| 6-2. Hydrogeologic Units for the Hydrogeologic Framework Model | 6-29 |
| 6-3. Coordinates of the Base-Case SZ Site-Scale Model Domain..... | 6-32 |
| 6-4. Vertical Grid Spacing Used in the SZ Site-Scale Flow Model | 6-36 |
| 6-5. SZ Computational Grid and HFM2006 Volume Comparisons by Unit | 6-40 |
| 6-6. SZ Computational Grid Nodes by Unit | 6-43 |
| 6-7. Hydrological Features in the SZ Site-Scale Flow Model | 6-50 |
| 6-8. Comparison of Observed Hydraulic Heads from the SZ Site-Scale Flow Model and Model Computed Head Data..... | 6-59 |
| 6-9. Calibration Parameters Used in the SZ Site-Scale Flow Model..... | 6-66 |
| 6-10. Hand Calibration Results used in the SZ Site-Scale Flow Model..... | 6-68 |
| 6-11. Comparison of Target and Site-Scale Volumetric/Mass Flow Rates | 6-74 |
| 7-1. Predicted and Observed Hydraulic Gradient for Identified Wells Used for Confidence Building During Development..... | 7-6 |
| 7-2. Wells Used in Validation of the Saturated Zone Site-Scale Flow Model with Observed and Predicted Water Levels..... | 7-10 |
| 7-3. Predicted and Observed Hydraulic Gradients for Post-Development Validation | 7-12 |
| 7-4. Transmissivities, Hydraulic Conductivities, and Permeabilities Determined in the Single-Well Hydraulic Tests Conducted in the Alluvium in NC-EWDP-19D Between July and November 2000 | 7-20 |
| 7-5. Permeabilities Calculated for the Lower Carbonate Aquifer..... | 7-22 |
| 7-6. Permeability Estimates for the Valley Fill Aquifer | 7-24 |
| 7-7. Permeability Estimates for the Welded Tuff Aquifer..... | 7-25 |
| 7-8. Permeabilities of the Lava Flow Aquifer..... | 7-26 |
| 8-1. Output Data..... | 8-5 |
| A3-1. Software Used in Support of this Scientific Analysis..... | A-2 |
| A4-1. Sources of Data..... | A-5 |
| A4-2. Sources of Data and Other Information..... | A-8 |
| A4-3. Summary of Groundwater Wells and Data Sources | A-11 |
| A5-1. Assumptions | A-52 |
| A6-1. Field Parameters and Major Ion Composition..... | A-65 |
| A6-2. Isotope and Trace Element Composition..... | A-74 |

TABLES (Continued)

| | Page |
|---|-------|
| A6-3. Calculated Geochemical Parameters of Groundwater Samples Used in this Report..... | A-129 |
| A6-4. Yucca Mountain Mineral Phase Compositions and Thermodynamic Data Used in PHREEQC Analyses | A-140 |
| A6-5. Chemical and Isotopic Composition of Perched Water at Yucca Mountain | A-152 |
| A6-6. Recharge Rates Based on the Chloride Mass Balance Method..... | A-167 |
| A6-7. Chemistry and Ages of Groundwaters from Seven Boreholes at Yucca Mountain..... | A-173 |
| A6-8. Sensitivity of the Permissible Fraction of Young Water Present in Groundwater to Dissolved Inorganic Carbon Concentration Assumed for the Old Component of the Mixed Groundwater..... | A-175 |
| A6-9. Sensitivity of the Permissible Fraction of Young Water Present in Groundwater to the Assumed ¹⁴ C Activity of the Old Component of the Mixed Groundwater ... | A-176 |
| A6-10. Mineral Phases and Exchange Reactions Considered in the PHREEQC Inverse Analyses..... | A-184 |
| A6-11. Calculated Groundwater Transit Times (in years) Between Well WT-3 and Various Depth Zones in Well NC-EWDP-19D..... | A-194 |
| | |
| B4-1. Geographic and Geologic Data Sources for New Nye County Boreholes and Zones..... | B-7 |
| B4-2. Field Parameters and Average Major Ion Compositions for New Wells | B-12 |
| B4-3. Average Isotope and Trace Element Compositions for New Wells | B-14 |
| B4-4. Additional Data on Field Parameters and Major Ion Compositions for Well Cited in Appendix A..... | B-15 |
| B4-5. Additional Data on Strontium Isotopic Compositions for Wells Cited in Appendix A..... | B-16 |
| B4-6. Additional Data on Uranium Isotope Values for Wells Cited in Appendix A | B-18 |
| B4-7. Additional Data on Sulfur Isotope Values for Wells Cited in Appendix A | B-19 |
| B4-8. Additional Data on Carbon Isotope Values for Wells Cited in Appendix A..... | B-19 |
| B4-9. Additional Data on Stable Hydrogen and Oxygen Isotope Values for Wells Cited in Appendix A..... | D-20 |
| | |
| D-1. Comparison of New Nye County Well Data with Corroborating Data..... | D-7 |
| D-2. Nye County Wells with Data to Be Evaluated and Corresponding Data Sources..... | D-11 |
| D-3. Nye County Wells with GPS Locations | D-12 |
| D-4. Land Surface Elevation and the Top and Bottom of the Open Intervals for Nye County Wells | D-12 |
| D-5. Nye County Water Level Measurements through 2/2005 | D-14 |
| D-6. Nye County Water Level Measurements for Phase V Wells through 11/2006..... | D-33 |

TABLES (Continued)

| | Page |
|--|-------------|
| F-1. Acquired Survey Data used to Create Input File for Verification Calculations | F-7 |
| F-2. Comparison of UTM Coordinates Obtained from Conversion of NSP and Geographic Coordinates | F-9 |
| F-3. UTM Coordinates for Selected Nye County EWDP Boreholes, Converted Using CORPSCON V.5.11.08 | F-9 |

INTENTIONALLY LEFT BLANK

ACRONYMS AND ABBREVIATIONS

| | |
|---------|--|
| ACC | accession number |
| ACM | alternative conceptual model |
| AR | Amargosa River: group of boreholes located on the west side of Amargosa Desert |
| AR/FMW | Group of boreholes located near the confluence of the Amargosa River and Fortymile Wash drainages |
| ASCII | ASCII |
| ATC | Alluvial Testing Complex |
| BSC | Bechtel SAIC Company, LLC |
| CFR | code of federal regulations |
| CF-SW | Crater Flat Southwest |
| CMB | chloride mass balance |
| CR | condition report |
| CRWW | Coffer Ranch Windmill Well |
| CVFE | control-volume finite element |
| DFGP | Desert Farms Garlic Plot |
| DIC | Dissolved inorganic carbon |
| DIRS | document reference system |
| DOC | dissolved organic carbon |
| DOE | Department of Energy |
| DOS | disk operating system |
| DTN | data tracking number |
| DVRFS | Death Valley Regional (ground water) Flow System |
| ESF | Exploratory Studies Facility |
| EWDP | Early Warning Drilling Program |
| FEHM | finite-element heat and mass transfer numerical analysis computer code |
| FEPs | features, events, and processes |
| FMW-E | Fortymile Wash-East: group of boreholes in the Amargosa Desert east of Fortymile Wash |
| FMW-N | Fortymile Wash-North: group of boreholes east and northeast of Yucca Mountain |
| FMW-S | Fortymile Wash-South: group of boreholes along or near the main channel of Fortymile Wash in Amargosa Desert |
| FMW-W | Fortymile Wash-West: group of boreholes in the Amargosa Desert west of Fortymile Wash |
| GF | Gravity Fault: group of boreholes located on east side of the Amargosa Desert |
| GSIS | geoscientific information system |
| HFM | hydrogeologic framework model |
| HFM2006 | revised hydrogeologic framework model |

| | |
|---------|--|
| HGU | hydrogeologic unit |
| LA | license application |
| LANL | Los Alamos National Laboratory |
| LHG | large hydraulic gradient |
| LM | Levenberg-Marquardt (optimization algorithm for PEST) |
| LW | Amargosa Valley (formerly Lathrop Wells): group of boreholes located along U.S. Highway 95 |
| MVA | middle volcanic aquifer |
| NAD-27 | North American Datum of 1927 |
| NAD-83 | North American Datum of 1983 |
| NC-EWDP | Nye County Early Warning Drilling Program |
| NSP | Nevada State Plane |
| NTS | Nevada Test Site |
| NWRPO | Nye County Waste Repository Program |
| OV/NWA | Oasis Valley/Northwest Amargosa Valley: group of boreholes located in that region |
| PC | personal computer |
| QAP | quality assurance plan |
| QARD | <i>Quality Assurance Requirements and Description</i> |
| RMSE | root-mean-square error |
| SCM | Software Configuration Management |
| SCW | Solitario Canyon Wash: western group of boreholes |
| SNL | Sandia National Laboratories |
| SSD | sum-of-squares difference |
| STN | software tracking number |
| SZ | saturated zone |
| TDOC | total dissolved organic carbon |
| TDS | total dissolved solids |
| TDMS | technical data management system |
| TIC | Technical Information Center |
| TM | Timber Mountain: group of boreholes north of Yucca Mountain |
| TSPA | total system performance assessment |
| TWP | technical work plan |
| UGTA | underground testing area |
| USGS | United States Geologic Survey |
| UTM | Universal Trans Mercator |
| UZ | unsaturated zone |

YM-S Yucca Mountain South
YMP Yucca Mountain Project
YMRP *Yucca Mountain Review Plan, Final Report*

HYDROGEOLOGIC UNITS AND CHEMICAL ELEMENTS

Tac Calico Hills formation
Tcb Bullfrog tuff of the Crater Flat Group
Tcp Prow Pass tuff of the Crater Flat Group
Tct Tram tuff of the Crater Flat Group
Tlr Lithic Ridge tuffs

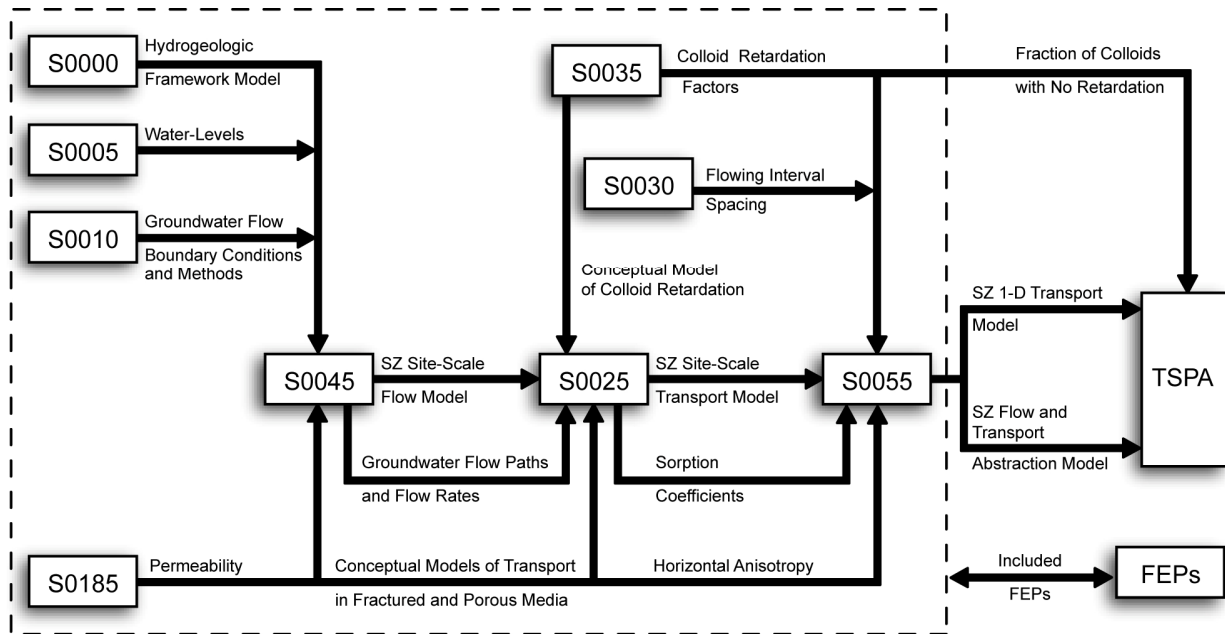
$\delta^{13}\text{C}$ delta carbon-13
 δD delta hydrogen-2, or delta deuterium
 $\delta^{18}\text{O}$ delta oxygen-18
 $\delta^{34}\text{S}$ delta sulfur-34
 $\delta^{87}\text{Sr}$ delta strontium-87

INTENTIONALLY LEFT BLANK

1. PURPOSE

The purpose of this model report is to document revision of *Saturated Zone (SZ) Site-scale Flow Model* (BSC 2004 [DIRS 170037]) for Yucca Mountain, Nevada, in accordance with SCI-PRO-006, *Models*. This report provides validation and confidence in the flow model developed in support of the total system performance assessment (TSPA) for the license application (LA). The output from this report provides the flow model used in *Site-Scale Saturated Zone Transport Model*, (SNL 2007 [DIRS 177392]), which in turn provides output to the *SZ Flow and Transport Model Abstraction* (SNL 2007 [DIRS 177390]). In particular, the output from the SZ site-scale flow model is used by the SZ site-scale transport model to simulate the groundwater flow pathways and radionuclide transport to the accessible environment for use in *SZ Flow and Transport Model Abstraction* (SNL 2007 [DIRS 177390]), which feeds the TSPA calculations. Figure 1-1 shows the relationship of this report to other saturated zone reports that also pertain to SZ flow and transport. The figure also depicts the relationship between SZ models and analyses. It should be noted that Figure 1-1 does not contain a complete representation of the data and parameter inputs and outputs of all saturated zone reports, nor does it show inputs external to this suite of saturated zone reports.

Since the development, calibration, and validation of the SZ site-scale flow model (CRWMS M&O 2000 [DIRS 139582]), more data have been gathered and analyses have been completed. The data include new stratigraphic and water-level data from Nye County wells, single- and multiple-well hydraulic testing data (SNL 2007 [DIRS 177394]), and new hydrochemistry data (Appendix B). New analyses include the 2004 transient Death Valley Regional (ground water) Flow System (DVRFS) model (Belcher 2004 [DIRS 173179]), the creation of a new hydrogeologic framework model (HFM), called HFM2006 (SNL 2007 [DIRS 174109], DTN: MO0610MWDHFM06.002 [DIRS 179352]), and the 2003 unsaturated zone (UZ) flow model (BSC 2004 [DIRS 169861]). The new data and analyses were used to construct the SZ site-scale flow model presented in this report to support TSPA-LA. The intended use of this work is to provide a flow model that generates flow fields that are used to simulate radionuclide transport in saturated volcanic rock and alluvium under natural-gradient flow conditions. Simulations of water-table rise were also conducted for use in downstream transport and abstraction modeling. The SZ site-scale flow model simulations were completed using the three-dimensional, finite-element heat and mass transfer computer code, FEHM V2.24, STN: 10086-2.24-02 [DIRS 179539]. Concurrently, the process-level transport model and methodology for calculating radionuclide transport in the SZ at Yucca Mountain using FEHM are described in *Site-Scale Saturated Zone Transport* (SNL 2007 [DIRS 177392]). The velocity fields are calculated by the flow model, described herein, independent of the transport processes, and are then used as inputs to the transport model. Justification for this abstraction is presented in *Saturated Zone Flow and Transport Model Abstraction* (SNL 2007 [DIRS 177390]).



| Legend | |
|---|--------------------------|
| S0000 - Hydrogeologic Framework Model | MDL-NBS-HS-000024 |
| S0005 - Water-Level Data Analysis | ANL-NBS-HS-000034 |
| S0010 - Recharge and Lateral Groundwater Flow Boundary Conditions | ANL-NBS-MD-000010 |
| S0025 - Site-Scale Saturated Zone Transport | MDL-NBS-HS-000010 |
| S0030 - Probability Distribution for Flowing Interval Spacing | ANL-NBS-MD-000003 |
| S0035 - Saturated Zone Colloid Transport | ANL-NBS-HS-000031 |
| S0045 - Site-Scale Saturated Zone Flow Model | MDL-NBS-HS-000011 |
| S0055 - Saturated Zone Flow and Transport Model Abstraction | MDL-NBS-HS-000021 |
| FEPs - Features, Events, and Processes in SZ Flow and Transport | DTN: MO0508SEPFEPPLA.002 |
| S0185 - Saturated Zone In-Situ Testing | ANL-NBS-HS-000039 |

NOTE: This figure is a simplified representation of the flow of information among SZ reports. See the most recent revision of each report for a complete listing of data and parameter inputs. This figure does not show inputs external to this suite of SZ reports.

FEPs = features, events, and processes; SZ = saturated zone; TSPA = total system performance assessment.

Figure 1-1. Generalized Flow of Information among Reports Pertaining to Flow and Transport in the SZ

This model report is governed by *Technical Work Plan: Saturated Zone Flow and Transport Modeling* (BSC 2006 [DIRS 177375]). All activities listed in the technical work plan (TWP) that are appropriate to the SZ site-scale flow model are documented in this report. The TWP (BSC 2006 [DIRS 177375]) cites procedures that were in effect at the time the work described in this report was planned and approved. Following the transition of the science work scope from Bechtel SAIC Company, LLC (BSC) to Sandia National Laboratories (SNL), new procedures have been issued since October 2, 2006.

Model-validation activities presented in this report lead to increased confidence that the model is a reasonable representation of groundwater flow likely to occur at Yucca Mountain near the repository site. Model confidence-building activities consist of the following comparisons between observed data and model simulations:

- Observed hydraulic heads and gradients not used for model development and calibration
- Hydraulic properties obtained from model calibrations and those obtained from field and laboratory testing
- Flowpaths obtained from the model and those inferred from analysis of field hydrochemistry and isotopic data.

Alternative conceptual models and the implications of these models for flow field, flowpaths, and transport times simulations are evaluated relative to the SZ site-scale flow model.

A number of relevant features, events, and processes (FEPs) are addressed in Section 6.2.

Uncertainty inherent to parameters, conceptualization, and modeling is discussed in Section 6 and propagated, as appropriate, in Section 8.

The SZ site-scale flow model is limited to steady state use (no transient conditions) for TSPA purposes. When using the SZ site-scale flow model for TSPA calculations, there are limitations that must be noted in regard to the following: changes to input parameter values, useable pathline distances, and overall model recharge fluxes. These are discussed more fully in Section 8.

Important technical issues addressed by this model report, and the sections in which they are discussed, include:

- Horizontal and vertical anisotropy, reasonable range for uncertainty (Sections 6.3.1.9, 6.4.3.11 and 6.7.1)
- Updated potentiometric data (Appendix E)
- Alternative conceptual flow models (Section 6.6)
- Validation of SZ site-scale flow model (Section 7)
- Comparison of volumetric and mass flow rates at the boundaries with those of the 2004 DVRFS model (Section 6.5.2.2).

Modeling objectives addressed in this model report are:

- Reflect the current understanding of the SZ flow

- Enhance model validation and uncertainty analyses
- Incorporate new data collected since the TSPA-SR (CRWMS M&O 2000 [DIRS 143665]).

This report is cited by *Features, Events, and Processes for Total System Performance Assessment* (SNL 2007 [DIRS 179476]).

This model report addresses the Condition Reports (CR) associated with previous versions as follow:

- CR 4734 identified an editorial error in a section callout in the previous revision of this report (BSC 2004 [DIRS 170037], p. 8-8). For this revision, cross-references have been checked and verified throughout the product development and review processes.
- CR 6012 identified two issues with the previous version (BSC 2004 [DIRS 170037]): the need to establish traceability for boundary fluxes used as calibration targets in the base-case flow model, and the need to assess the impact of differences between the boundary fluxes documented in the flow model analysis and model report (AMR) and those in the boundary flux report (BSC 2004 [DIRS 170015]). Sections 6.3.1.6, 6.4.3.8, 6.5.2.2, and Appendix C establish the traceability of the boundary fluxes extracted from the 2004 DVRFS model and used as calibration targets in the SZ site-scale flow model.
- CR 6493 identified as an issue that hydraulic heads simulated by the SZ flow alternative conceptual models appear to be unreasonably high in part of the model domain. This CR is no longer applicable because there are no calibrated alternative conceptual models in this report. Nevertheless, the revised, calibrated SZ site-scale flow model (Section 6.5) shows no such high heads.
- CR 6767 raised a question about the possible need to incorporate new technical data produced by the USGS on ^{14}C and $^{234}\text{U}/^{238}\text{U}$ activity ratios into the delineation of groundwater flow paths using geochemical indicators. Appendix B incorporates geochemical and isotopic data (including ^{14}C and $^{234}\text{U}/^{238}\text{U}$ ratios) that were not available for use in earlier versions and evaluates the consistency delineation of groundwater flowpaths.
- CR 6842 identified an incorrect software name and reference numbers in Table 3-1 of the previous revision. This report lists the correct software names in Table 3-1 and in Section 9. To prevent recurrence, confirmation across the software baseline report, DIRS, and this model report was included during the checking process.
- CR 7089 identified editorial issues in the previous revision. Because this is a complete revision of the SZ site-scale flow model, these editorial issues are no longer applicable.

- CR 7182 questioned the use of head boundaries with no vertical head variation. Section 6.3.1.6 presents the rationale for not varying the head vertically.
- CR 8337 identified errors in the constant head boundary condition specified along the southern boundary of the alternate SZ flow models. Because this is a complete revision of the SZ site-scale flow model, and there are no calibrated alternative models presented in this report), this CR is no longer applicable. Despite the inapplicability of this CR, care was taken to ensure that the southern boundary was correctly specified as the heads extracted from the potentiometric surface (Appendix E).

INTENTIONALLY LEFT BLANK

2. QUALITY ASSURANCE

Development of this model report and the supporting modeling activities are subject to the Office of Civilian Radioactive Waste Management Quality Assurance Program as indicated in the TWP (BSC 2006 [DIRS 177375]) developed under LP-2.29Q-BSC, *Planning for Science Activities*. Approved quality assurance procedures identified in the TWP (BSC 2006 [DIRS 177375], Section 4) have been used to conduct and document the activities described in this model report. The TWP (BSC 2006 [DIRS 177375], Section 8) also identifies the methods used to control the electronic management of data.

Planning and preparation of this report was initiated under the BSC QA Program. Therefore, forms and associated documentation prepared prior to October 2, 2006, the date this work transitioned to the Lead Laboratory, were completed in accordance with BSC procedures. Forms and associated documentation completed on or after October 2, 2006 were prepared in accordance with Lead Laboratory procedures.

This model report provides calibrated values for hydrologic properties of the SZ portion of the lower natural barrier (i.e., SZ below and downgradient from the repository), which is important to the demonstration of compliance with the postclosure performance objectives defined at 10 CFR 63.113 [DIRS 176544]. Therefore, the lower natural barrier is classified in *Q-List* (BSC 2005 [DIRS 175539], Table A-1) as “SC” (Safety Category), reflecting its importance to waste isolation, as defined in LS-PRO-0203, *Q-List and Classification of Structures, Systems, and Components*. This report contributes to the analysis and modeling data used to support performance assessment; the conclusions do not directly impact engineered features important to safety, as defined in LS-PRO-0203.

INTENTIONALLY LEFT BLANK

3. USE OF SOFTWARE

3.1 SOFTWARE TRACKED BY CONFIGURATION MANAGEMENT

The computer codes used directly in the SZ site-scale flow model are summarized in Table 3-1. Table A3-1 lists additional software used in the hydrochemistry analysis to support an indirect corroboration activity for validation (see Appendix A). Section E2 discusses software used to develop the potentiometric surface. The qualification status of the software is indicated in the Software Configuration Management (SCM) database. All software was obtained from SCM and is appropriate for the application. Qualified codes were used only within the range of validation as required by IM-PRO-003, *Software Management*. All software baselined after October 2, 2006 was qualified per IT-PRO-0012, *Qualification of Software*, and validated per IM-PRO-005 *Software Independent Verification and Validation*. Computer codes listed in Table 3-1 were selected for use in the analysis report because they were appropriate for the intended use. Software used directly in modeling tasks also satisfy at least one of the following conditions (as documented in the table footnotes) in that they were:

- Developed specifically for the tasks considered in this report
- Best available codes for modeling conditions specific to the YMP.

The codes developed specifically for the tasks considered in this report and for the YMP were validated for the parameter ranges expected for Yucca Mountain. The range of use and the limitations on output of each code are specified in the Software Management Report of each code. As it can be concluded from these reports, the limitations on input and output should only be considered when these codes are used outside of the YMP. Otherwise, no special limitations on input and output exist. The codes that fall into one of the categories above are described in Sections 3.1.1 through 3.1.4.

Table 3-1. Computer Codes Used in the SZ Site-Scale Flow Model

| Software Name and Version (V) | Software Tracking Number (STN) | Description | Computer Type, Platform, and Location | Date Base-lined |
|---|--------------------------------|--|--|-----------------|
| CORPSCON V.5.11.08 [DIRS 155082] | 10547-5.11.08-00 | Software package for conversion of coordinates | Windows NT 4.0 | 8/27/01 |
| FEHM V2.24 ^a [DIRS 179539] | 10086-2.24-02 | Solution to SZ flow | PC or Sun Ultra Sparc with Sun Solaris 5.7 or 5.8 operating system | 12/1/06 |
| LaGriT V1.1 ^a [DIRS 173140] | 10212-1.0-00 | Software package for grid generation, analysis, and visualization | Sun Ultra Sparc with Sun OS 2.7 operating system at LANL | 8/8/01 |
| PEST V5.5 [DIRS 161564] | 10289-5.5-00 | Preconditioning and parameter optimization for FEHM [DIRS 179539] runs | Sun Ultra Sparc with Sun Solaris 5.7 or 5.8 operating system at LANL | 12/3/02 |

Table 3-1. Computer Codes Used in the SZ Site-Scale Flow Model (Continued)

| Software Name and Version (V) | Software Tracking Number (STN) | Description | Computer Type, Platform, and Location | Date Base-lined |
|--|---------------------------------------|--|---|------------------------|
| EarthVision 5.1 [DIRS 167994] | 10174-5.1-00 | Commercial software for 3D model building and visualization used for contouring, plotting, and visualization of the data and for evaluation of results | Silicon Graphics Octane workstation running IRIX 6.5 | 09/18/00 |
| Extract V1.0 ^b [DIRS 163070] | 10955-1.0-00 | Pre/postprocessor used to extract lateral flow data from the USGS regional flow model | Sun UltraSPARC - SunOS 5.7 operating system at SNL | 12/11/02 |
| Extract V1.1 ^b [DIRS 163071] | 10955-1.1-00 | Pre/postprocessor used to extract lateral flow data from the USGS 2001 regional flow model | Sun UltraSPARC - SunOS 5.7 operating system at SNL | 12/11/02 |
| EXT_RECH V1.0 ^b [DIRS 163072] | 10958-1.0-00 | Pre/postprocessor used to extract recharge data from the USGS regional flow model | Sun UltraSPARC - SunOS 5.7 operating system at SNL | 12/11/02 |
| Mult_Rech V1.0 ^b [DIRS 163073] | 10959-1.0-00 | Pre/postprocessor that scales recharge data from the USGS regional flow model and maps the data to a new grid | Sun UltraSPARC - SunOS 5.7, Solaris 2.7 operating system at SNL | 12/18/02 |
| Xread_Distr_Rech V1.0 ^b [DIRS 163074] | 10960-1.0-00 | Pre/postprocessor used to extract recharge data from the USGS 1999 regional flow model | Sun UltraSPARC - SunOS 5.7 operating system at SNL | 12/11/02 |
| Xread_Distr_Rech_UZ V1.0 ^b [DIRS 163075] | 10961-1.0-00 | Pre/postprocessor that maps recharge data onto a new grid excluding the UZ flow model region | Sun UltraSPARC - SunOS 5.7 operating system at SNL | 12/11/02 |
| Xread_Reaches V1.0 ^b [DIRS 163076] | 10962-1.0-00 | Pre/postprocessor that maps local recharge from four stream channels onto a new grid | Sun UltraSPARC - SunOS 5.7 operating system at SNL | 12/11/02 |
| Xwrite_Flow_New V1.0-125 ^b [DIRS 163077] | 10963-1.0-125-00 | Used both to map the combined UZ and SZ site-scale fluxes onto a 125-m grid and to create a flux file that is compatible with FEHM [DIRS 179539] flow macros | Sun UltraSPARC - SunOS 5.7 operating system at SNL | 12/11/02 |

Table 3-1. Computer Codes Used in the SZ Site-Scale Flow Model (Continued)

| Software Name and Version (V) | Software Tracking Number (STN) | Description | Computer Type, Platform, and Location | Date Base-lined |
|--|--------------------------------|---|--|-----------------|
| Zones V1.0 ^b [DIRS 163078] | 10957-1.0-00 | Used to extract zonal designation data from the USGS 2001 regional flow model | Sun UltraSPARC - SunOS 5.7 operating system at SNL | 12/11/02 |

^a Developed for the YMP.

^b Developed specifically for the tasks considered in this report.

DOS = disk operating system; HFM = hydrogeologic framework model; LANL = Los Alamos National Laboratory; PC = personal computer; SNL = Sandia National Laboratories; SZ = saturated zone; USGS = U.S. Geological Survey; UZ = unsaturated zone.

3.1.1 Parameter Optimization

The parameter estimation code PEST V5.5 (STN: 10289-5.5-00; [DIRS 161564]) is used to perform the parameter optimization for the hydrogeologic and feature permeabilities. The PEST code is based on the Levenberg-Marquardt (LM) algorithm. This software was not used to generate flow model output. Rather, it is used to calibrate the flow model by minimizing the difference between observed and simulated head and boundary fluxes values.

3.1.2 Flow Modeling

FEHM V2.24 (STN: 10086-2.24-02; [DIRS 179539]) is used to solve for a steady-state flow solution and to provide model output. The range of validation for the FEHM code was developed with the YMP specific data. Consequently, the input and output parameters are within their validation ranges.

3.1.3 Particle Tracking

The FEHM code is used within its validated range to determine the steady-state flow solution (see Section 3.1.2). FEHM has two different particle-tracking routines and herein the *sptr* macro is used, but only insofar as to illustrate flowpaths. The particle-tracking portion of FEHM is discussed extensively in *Site-Scale Saturated Zone Transport* (SNL 2007 [DIRS 177392], Section 6.4.2).

3.1.4 Grid Generation

The grid generation software package LaGriT V1.0 (STN: 10212-1.1-00; [DIRS 173140]) is used within its validation limits for creation, analysis, and visualization of grids. LaGriT is a set of software macros that uses the HFM conceptual model data to create computational grids. The software macros translate the coordinate and attribute information into a form that is valid for finite-element heat and mass (FEHM) compilations.

3.2 EXEMPT SOFTWARE

Several additional, exempt (IM-PRO-003), commercially available software packages were used for data handling, formatting, and data visualization in the preparation of SZ site-sale flow

Model. These additional software packages are Microsoft Access (97 and 2000) and Microsoft Excel (97 and 2003 SP2). Each of these additional software packages was used on the Windows 2000 platform. No calculations were performed by these commercial software packages and the only output is in the form of visualizations, such as those found in Figures 6-14 through 6-17 and the appendices. Input files or sources are identified with each figure. Surfer was used for visualization and is therefore exempt per IM-PRO-003, Section 2.0, 5th paragraph, 2nd dash. Access and Excel were used for formatting data and were exempt per IM-PRO-003, Section 2.0, 5th paragraph, 1st dash. Each of these exempt software packages is controlled by YMP Software Configuration Management.

- *Excel 97* or 2003-SP2 was used to preprocess data from the U.S. Geological Survey (USGS) traces for FEHM zone definitions as well as for other standard calculations and visualizations. The calculation of basic statistics was used with standard functions only.
- *Surfer* for Windows, v8.06.39 was used for plotting and visualization of analysis results in figures shown in this report. The results were visually checked for correctness.
- *Igor Pro*, v4.091 was used for plotting and visualization of analysis results in some figures shown in this report. The results were visually checked for correctness.
- *Microsoft Access* 1997 SR2, was used to identify model nodes that are located a specified distance from an x,y coordinate.
- *GMV* and *Adobe Illustrator*, v10 were used to visualize and illustrate the computational mesh, geochemical analyses, and related data.
- *AquaChem*, V3.7, was used to create trilinear diagrams showing proportions of major ions in groundwater and $x-y$ scatter plots.
- *Adobe Illustrator*, v10 was used to create flow-path maps.

Outputs from *Excel*, *Surfer*, *Igor*, *Microsoft Access*, *GMV*, *Adobe Illustrator*, and *AquaChem* were visually checked for correctness. This output can be found in the Technical Data Management System (TDMS) within data packages that have been assigned data tracking number (DTN) numbers. The DTNs are identified in appropriate places throughout Section 6 to allow the independent reviewer to reproduce or verify results by visual inspection or hand calculation.

AutoCad 2002 and *EarthVision 7.5.2* were used for data visualization and are, therefore, exempt under of IM-PRO-003, Paragraph 1.4.2. *UltraEdit V11.10* was used for formatting data and was exempt under IM-PRO-003, Paragraph 1.4.1. Each of these exempt software packages is controlled by YMP Software Configuration Management.

3.3 PROTOTYPE SOFTWARE

PEST V11.1 (STN: 611582-11.1; [DIRS 179480]) was used as a prototype in advancing science analysis. This software was not used in quality-affecting work; rather, the earlier qualified

version *PEST V5.5* (STN: 10289-5.5-00; [DIRS 161564]) was used for quality-affecting work. *PEST V11.1* was used to analyze, in a prototype/scoping manner, the FEHM predictive uncertainty for specific discharge, which was calculated with *SPDIS.EXE* (STN: 611598-00-00; [DIRS 180546]).

INTENTIONALLY LEFT BLANK

4. INPUTS

4.1 DIRECT INPUT

Input information used in this model report comes from several sources, which, along with their DTNs, are summarized in Table 4-1. The data referenced in Table 4-1 contain information necessary to construct the numerical model, set boundary conditions, calibrate the model, and check the calibration. The data are fully appropriate for the SZ site-scale flow model. All data listed in Table 4-1 are qualified or will be qualified according to SCI-PRO-001, *Qualification of Unqualified Data*, upon finalization of this report. Per SCI-PRO-006 (Attachment 2), no data used as input and listed in Table 4-1 are used for model validation.

Table 4-1. Direct Input Data Sources

| Data Description | Data Tracking Number | File Name |
|---|---|---|
| Hydraulic head data and well locations as described by BSC 2004 [DIRS 170009] | GS010908312332.002 [DIRS 163555] ^a | <i>mean312411.xls</i> |
| Potentiometric surface | MO0409SEPPSMP.000 [DIRS 179336] | <i>S00005_fig6-2.pdf</i> |
| Plot of temperature profiles in wells | MO0102DQRBTEMP.001 [DIRS 154733] | <i>All</i> |
| Fault locations | GS010608312332.001 [DIRS 155307] | <i>tert_flts.e00</i> |
| Fault locations (U.S. Highway 95) | GS010908314221.001 [DIRS 162874] | <i>All</i> |
| HFM for SZ site-scale flow and transport model, containing unit surfaces | MO0610MWDHFM06.002 [DIRS 179352] | <i>output.zip</i> |
| UZ flow model output | LB03023DSSCP9I.001 [DIRS 163044] | <i>Meshes.tar.gz</i> <i>preq_1A.tar.gz</i> <i>preq_mA.tar.gz</i> <i>preq_uA.tar.gz</i> |
| Fortymile Wash infiltration | MO0102DQRGWREC.001 [DIRS 155523] | <i>All</i> |

^a This DTN was used to establish well locations and water levels for model calibration. While this same DTN was used in validation (Appendix A), it was used solely to establish a common frame of reference (i.e., common well locations were used, but water levels were not used in the analysis in Appendix A).

HFM = hydrogeologic framework model; SZ = saturated zone.

The data listed in Table 4-1 are direct model inputs, after appropriate manipulation by the software listed in Table 3-1.

Table 4-2. Intermediary Direct Input Data Sources (see also Table 8-1)

| Data Description | Data Tracking Number | File Name |
|---|---------------------------------|---|
| Lateral mass flow targets and infiltration boundary conditions | SN0612T0510106.003 ^a | <i>wt_250_04.dat</i> <i>east_bdy_2004</i> <i>north_bdy_2004</i> <i>south_bdy_2004</i> <i>west_bdy_2004</i> <i>Analysis.xls</i> |
| Nye County Early Warning Program well location, open interval, and water-level data | SN0702T0510106.007 ^b | <i>All</i> |

^a See Appendix C for development and qualification of this DTN for intended use in this report.

^b See Appendix D for development and qualification of this DTN for intended use in this report.

The data listed in Table 4-2 are direct model inputs that come from intermediary product output as developed and qualified in Appendices C and D.

4.2 CRITERIA

The general requirements to be satisfied by the TSPA are stated at 10 CFR Part 63 [DIRS 176544]. The acceptance criteria that will be used by the NRC to determine whether the technical requirements have been met are identified in *Yucca Mountain Review Plan, Final Report* (YMRP) (NRC 2003 [DIRS 163274]).

Acceptance Criteria from YMRP Section 2.2.1.3.8.3 (NRC 2003 [DIRS 163274]), Flow Paths in the Saturated Zone

The applicable acceptance criteria in the YMRP (NRC 2003 [DIRS 163274], Section 2.2.1.3.8.3) are given below. How they are addressed by this report is described in Section 8.4.

Acceptance Criterion 1: *System Description and Model Integration Are Adequate.*

- (1) Total system performance assessment adequately incorporates important design features, physical phenomena, and couplings, and uses consistent and appropriate assumptions, throughout the flowpaths in the SZ abstraction process;
- (2) The description of the aspects of hydrology, geology, geochemistry, design features, physical phenomena, and couplings, that may affect flowpaths in the SZ, is adequate. Conditions and assumptions in the abstraction of flowpaths in the SZ are readily identified, and consistent with the body of data presented in the description;
- (4) Boundary and initial conditions used in the total system performance assessment abstraction of flowpaths in the SZ are propagated throughout its abstraction approaches. For example, abstractions are based on initial and boundary conditions consistent with site-scale modeling and regional models of the Death Valley regional groundwater flow system;
- (5) Sufficient data and technical bases to assess the degree to which features, events, and processes have been included in this abstraction are provided;
- (6) Flowpaths in the SZ are adequately delineated, considering natural site conditions;
- (7) Long-term climate change, based on known patterns of climatic cycles during the Quaternary period, particularly the last 500,000 years, and other paleoclimate data, are adequately evaluated;
- (8) Potential geothermal and seismic effects on the ambient SZ flow system are adequately described and accounted for;

- (9) The impact of the expected water table rise on potentiometric heads and flow directions, and consequently on repository performance, is adequately considered; and
- (10) Guidance in NUREG-1297 (Altman et al. 1988 [DIRS 103597] and NUREG-1298 (Altman et al. 1988 [DIRS 103750]), or other acceptable approaches for peer review and data qualification is followed.

Acceptance Criterion 2: *Data Are Sufficient for Model Justification.*

- (1) Geological, hydrological, and geochemical values used in the license application to evaluate flowpaths in the SZ are adequately justified. Adequate descriptions of how the data were used, interpreted, and appropriately synthesized into the parameters are provided;
- (2) Sufficient data have been collected on the natural system to establish initial and boundary conditions for the abstraction of flowpaths in the SZ;
- (3) Data on the geology, hydrology, and geochemistry of the SZ used in the total system performance assessment abstraction are based on appropriate techniques. These techniques may include laboratory experiments, site-specific field measurements, natural analogue research, and process-level modeling studies. As appropriate, sensitivity or uncertainty analyses, used to support the U.S. Department of Energy total system performance assessment abstraction, are adequate to determine the possible need for additional data; and
- (4) Sufficient information is provided to substantiate that the mathematical groundwater modeling approach and model(s) are calibrated and applicable to site conditions.

Acceptance Criterion 3: *Data Uncertainty Is Characterized and Propagated Through the Model Abstraction.*

- (1) Models use parameter values, assumed ranges, probability distributions, and bounding assumptions that are technically defensible, reasonably account for uncertainties and variabilities;
- (2) Uncertainty is appropriately incorporated in model abstractions of hydrologic effects of climate change, based on a reasonably complete search of paleoclimate data;
- (3) Uncertainty is adequately represented in parameter development for conceptual models, process-level models, and alternative conceptual models, considered in developing the abstraction of flowpaths in the SZ. This may be done either through sensitivity analyses or through use of conservative limits. For example, sensitivity analyses and/or similar

analyses are sufficient to identify SZ flow parameters that are expected to significantly affect the abstraction model outcome; and

- (4) Where sufficient data do not exist, the definition of parameter values and conceptual models is based on appropriate use of expert elicitation, conducted in accordance with NUREG-1563 (Kotra et al. 1996 [DIRS 100909]). If other approaches are used, the U.S. Department of Energy adequately justifies their uses.

Acceptance Criterion 4: *Model Uncertainty Is Characterized and Propagated Through the Model Abstraction.*

- (1) Alternative modeling approaches of features, events, and processes are considered and are consistent with available data and current scientific understanding, and the results and limitations are appropriately considered in the abstraction;
- (2) Conceptual model uncertainties are adequately defined and documented, and effects on conclusions regarding performance are properly assessed. For example, uncertainty in data interpretations is considered by analyzing reasonable conceptual flow models that are supported by site data, or by demonstrating through sensitivity studies that the uncertainties have little impact on repository performance;
- (3) Consideration of conceptual model uncertainty is consistent with available site characterization data, laboratory experiments, field measurements, natural analogue information and process-level modeling studies; and
- (4) Appropriate alternative modeling approaches are consistent with available data and current scientific knowledge, and appropriately consider their results and limitations, using tests and analyses that are sensitive to the processes modeled.

Acceptance Criteria from Section 2.2.1.1.3 (NRC 2003 [DIRS 163274]), System Description and Demonstration of Multiple Barriers

Acceptance Criterion 3: *Technical Basis for Barrier Capability is Adequately Presented.*

The technical bases are consistent with the technical basis for the performance assessment. The technical basis for assertions of barrier capability is commensurate with the importance of each barrier's capability and associated uncertainties.

4.3 CODES, STANDARDS, AND REGULATIONS

No codes, standards, or regulations other than those identified in Section 4.1 were used in this model report.

5. ASSUMPTIONS

A list of the assumptions used in this model report is provided in Table 5-1. The rationale and confirmation status for each status assumption is also provided. The upstream assumptions associated with the rationale below do not impact the results of the model.

Table 5-1. Assumptions

| No. | Assumption | Rationale | Location in this Report |
|-----|--|--|-------------------------|
| 1 | Horizontal anisotropy in permeability, as it applies to the fractured and faulted volcanic units along the flowpaths, is adequately represented by a permeability tensor that is oriented in the north-south and east-west directions. | This assumption is introduced due to the difficulty to (1) establish with certainty the direction of horizontal anisotropy and to align the model axes along the principle axes or (2) build the model with a 9-component tensor. One analysis of the probable direction of horizontal anisotropy shows that the direction of maximum transmissivity is N 33°E (Winterle and La Femina 1999 [DIRS 129796], p. iii), indicating that the anisotropy applied on the SZ site-scale model grid is within approximately 30° of the inferred anisotropy. | Used throughout |
| 2 | The hydrogeologic properties, including permeabilities, for all units in the SZ site-scale flow model may be represented with homogeneous values. These properties are uniform within each stratigraphic unit. | This assumption is introduced due to the lack of information on the areal heterogeneity within the SZ. The flow model is designed to simulate the groundwater flow field at a scale of many kilometers. For simulating flow at that scale, effective flow parameters are generally acceptable. Thus, the use of homogeneous properties within a particular flow unit is acceptable. The calibration process provides "best fit" parameters for the SZ model. Where appropriate, additional zones or parameters are supplied to represent spatial differences in hydrogeology. These zones are justified in the sections in which they are used (see, for example, Sections 6.4.3.1 and 6.4.3.4). | Used throughout |

DVRFS = Death Valley Regional Flow System; LA = license application; NTS = Nevada Test Site; SZ = saturated zone.

INTENTIONALLY LEFT BLANK

6. MODEL DISCUSSION

6.1 MODELING OBJECTIVES

The purpose of the SZ site-scale flow model is to describe the steady-state flow of groundwater as it moves from the water table below the repository, through the SZ, and to the accessible environment. The flow model estimates the SZ advective processes that control the movement of groundwater and dissolved radionuclides and colloidal particles that might be present.

The previous versions of the SZ site-scale flow model were developed in support of the TSPA-SR (CRWMS M&O 2000 [DIRS 153246]) and the TSPA-LA (BSC 2004 [DIRS 170037]). This model revision includes the following modifications to: (1) reflect the current understanding of SZ flow, (2) enhance model validation and uncertainty analyses, (3) improve locations and definitions of fault zones, (4) enhance grid resolution (500-m grid spacing to 250-m grid spacing), and (5) incorporate new data collected since the TSPA-SR:

- Implementation of the updated hydrogeologic framework model (HFM) that incorporates recent geologic data obtained from the Nye County Early Warning Drilling Program (DTN: MO0610MWDHFM06.002 [DIRS 179352]) and the 2004 DVRFS (Belcher 2004 [DIRS 173179])
- A potentiometric surface updated with water-level data from Phases III and IV of the NC-EWDP (Output DTN: MO0611SCALEFLW.000)
- Additional water-level calibration target data from Phases III and IV of the Nye County Early Warning Drilling Program (Output DTN: SN0702T0510106.007)
- Boundary volumetric/mass flow rates and recharge data from the 2004 DVRFS (Belcher 2004 [DIRS 173179]) and the 2003 UZ flow model (BSC 2004 [DIRS 169861])
- Use of field and laboratory tests (hydraulic and tracer data collected since TSPA-SR) to establish and confirm the conceptual model for flow, constrain model parameter calibration, and provide data for model validation and confidence building (SNL 2007 [DIRS 177394], Section 6).

This modeling analysis is a direct feed to *Site-Scale Saturated Zone Transport* (SNL 2007 [DIRS 177392]) because it provides the SZ flow fields for transport calculations.

6.2 FEATURES, EVENTS, AND PROCESSES CONSIDERED IN THE MODEL

As stipulated in *Technical Work Plan for: Saturated Zone Flow and Transport Modeling* (BSC 2006 [DIRS 177375]), this model report addresses the FEPs pertaining to SZ flow that are included (i.e., Included FEPs) for TSPA-LA listed in Table 6-1. SZ FEPs that were excluded (i.e., Excluded FEPs) for TSPA-LA are described in *Features, Events, and Processes for the Total System Performance Assessment* (SNL 2007 [DIRS 179476]). Table 6-1 provides a list of FEPs that are relevant to this model analysis in accordance with their assignment in the LA FEP list (DTN: MO0508SEPFELA.002 [DIRS 175064]). Specific reference to the various sections

within this document where issues related to each FEP are addressed is provided in Table 6-1. A detailed discussion of these FEPs as well as their implementation in TSPA-LA is documented in *Features, Events, and Processes for the Total System Performance Assessment* (SNL 2007 [DIRS 179476]).

Table 6-1. Features, Events, and Processes Included in TSPA-LA and Relevant to this Model Report

| FEP No. | FEP Name | Sections Where Disposition is Described | Discussed in Supporting Documents |
|--------------|--|---|--|
| 1.2.02.01.0A | Fractures | Sections 6.3.1.10, 6.4.3.7 | Upstream Feeds ^a BSC 2004 [DIRS 170014] Corroborating ^b SNL 2007 [DIRS 177394] |
| 1.2.02.02.0A | Faults | Sections 6.3.1.10, 6.4.3.7 | Upstream Feeds ^a SNL 2007 [DIRS 174109] DTNs: GS010608312332.001 [DIRS 155307], GS010908314221.001 [DIRS 162874] Corroborating ^b BSC 2006 [DIRS 177394] |
| 1.3.07.02.0A | Water table rise affects SZ | Section 6.6.4 | Upstream Feeds ^a BSC 2006 [DIRS 177394] |
| 2.2.03.01.0A | Stratigraphy | Sections 6.3.1.2, 6.4.3.1, 6.4.3.3, 6.4.3.10 | Upstream Feeds ^a SNL 2007 [DIRS 174109]; Corroborating ^b BSC 2004 [DIRS 170014] BSC 2006 [DIRS 177394] |
| 2.2.03.02.0A | Rock properties of host rock and other units | Sections 6.4.3.1, 6.4.3.3, 6.4.3.10 | Upstream Feeds ^a SNL 2007 [DIRS 174109] Corroborating ^b BSC 2006 [DIRS 177394] |
| 2.2.07.12.0A | Saturated groundwater flow in the geosphere | Sections 6.3.1.1, 6.4.1, 6.4.2; Figures 6-1; A-6.7.6, A-6.7.7, A-6.7.8, A-6.7.9, and A-6.7.11 | Upstream Feeds ^a DTN: MO0507SPAINHFM.000 [DIRS 174523] Corroborating ^b BSC 2004 [DIRS 170014] BSC 2006 [DIRS 177394] |
| 2.2.07.13.0A | Water-conducting features in the SZ | Sections 6.3.1.2, 6.4.3.7 | Upstream Feeds ^a SNL 2007 [DIRS 174109] Corroborating ^b BSC 2004 [DIRS 170014] BSC 2006 DIRS 177394] |
| 2.2.07.15.0A | Advection and dispersion in the SZ | Sections 6.4.1, 6.4.2 | Upstream Feeds ^a DTN: MO0507SPAINHFM.000 [DIRS 174523] Corroborating ^b BSC 2006 [DIRS 177394] |
| 2.2.10.03.0A | Natural geothermal effects on flow in the SZ | Sections 6.3.2 and 6.4.3.10 | Upstream Feeds ^a SNL 2007 [DIRS 174109] |
| 2.2.12.00.0B | Undetected features in the SZ | Section 6.3.2 | Upstream Feeds ^a SNL 2007 [DIRS 174109] |

^a Aspects of the SZ FEPs screening position adopted in this report are a result of SZ analyses performed in a directly upstream SZ model or analyses. N/A indicates that there are no upstream feeds.

^b Corroborating-SZ analysis or model report that indirectly supports the FEP topic.

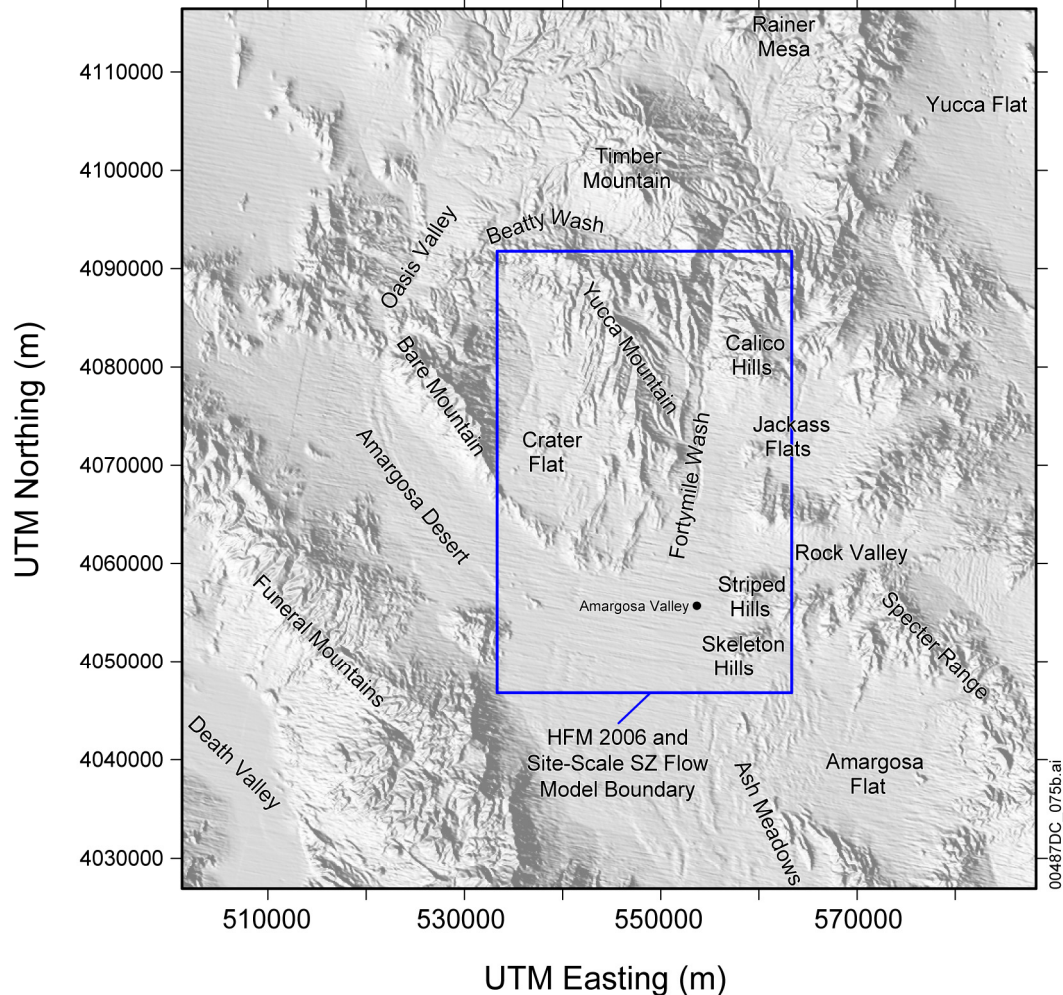
FEP = features, events, and processes; SZ = saturated zone.

6.3 THE CONCEPTUAL MODEL

Yucca Mountain is located in the Great Basin about 150 km northwest of Las Vegas, Nevada. The mountain consists of a series of fault-bounded blocks of ash-flow and ash-fall tuffs and a smaller volume of lava deposited between 14 and 11 Ma (one million years (refers to age)) from a series of calderas located a few to several tens of kilometers to the north (Sawyer et al. 1994 [DIRS 100075]). Yucca Mountain itself extends southward from the Pinnacles Ridge toward the Amargosa Desert, where the tuffs thin and pinch out beneath the alluvium (Figure 6-1). The tuffs dip 5 to 10 degrees to the east over most of Yucca Mountain.

The Solitario Canyon Fault separates Yucca Mountain from Crater Flat, which is in the western portion of the model domain. Crater Flat is west of Yucca Mountain and separated from it by Solitario Canyon, which is the surface expression of the Solitario Canyon Fault—a steeply dipping scissored fault with down-to-the-west displacement of as much as 500 m in southern Yucca Mountain (Day et al. 1998 [DIRS 100027], pp. 6 to 7). Underlying Crater Flat are thick sequences of alluvia, lavas, and tuffs that have been locally cut by faults and volcanic dikes. East of Yucca Mountain, and separated from it by Fortymile Wash, is Jackass Flats, which is underlain by a thick sequence of alluvium and volcanic rocks. Timber Mountain, approximately 25 km to the north of the repository area, is a resurgent dome within the larger caldera complex when eruptions supplied the tuffs at Yucca Mountain.

The SZ site-scale flow model presented in this report describes our current state of knowledge of the saturated flow system. The boundaries of the numerical model for SZ flow and transport are indicated on Figure 6-1 in blue. The domain was selected to be: (1) coincident with grid cells of the DVRFS model (DTN: MO0602SPAMODAR.000 [DIRS 177371]) where site-scale model (FEHM) nodes correspond to regional model (MODFLOW-2000) cell corners in the horizontal plane; (2) sufficiently large to reduce the effects of boundary conditions on estimating permeabilities and calculated flow fields near Yucca Mountain; (3) sufficiently large to assess groundwater flow at distances beyond the 18-km compliance boundary from the repository area; (4) small enough to minimize the model size for computational efficiency and to include structural feature detail affecting flow; (5) thick enough to include part of the regional Paleozoic carbonate aquifer (the bottoms of the site- and regional-scale models are equal at -4,000 m below sea level); and (6) large enough to include borehole data from the Amargosa Desert at the southern end of the modeled area. The hydrogeologic setting of the SZ flow system in the vicinity of Yucca Mountain was summarized by Luckey et al. (1996 [DIRS 100465], p. 13). Yucca Mountain is part of the Alkali Flat-Furnace Creek sub-basin of the Death Valley groundwater basin (Waddell 1982 [DIRS 101062], pp. 15 to 16). Discharge within the sub-basin occurs at Alkali Flat (Franklin Lake Playa) and, possibly, Furnace Creek in Death Valley (Figure 6-1). Water inputs to the sub-basin include groundwater inflow/outflow along the northern, eastern, and western boundaries of the sub-basin, recharge from precipitation in high-elevation areas of the sub-basin, and recharge from surface runoff in Fortymile Canyon and Fortymile Wash. North and northeast of Yucca Mountain, recharge from precipitation also occurs at Timber Mountain, Pahute Mesa, Rainier Mesa, and Shoshone Mountain (Luckey et al. 1996 [DIRS 100465], p. 13).



Source: DTN:GS010908314221.001 [DIRS 162874].

NOTE: The blue rectangle indicates the boundary of the SZ flow and transport models.

SZ = saturated zone; UTM = Universal Transverse Mercator.

Figure 6-1. Important Physiographic Features Near Yucca Mountain Including Some of Those Explicitly Included the SZ Site-Scale Flow Model

The general conceptual model of flow in the SZ site-scale flow model domain is that groundwater flows southerly from recharge areas of higher precipitation at higher elevations north of Yucca Mountain, through the Fortymile Wash and toward the Amargosa Desert (see Appendices A and B). Within the model domain, recharge occurs from infiltration of both precipitation and flood-flows through Fortymile Wash and its tributaries. In the southeastern part of the model area (within the Ash Meadows groundwater basin), considerable flows enter and exit the area through the lower carbonate aquifer system (BSC 2004 [DIRS 170015], Section 6.2). This aquifer system is believed to underlie much of the Alkali Flat-Furnace Creek groundwater basin based on inferences from Death Valley regional groundwater flow data (Belcher 2004 [DIRS 173179], Figure F-46). However, the flow patterns of groundwater in this area and their relationship to flow in the Ash Meadows groundwater basin system are poorly understood. Outflow from the SZ site-scale flow model area occurs primarily across the

southern boundary of the model. The constant head boundary condition applied to the southern boundary reflects head decreases from pumping by irrigation wells in the Amargosa Farms area. Although the irrigation wells are not explicitly modeled in the SZ site-scale model, the effects of this pumping are reflected in the lower heads of the southern boundary condition.

6.3.1 Key Features

Several important physiographic features are shown in Figure 6-2. Within the boundaries of the model domain, there are at least seven primary components that affect the local flow system and potential radionuclide transport:

- HFM and the faults
- Solitario Canyon Fault
- Recharge to SZ
- Crater Flat Tuff hydrogeologic units
- Shallow alluvial aquifer of Fortymile Wash
- Regional carbonate aquifer
- Large, moderate, and small hydraulic gradients.

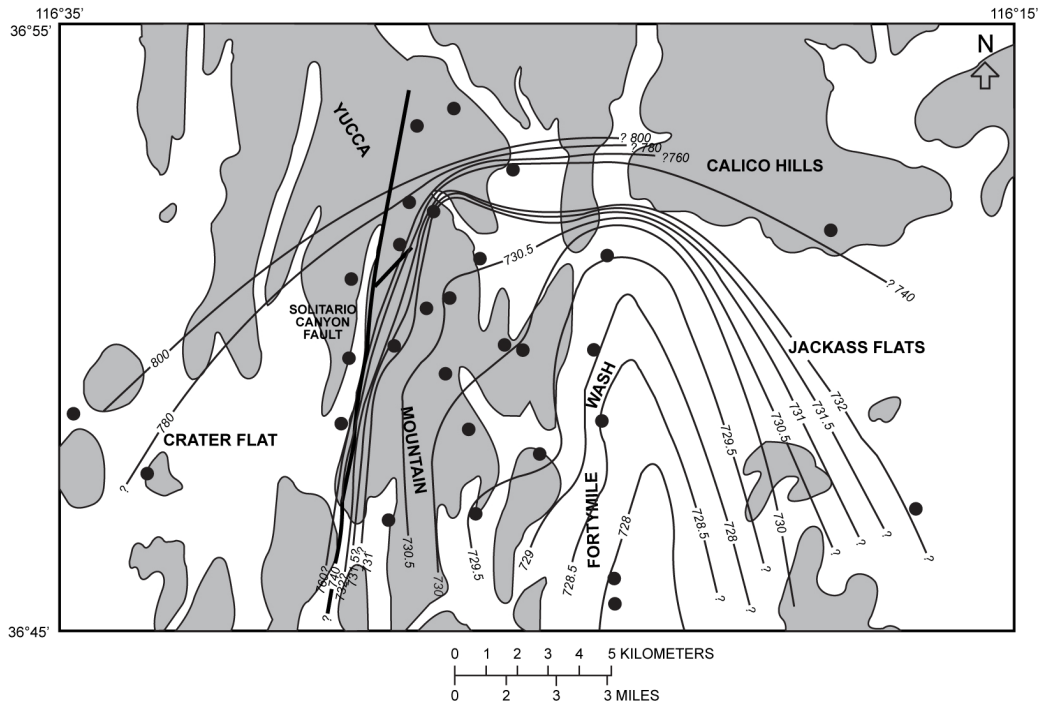
The HFM (SNL 2007 [DIRS 174109]) is a conceptual model providing a three-dimensional interpretation of the hydrostratigraphic unit locations and the structure within the SZ site-scale flow and transport model domain. The HFM does not provide any hydraulic parameters; rather, it provides a conceptualization of hydrogeologic units that serves as the basis for calibrating hydraulic parameters. Faults are superimposed on the HFM as described in Sections 6.4.3.1 and 6.4.3.7.

The Solitario Canyon Fault is important because it could provide a vertical flowpath from the surface to the SZ. Depending on its conceptualization, it also acts as a barrier to flow that might otherwise travel from Crater Flat to Yucca Mountain.





Recharge to the SZ is important because it impacts transport time of radionuclides that could potentially escape from the repository. Flow through the lateral boundaries from the steady-state stress period of the 2004 DVRFS (Belcher 2004 [DIRS 173179]) supplies target boundary volumetric/mass flow rates for the site-scale model. Vertical recharge due to infiltration of rain and runoff at the land surface contributes to a small downward gradient below and around the repository.

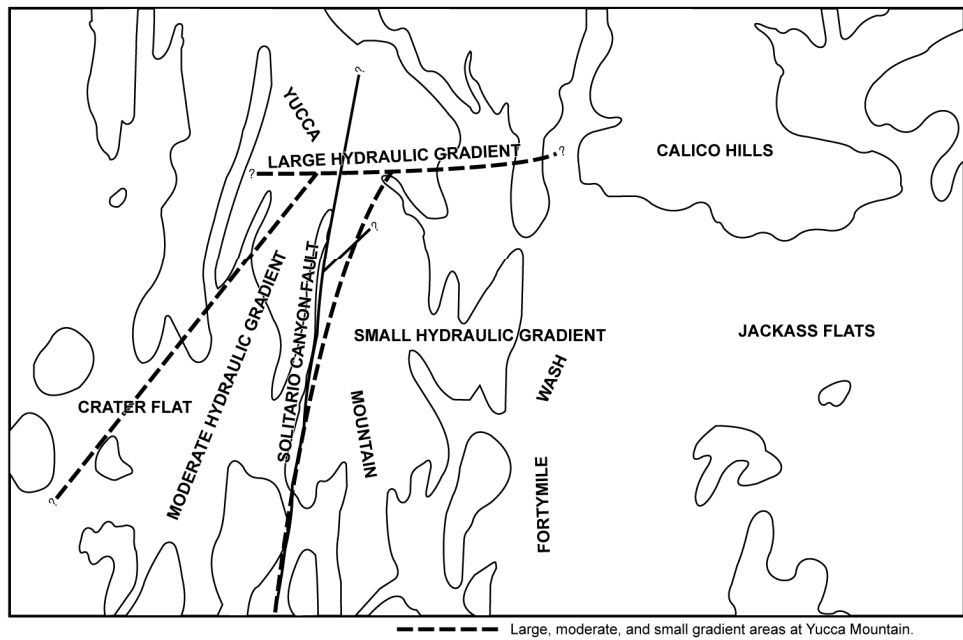
The three Crater Flat tuffs are likely to be among the more permeable hydrogeologic units near the repository and, thus, are the most likely paths for potential radionuclide transport. Calibrated values of these three permeabilities will be representative of not only these units in the HFM, but also functions of the model formulation and contamination by cross correlations. A discussion of parameter and prediction uncertainties is presented in Section 6.7.

The shallow alluvial aquifer in Fortymile Wash is important because it bounds the likely flowpaths for fluid leaving the repository area and also has desirable retardation characteristics for many radionuclides.



EXPLANATION

| | | | |
|--|----------|--|--|
|  | Alluvium |  | Potentiometric contour--Shows altitude of potentiometric surface, 1993. Contour interval in meters, is variable. Datum is sea level. |
|  | Bedrock |  | Well location |



Source: Tucci and Burkhardt (1995 [DIRS 101060], Figures 2, 4, and 5).

NOTE: An updated potentiometric surface is developed in Appendix E.

Figure 6-2. Potentiometric Surface Map and Gradient Areas Developed Using Water-Level Data from 1993

The regional carbonate aquifer underlies the likely flowpaths for fluid leaving the repository area. This aquifer also provides an upward gradient that keeps the flowpaths shallow and effectively isolates the local Yucca Mountain system from the regional carbonate aquifer. Much of the flow through the model domain passes through the lower carbonate aquifer.

In Figure 6-2, the large, moderate, and small hydraulic gradients control the flow field below and downgradient from the repository. It is important to accurately represent these gradients to ensure consistency between model results and the inferred potentiometric surface.

Hydrochemical studies conducted at and near Yucca Mountain over the last 25 years are summarized in Appendices A and B. Appendix A summarizes data that were available up to approximately 2002, whereas Appendix B examines data that have come available since then. The appendices provide analyses of groundwater recharge rates, flow directions and velocities, and mixing proportions of water from different source areas based on geochemical and isotopic constraints. They also provide an evaluation of chemical reactions in the groundwater system, the evolution of groundwater as it moves along a flowpath, and groundwater-mixing relationships. The appendices also examine groundwater residence times based on ^{14}C ages. Appendix A evaluates water/rock interactions to provide a basis for ^{14}C age corrections. Appendix B presents a comparison of ^{14}C ages based on organic and inorganic carbon ages. The appendices provide a comparison of patterns of groundwater movement outlined by the SZ flow model with flow patterns inferred strictly from hydrochemical and isotopic data. In this way, the combined analyses documented in the appendices serve as an independent corroboration of the SZ site-scale flow model.

6.3.1.1 Groundwater Flow

As described by Luckey et al. (1996 [DIRS 100465], p. 17), the Tertiary volcanic section at Yucca Mountain consists of a series of ash flow and bedded ash fall tuffs that contain minor amounts of lava and flow breccia. Individual ash flow tuffs may be several hundred meters thick, whereas bedded ash fall tuffs generally are less than a few tens of meters thick. Ash flow tuffs range from nonwelded to densely welded, and the degree of welding varies both horizontally and vertically in a single flow unit. Nonwelded ash flow tuffs, when unaltered, have moderate to low matrix permeability but high porosity. Permeability is decreased by secondary alteration, and fractures are infrequent and often closed in the low-strength nonwelded tuffs. Consequently, these rocks generally constitute laterally extensive SZ confining units in the Yucca Mountain area. The properties of partly welded tuffs vary between those of fractured, welded tuffs and those of altered, nonwelded tuffs. The densely welded tuffs generally have minimal primary porosity and water-storage capacity, but they can be highly fractured. Where interconnected, fractures can easily transmit water, and highly fractured units function as aquifers. In general, the bedded ash fall tuffs have high primary porosity and can store large amounts of water. Their matrix permeability is moderate to low, depending on the degree of alteration. North of Yucca Mountain, the Claim Canyon caldera has altered the geologic units in the region yielding changes in their hydrogeologic properties. The bedded ash fall tuffs generally function as confining units, at least when compared to less porous but densely fractured ash flow tuffs. Lavas, flow breccias, and other minor rock types are neither thick nor widely distributed in the Yucca Mountain area. Their hydraulic properties probably are as variable as the properties of the ash flow tuffs, but the relatively limited spatial distribution of

these minor rock types makes them generally unimportant to the hydrogeology of Yucca Mountain.

Luckey et al. (1996 [DIRS 100465], p. 17) state that even fractured tuffs and lavas may not easily transmit water because lithostatic loading keeps the fractures closed. In addition, where volcanic glass has been partly replaced by zeolites and clays, particularly in the originally glassy nonwelded tuffs, these secondary minerals substantially decrease permeability and slow groundwater flow through the rock. The degree of alteration can affect the water-transmitting characteristics of the volcanic sequence. Alteration, particularly in the Calico Hills Formation, increases toward the north of Yucca Mountain and probably accounts for the apparent decrease in hydraulic conductivity to the north. Alteration also tends to increase with depth and is pervasive below the Calico Hills Formation.

Fractures vary in length, orientation, connectivity, aperture width, and amounts and types of coatings, all of which may affect flow. The physical parameters of fractures are characterized by outcrop mapping, borehole logging, and mapping in the Exploratory Studies Facility. In the UZ, water seeps were not observed during outcrop mapping or during mapping in the Exploratory Studies Facility.

Fractures at Yucca Mountain originated as a result of initial cooling of the volcanic deposits and later as a result of tectonic activity. For example, in the Tiva Canyon welded hydrologic unit, two sets of vertically-oriented cooling fractures were observed dipping nearly vertically and striking toward the northwest and northeast. A third set of tectonic joints commonly abuts the cooling joints, and these three sets of joints form an orthogonal, three-dimensional network. An extensive discussion of fractures in the Yucca Mountain area is presented in *Yucca Mountain Site Description* (BSC 2004 [DIRS 169734], Section 3.5).

Fracture aperture characteristics are poorly known from direct observation, and for modeling, reliance is placed on indirect effects such as changes in permeability. In general, the stress due to overburden loading across high-angle fractures will be less than across low-angle fractures, resulting in higher vertical than horizontal permeability. Stratification effects will also be present in many units. This will tend to have the opposite effect; that is, the horizontal permeability will be larger than the vertical permeability.

The volcanic rocks consist of alternating layers of welded and nonwelded ash flow and ash fall (bedded) tuff deposits. Each of the ash flow units is underlain by an associated bedded tuff layer. The ash flow units vary in degree of welding (or recrystallization). Maximum welding is generally found near the center of the ash flow, where heat was retained the longest, and the degree of welding decreases upward and downward toward the ash flow boundaries.

The welded units typically have low matrix porosities and high fracture densities, whereas the nonwelded and ash fall units have relatively higher matrix porosities and lower fracture densities. The fracture density correlates to the degree of welding of the volcanic rocks.

Where glassy tuff has been saturated for long periods (e.g., beneath the water table), the original glassy material generally has been altered to zeolite or clay minerals. Such alteration does not affect porosity greatly because pore spaces are not filled, but the permeability of the rocks is

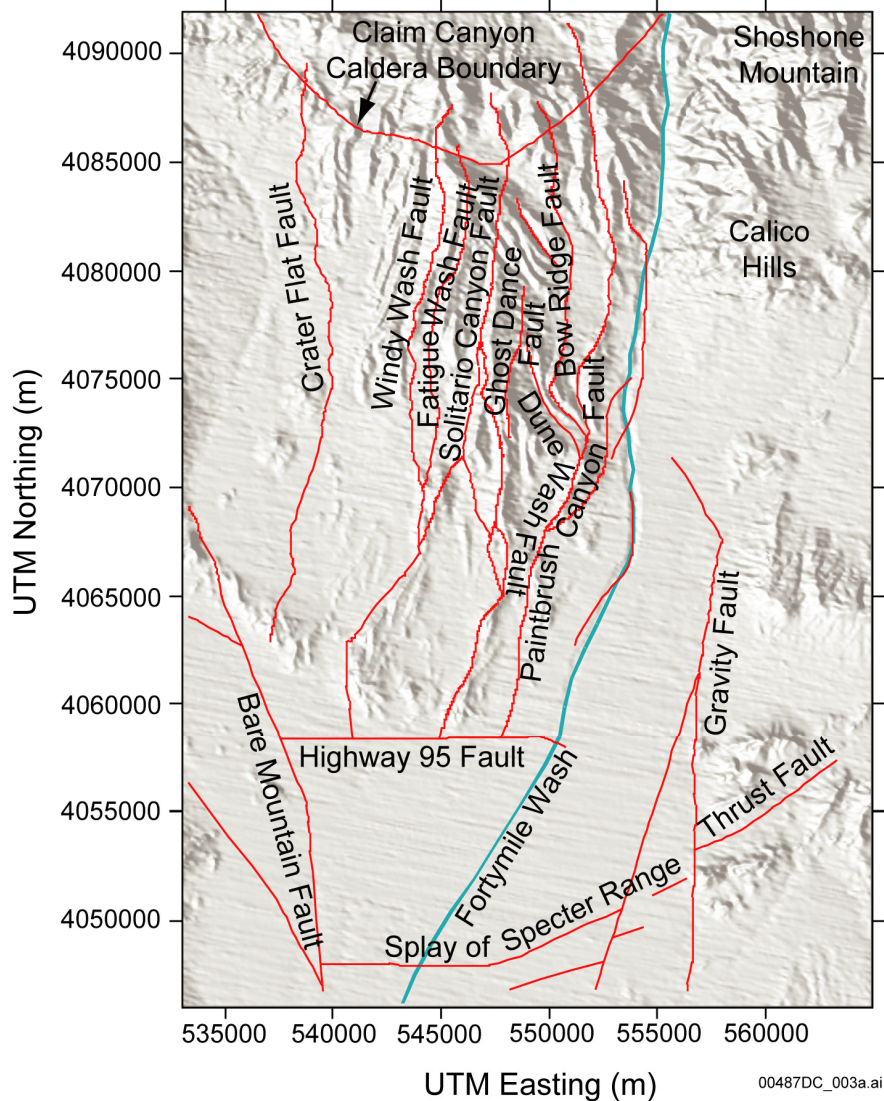
greatly reduced by alteration of the connectivity between the pore spaces. Alteration of silica to zeolites or clay minerals is not an important factor in densely welded zones because cooling fractures dominate permeability.

The SZ flow system to the south of Yucca Mountain transitions from a fractured tuff aquifer to a valley-fill (alluvium) aquifer before reaching the approximately 18-km performance compliance boundary at the southern boundary of the Nevada Test Site (NTS). Underlying Crater Flat is a thick sequence of alluvium, lavas, and tuffs that have been locally cut by faults and volcanic dikes. East of Yucca Mountain, and separated from it by Fortymile Wash, is Jackass Flats, which is underlain by a thick sequence of alluvium and volcanic rocks. Characterization of the valley-fill system was conducted just outside the southwest corner of NTS at the Alluvial Testing Complex (ATC), which is the site of Nye County Early Warning Drilling Program (NC-EWDP) well NC-EWDP-19D, and at NC-EWDP-22S, which is about 4.5 km north–northeast of the ATC. Single- and cross-well tracer tests were conducted in these wells and tests indicated producing zones with permeabilities consistent with other alluvial systems (3 to 20×10^{-12} m²) interbedded with lower permeability (0.1×10^{-12} m²) clay-rich zones (SNL 2007 [DIRS 177394], Sections 6.4.5 and F7). In addition to flow in the volcanic rocks and alluvium in the SZ, a significant portion of the groundwater flows through the lower carbonate aquifer.

In general, it is believed that the matrix porosity of the ancient marine limestones and dolomites of the lower carbonate aquifer is negligible (Winograd and Thordarson 1975 [DIRS 101167], p. C14), and that the large discharge from that aquifer system at Ash Meadows is due to flow through solution-enlarged fractures and along faults (Dudley and Larson 1976 [DIRS 103415], pp. 5 and 9). Borehole UE-25 p#1 penetrates the lower carbonate aquifer near Yucca Mountain. Another deep well, NC-EWDP-2DB was completed in the carbonate aquifer as part of the NC-EWDP. These deep wells helped improve the understanding of hydrologic conditions in the aquifers, including the deep carbonate aquifer, and helped to confirm the direction and magnitude of groundwater flow in that aquifer. Significant upward gradients were observed in wells UE-25 p#1 and NC-EWDP-2DB (BSC 2004 [DIRS 170009], Table 6-4).

6.3.1.2 Hydrologic Features

HFM2006 represents the distribution of geologic units within the SZ site-scale flow model (SNL 2007 [DIRS 174109], Section 6.4). Faults and other hydrogeologic features (Figure 6-3) such as zones of alteration that affect SZ flow were also included. Locations of faults come from fault trace maps that are derived from data collected during borehole drilling as well as locations where the faults intersect the land surface. Faults in the model area dip at various angles, but most are high-angle faults. Faults believed important to flow near Yucca Mountain are modeled explicitly. Given the large uncertainties in their orientations, faults were simply treated as vertical features. Section 6.4.3.1 discusses how these features were constructed in the HFM. Figure 6-3 illustrates many observed faults in the Yucca Mountain region, but not all of these were explicitly included in the model.



Source: DTN: GS010908314221.001 [DIRS 162874] (faults).

NOTE: The geographic coordinates of the different geologic features are the result of interpretation of the geologic map, including geologic cross sections, and lithostratigraphic and structural data from boreholes as described in *Hydrogeologic Framework Model for the Saturated Zone Site Scale Flow and Transport Model* (SNL 2007 [DIRS 174109]). The conversion of the geographic coordinates was done using standard Geographic System Information (GIS) functions. Here, the location of the U.S. Highway 95 Fault was modified based on a subsequent USGS interpretation (DTN: GS010908314221.001 [DIRS 162874]).

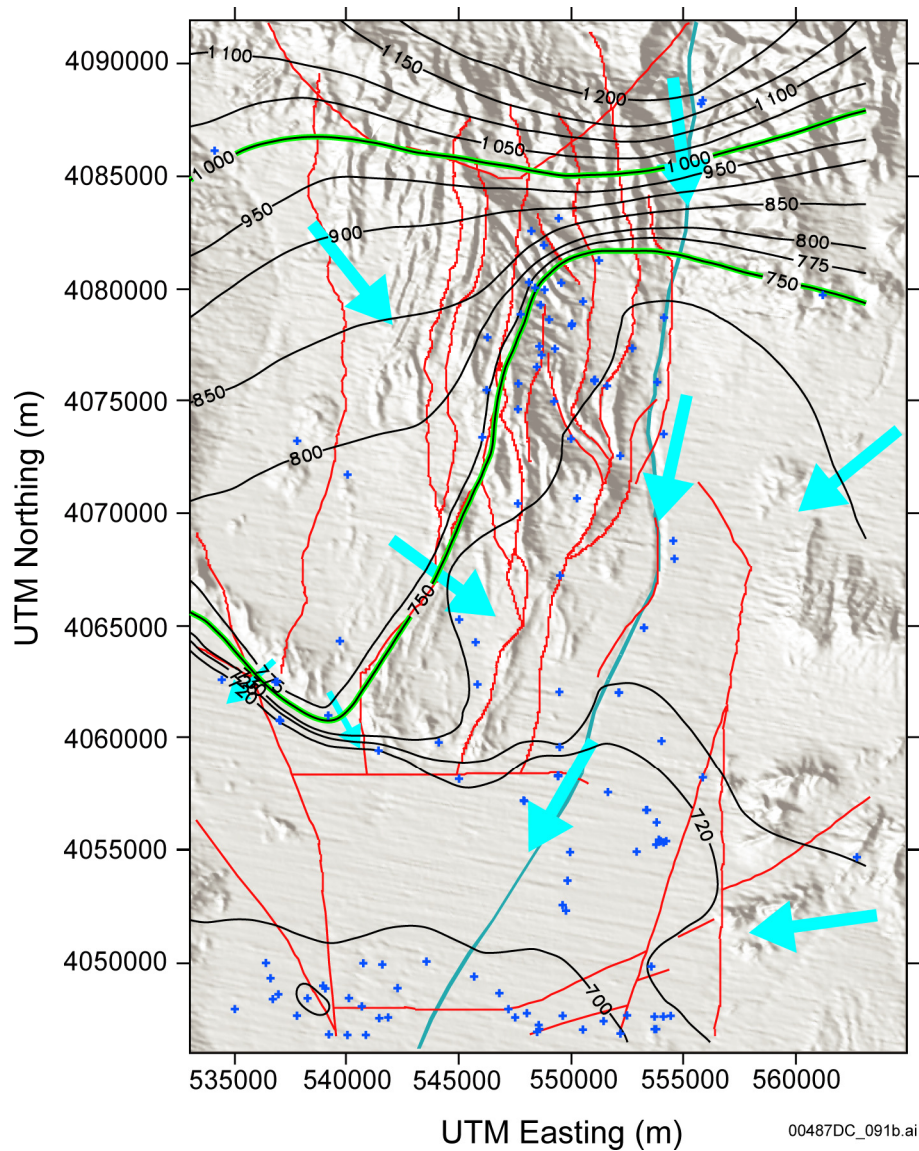
UTM = Universal Transverse Mercator.

Figure 6-3. Location of Faults in the Yucca Mountain Region

6.3.1.3 Flow Field

Using the potentiometric surface map (Figure 6-4 and Appendix E) the general direction of groundwater flow within the SZ site-scale flow and transport model domain for the horizontally isotropic case is from north to south. That is, the direction of flow is generally perpendicular to the water-level contours (anisotropic media may have flowpaths in directions non-orthogonal to the water-level contours). Based on the interpretation of the water-level data, the water table

exhibits a steep gradient throughout the northern part of the model area (north of the repository) and the contours curve southward to the west of Crater Flat (see Appendix E).



Source: DTN: GS010908314221.001 [DIRS 162874] (Faults)

Output DTN: MO0611SCALEFLW.000 (Water-level contours from Appendix E).

NOTE: The inferred groundwater flow directions are based on Assumption 1 in Appendix A (see Table A5-1). The red lines are selected faults; blue crosses indicated the location of hydraulic head measurements. The potentiometric surface is in black and inferred flow directions are indicated with blue arrows.

UTM = Universal Transverse Mercator.

Figure 6-4. Potentiometric Surface and Inferred Flow Directions

Several faults are interpreted as barriers to groundwater flow based on field data near the Solitario Canyon Fault, west of the repository, which demonstrates a differential of about 45 m (148 ft) in the potentiometric surface (Figure 6-4). In Crater Flat and on the southern part of

Yucca Mountain, flow is directed nearly easterly toward Fortymile Wash. A more-detailed water-level map of the immediate vicinity of Yucca Mountain (Figure 6-2) indicates that flows from the west and east converge at Fortymile Wash and turn southward toward the Amargosa Desert. The cause of the easterly gradient in Crater Flat and southern Yucca Mountain may be the U.S. Highway 95 Fault that acts as a groundwater barrier near the northern margin of the Amargosa Desert. Figure 6-2 is a water-level map using 1993 data, but newer data do not contradict any part of this discussion (see derivation of the potentiometric surface in Appendix E).

As discussed in Section 6.3.2.5, the potentiometric level in well UE-25 p#1, which penetrates the lower carbonate aquifer, is about 752 m (2,467 ft), 21 m (69 ft) higher than in nearby wells. This result indicates a potential for upward flow from the lower carbonate aquifer; however, other lines of evidence suggest that such flow is small. The direction of flow and hydraulic gradient cannot be determined from a single well; however, regional relationships suggest that the general direction of flow in the lower carbonate aquifer should be southerly to southeasterly in the SZ site-scale flow model domain (NRC 1998 [DIRS 107770], p. 109). South of the model domain, there is geochemical evidence for a westward component of flow in the carbonate aquifer (Appendix B, Figure B6-15).

Most monitoring wells in the Yucca Mountain area show little variation in water level over time (Luckey et al. 1996 [DIRS 100465], p. 29). In contrast, water levels in the heavily pumped Amargosa Farms area have declined substantially since intensive irrigation development began in the 1950s. Kilroy (1991 [DIRS 103010], p. 18) reported a water level decline of as much as 9 m (30 ft) by 1987, and La Camera and Locke (1997 [DIRS 103011], Figure 4) show an additional decline of about 3.4 m (11 ft) through 1996 at well AD-5, about 14 km (8.7 mi) southwest of the Amargosa Valley.

6.3.1.4 Large, Moderate, and Small Hydraulic Gradients

Three regions of distinct hydraulic gradients of the potentiometric surface at Yucca Mountain (Figure 6-4) are recognized: (1) a large hydraulic gradient (LHG) of 0.13 between water-level altitudes of 1,030 m (3,380 ft) and 750 m (2,460 ft) to the north of Yucca Mountain, (2) a moderate hydraulic gradient of 0.05 west of the crest of Yucca Mountain, and (3) a small hydraulic gradient of 0.0001 to 0.0003 extending from the Solitario Canyon Fault to Fortymile Wash. These gradients are evident on detailed potentiometric surface maps presented by Ervin et al. (1994 [DIRS 100633]), Tucci and Burkhardt (1995 [DIRS 101060]), as well as on the maps with large contour intervals compiled by D'Agnese et al. (1997 [DIRS 100131]). The large contour-interval maps do not portray the small or moderate gradients adequately because of limitations imposed by contour intervals; however, the large gradient is recognizable on all of these maps.

Luckey et al. (1996 [DIRS 100465]) present detailed descriptions of these gradient features and discuss interpretations of their causes. The LHG has been the subject of numerous theories and could be the result of the Claim Canyon caldera and its associated alteration of hydrogeologic properties. Permeability changes in similar environments have been studied by economic geologists (Norton and Knapp 1977 [DIRS 147379]). The LHG is discussed by Luckey et al. (1996 [DIRS 100465], pp. 21 to 25) and their theories regarding its genesis are summarized here:

- The gradient is the result of flow through the upper volcanic confining unit, which is nearly 298-m (984-ft) thick near the large gradient. This large thickness of low-permeability material creates a barrier to flow that causes water to back up behind it, increasing hydraulic head to the north, and leading to the large gradient.
- The gradient represents a semi-perched system where flow in the upper and lower aquifers is predominantly horizontal, while flow in the upper confining unit would be predominantly vertical. In this scenario, the large hydraulic gradient is a manifestation of water leaking out of the upper aquifer, through the confining unit, and into the lower aquifer. Farther south, water has drained out of the perched aquifer and now only the lower heads of the deeper aquifer are measured. The difference in heads between the northern-perched water levels and the southern deeper aquifer levels is manifested as a large gradient.
- The gradient represents a drain down a buried fault from the volcanic aquifers to the lower carbonate aquifer. In this case water levels drop quickly as the feature is approached from the north much in the same way water levels drop into the cone of depression caused by a pumping well. In this case, the feature is linear; the result is a region of steep hydraulic gradient rather than a cone of depression around a single well.
- The gradient represents a spillway in which a fault marks the effective northern limit of the lower volcanic aquifer. In this scenario, water flows more readily in the lower volcanic aquifer, which is located south of the LHG. This effectively “drains off” the high hydraulic heads and establishes a lower water level. North of this location, the lower permeabilities create a barrier to flow that maintains high water levels.
- The large gradient results from the presence at depth of the Eleana formation, a part of the Paleozoic upper confining unit, which overlies the lower carbonate aquifer in much of the Death Valley region. The Eleana formation is absent at borehole UE-25 p#1 at Yucca Mountain, which penetrated the lower carbonate aquifer directly beneath the lower volcanic confining unit.

It is important to accurately represent the LHG in the numerical model and to understand how it affects estimates of groundwater specific discharge and flowpaths from below the repository. To model the LHG, the concept of a hydrogeologically altered portion of the model domain representing the Claim Canyon caldera complex is introduced (see Section 6.3.1.11). It is explicitly included in the SZ site-scale model construction as a zone of altered (decreased) permeability. Because the LHG occurs north of Yucca Mountain, changes in the model’s simulated pathlines from the repository due to the LHG conceptualization (so long as it is represented in some form) are minimal as long as the gradients downstream of Yucca Mountain are modeled accurately.

The cause of the moderate hydraulic gradient is better understood than that of the LHG, and Luckey et al. (1996 [DIRS 100465], p. 25) suggest that the Solitario Canyon Fault and its splays function as a barrier to flow from west to east due to the presence of low-permeability fault gouge or to the juxtaposition of more permeable units against less permeable units.

The small hydraulic gradient occupies most of the repository area and the downgradient area eastward to Fortymile Wash. Over a distance of 6 km (3.7 mi) between the crest of Yucca Mountain and Fortymile Wash, the hydraulic head declines only about 2.5 m (8.2 ft). The small gradient could indicate highly transmissive rocks, little groundwater flow in this area, or a combination of both (Luckey et al. 1996 [DIRS 100465], p. 27).

The potentiometric map (Appendix E), which includes head data from the recently drilled NC-EWDP boreholes, indicates that the small hydraulic gradient extends southward to U.S. Highway 95.

6.3.1.5 Vertical Gradients

Information on vertical hydraulic gradients in the SZ is available from NC-EWDP wells (BSC 2004 [DIRS 170009]) and from *Ground-Water Conditions in Amargosa Desert, Nevada-California, 1952-87* (Kilroy 1991 [DIRS 103010]) for wells in the Amargosa Desert. The following discussion of vertical gradients is based on the work by Luckey et al. (1996 [DIRS 100465], pp. 27 to 29) and *Water-Level Data Analysis for the Saturated Zone Site-Scale Flow and Transport Model* (BSC 2004 [DIRS 170009], Sections 6.3.2 and 7.1.1).

Water-Level Data Analysis for the Saturated Zone Site-Scale Flow and Transport Model (BSC 2004 [DIRS 170009], Section 6.3.2) reports on potentiometric level measurements in multiple depth intervals in 17 boreholes at Yucca Mountain. Differences in potentiometric levels at different depth intervals in the same borehole ranged from as little as 0.10 m (0.33 ft) in borehole USW H-4 to as much as 54.7 m (179.5 ft) in USW H-1 (BSC 2004 [DIRS 170009], Table 6-4). Downward gradients were also observed with a maximum head difference of -38 m (125 ft) at NC-EWDP-1DX. Aside from well NC-EWDP-1DX located along U.S. Highway 95 south of Crater Flat, the largest head differences were between the lower carbonate aquifer or the adjoining lowermost lower volcanic confining unit and the overlying lower volcanic aquifer. Between the upper part of the lower volcanic confining unit and the lower volcanic aquifer the differences in potentiometric levels generally were 1 m (3 ft) or less.

Some potentiometric levels were higher in the lower intervals of the volcanic rocks than in the upper intervals, indicating a potential for upward groundwater movement. Of 17 wells with the ability to measure a vertical gradient, six showed a significant (> 5 m [16.4 ft]) upward gradient (USW H-1, USW H-3, UE-25 p#1, NC-EWDP-2D/-2DB, NC-EWDP-4PA/-4PB, and NC-EWDP-19P/-19D), six showed essentially no (< 2 m [6.6 ft]) head differences between uppermost and lowermost monitored intervals (USW H-4, USW H-5, USW H-6, UE-25 c#3, NC-EWDP-9SX, and NC-EWDP-12PA/-12PB/-12PC), and five showed a downward gradient (UE-25 b#1, USW G-4, UE-25 J-13, NC-EWDP-1DX, NC-EWDP-3S/3D). Overall, it appears that there is a notable upward vertical gradient between the lower and upper volcanic aquifer at locations nearest Yucca Mountain (USW H-1, USW H-3, and UE-25 p#1). Away from Yucca Mountain the direction of the vertical hydraulic gradient varies from location to location. For example, at locations UE-25 J-13, NC-EWDP-1DX, and NC-EWDP-3S, there is a downward gradient in the upper portion of the volcanic units. For wells in the lower Fortymile Wash, such as NC-EWDP-2D/2DB, NC-EWDP-4PA/-4PB, NC-EWDP-9SX (probes 1 and 2), NC-EWDP-12PA/-12PB, and NC-EWDP-19P/-19D, the gradients are slightly to moderately upward.

Potentiometric levels in the Paleozoic carbonate aquifer in borehole UE-25 p#1 are about 752 m (2,467 ft), or about 21.4 m (70.2 ft) higher than levels in the overlying lower volcanic aquifer. The potentiometric levels in the Paleozoic carbonate aquifer in borehole NC-EWDP-2DB is about 7.2 m (23.6 ft) higher than the overlying volcanic unit at NC-EWDP-2D. These data indicate a potential for upward groundwater movement from the Paleozoic rocks to the volcanic rocks. Because of the large difference in potentiometric levels in these two aquifers, they seem to be hydraulically separated (Luckey et al. 1996 [DIRS 100465], p. 28). Testing at the C-wells complex in 1984 suggested a hydraulic connection between the lower volcanic aquifer and the carbonate aquifer; however, testing in 1995 and 1996, using more-reliable water-level measurement equipment did not confirm the hydraulic connection (Luckey et al. 1996 [DIRS 100465], p. 28).

In borehole UE-25 p#1, the lowermost 70 m (230 ft) of the older tuffs (lower volcanic confining unit) had potentiometric levels similar to those in the carbonate aquifer, indicating a hydraulic connection between the lowermost part of the lower volcanic confining unit and the carbonate aquifer. Such a connection could be expected in the hanging-wall rocks adjacent to a fault; and, this type of connection is supported by calcification of the basal tuffs in the borehole. The remaining 237 m (778 ft) of the lower volcanic confining unit had a potentiometric level similar to that of the lower volcanic aquifer (Luckey et al. 1996 [DIRS 100465], p. 28). The upward hydraulic gradient observed in wells NC-EWDP-2D/-2DB supports the conceptual model that water levels in the carbonate aquifer are higher than in the overlying volcanic units in portions of the SZ site-scale flow model domain (BSC 2004 [DIRS 170009], Section 7.1.1).

No obvious spatial patterns in the distribution of vertical hydraulic gradients around Yucca Mountain are apparent; however, some generalizations can be made as to the distribution of potentiometric levels in the lower sections of the volcanic rocks. Potentiometric levels in the lower volcanic confining unit are relatively high (altitude greater than 750 m [2,477 ft]) in the western and northern parts of Yucca Mountain and are relatively low (altitude about 730 m [2,411 ft]) in the eastern part of Yucca Mountain. Based on potentiometric levels that were measured in borehole UE-25 p#1 and NC-EWDP-2D/-2DB, the potentiometric levels in the lower volcanic confining unit in boreholes USW H-1, USW H-3, USW H-5 and USW H-6 may reflect the potentiometric level in the carbonate aquifer. Boreholes UE-25 b#1 and USW G-4 do not seem to fit the pattern established by the other boreholes. These two boreholes penetrated only 31 m (102 ft) and 64 m (210 ft), respectively, into the lower volcanic confining unit and had potentiometric levels (about 730 m [2,395 ft]) that were similar to potentiometric levels in the lower volcanic aquifer. Penetration of the other four boreholes into the lower volcanic confining unit ranged from 123 m (403 ft) in borehole USW H-3 to 726 m (2,382 ft) in borehole USW H-1. In boreholes USW H-1, USW H-3, USW H-5, and USW H-6, the potentiometric levels in the lower volcanic confining unit are influenced by the potentiometric level in the carbonate aquifer (Luckey et al. 1996 [DIRS 100465], p. 29). *Water-Level Data Analysis for the Saturated Zone Site-Scale Flow and Transport Model* (BSC 2004 [DIRS 170009], Section 6.3.2) notes that the water levels measured in USW UZ-14 and USW H-5 are somewhat anomalous and are likely due to features or processes not included in this flow model. Such interpretations are bases for limiting the impact of these data on model results by reducing their importance during calibration (see Section 6.5.1.2).

At several wells, including USW H-1 and USW H-6, small hydraulic gradient reversals at several depths are observed (BSC 2004 [DIRS 170009], Table 6-4). These small reversals may be explained by small-scale heterogeneities in the hydrostratigraphic units or measurement errors (BSC 2004 [DIRS 170009], Section 6.3.2). The confidence in the vertical hydraulic head differences is greatest for the locations with the largest hydraulic head differences.

Vertical hydraulic gradients could have an important impact on the analysis of the effectiveness of the SZ as a barrier to radionuclide transport in that they keep the flowpath from the repository in the shallow groundwater. Based on available data, a spatially extensive upward gradient can be inferred between the carbonate aquifer and the volcanic aquifers, which indicates that, at least for the immediate Yucca Mountain area, radionuclide transport would be restricted to the volcanic system (BSC 2004 [DIRS 170009], Section 7.1.1). Insufficient data are available to specify an upward gradient in the constant-head boundaries.

Kilroy (1991 [DIRS 103010], pp. 11 to 16, Table 3) presents vertical gradient data for 21 nested piezometers, one well cluster, and one river and well pair in the Amargosa Desert area. However, none of these locations is within the area of the SZ site-scale model domain. Upward gradients generally were associated with freshwater limestones, carbonate rock outcrops, and structural features (Kilroy 1991 [DIRS 103010], p. 16). The association with carbonate rocks is attributed to a hydraulic connection with the carbonate aquifer regional flow system and, especially, to the Spotted Range-Mine Mountain fault zone, which is a conduit for flow from the carbonate aquifer to the basin fill.

6.3.1.6 Lateral Boundary Conditions

The constant head boundary conditions used in the SZ site-scale flow model are derived from hydraulic heads extracted from the potentiometric surface (Appendix E). The data are used to form fixed-head boundary conditions on the lateral sides of the model that may vary horizontally along the boundaries, but not in the vertical direction. Constant vertical head yields no vertical flows at the boundaries. These boundary conditions contrast with the observed upward gradient in the area near well UE-25 p#1, which is near the center of the model domain. Nevertheless, upward gradients can be obtained away from the boundaries despite the applied boundary conditions. This is because permeability differences between the hydrogeologic units propagate the high head in the north of the model through the higher permeability carbonate rocks farther into the model interior than the lower permeability volcanic confining unit overlaying the carbonate rocks. Furthermore, conceptually, the high heads in the northern thermally altered region may propagate increased pressures through the regional lower carbonate aquifer that subsequently provides an upward gradient in the southern, low-head portion of the model domain overlain by confining volcanic units. Overall, there are insufficient data (see Section 6.3.2.5) to specify a vertical gradient in constant head boundary conditions (only six of the 17 wells with vertical gradient measurements showed a significant upward gradient).

Of special note is the southern boundary of the model, which is near a large number of wells in the Amargosa Valley. Near the southern boundary, numerous measurements have been taken over the last 100 years. Some of the earlier measurements represent predevelopment states, while later measurements reflect changes in water levels due to pumping. The boundary conditions represent water levels affected by pumping and are described by *Recharge and*

Lateral Groundwater Flow Boundary Conditions for the Saturated Zone Site-Scale Flow and Transport Model (BSC 2004 [DIRS 170015], Sections 6.5 and 6.7).

Most of the inflows to, and outflows from, the SZ site-scale flow model occur as groundwater flows across the lateral boundaries. The best estimates of flow rates are the cell-by-cell fluxes calculated by the 2004 DVRFS (Belcher 2004 [DIRS 173179]; see also Appendix C). Fluxes from the steady-state stress period were used during the calibration of the SZ site-scale flow model as targets. These fluxes provide some consistency with the regional-scale flow model, which is based on a regional mass balance and calibrated to spring flow data. There are differences between the regional- and site-scale flow models due to notable differences in their conceptual models including the use of different grid resolutions and methods to simulate flow. Thus, it was necessary to average the fluxes over many grid blocks on each side of the model. Output from the regional flow model is linked to the SZ site-scale flow model during calibration. Volumetric/mass flow rates derived from the regional flow model are provided as calibration targets during SZ site-scale flow model calibration in much the same way that water levels are used for targets. Data from the regional model are qualified for use in this report (Appendix C). Because of the differences in the two models, only general agreement on volumetric/mass flow rates between the two models is expected, and obtained.

Consistent with the regional flow model, the bottom boundary condition of the SZ site-scale flow model has zero-flux specified. Direct evapotranspiration from the water table is not considered in this analysis because depth to water is too great for this process to be important. The top boundary condition was a specified flux recharge map described in Section 6.3.1.7, portions of which are derived from the regional model, the UZ model, and streamflow studies along Fortymile Wash. Because the flow model is a steady-state model, there are no boundary condition temporal variation requirements.

6.3.1.7 Recharge

The recharge to the flow model was derived from three sources: regional-scale SZ model (Belcher 2004 [DIRS 173179]), the 2003 UZ flow model (BSC 2004 [DIRS 169861]), and Fortymile Wash data (Savard 1998 [DIRS 102213]), see Section 6.4.3.9. Recharge from the UZ site-scale model (percolation flux) was taken as the flow through the base of that model, the domain of which includes approximately 40 km² (19.3 mi²) that defines the footprint of Yucca Mountain, but is only a small fraction of the SZ model domain. The UZ flow model uses dual permeability, and accordingly, the output includes volumetric/mass flow rates for fracture and matrix flow. These data are combined into a total volumetric flow rate and an average percolation flux (BSC 2004 [DIRS 170015], Table 6-4 and Figure 6-4).

The technique for estimating recharge from all three sources is detailed in *Recharge and Lateral Groundwater Flow Boundary Conditions for the Saturated Zone Site-Scale Flow and Transport Model* (BSC 2004 [DIRS 170015], Figure 6-8 and Section 6.2.4), but is summarized here:

- The distributed vertical recharge, primarily in the northernmost portion of the SZ site-scale flow model domain, was extracted from the 2004 SZ regional-scale flow model (DTN: MO0602SPAMODAR.000 [DIRS 177371]). No recharge within the UZ

flow model area was included from the regional flow model because this was accounted for separately as percolation through the unsaturated zone by the UZ model (see below).

- The recharge through each node of the UZ flow model is extracted and the corresponding recharge to the SZ site-scale flow model node was calculated (the UZ flow model grid is finer than the SZ site-scale grid).
- Estimates of recharge from the infiltration of surface flows in Fortymile Wash are given by linear reaches (discrete segments) along the wash. Recharge estimates were interpolated to at least a 500-m (1,640-ft) -wide recharge zone for most of the wash and a broader area of distributary channels in the Amargosa Desert (BSC 2004 [DIRS 170015], Table 6-3, Figure 6-6).

6.3.1.8 Discharge

There is no measurable natural discharge (i.e., springs or evapotranspiration within the SZ site-scale flow model domain); therefore, natural discharge to the surface is not considered.

6.3.1.9 Heterogeneity

Physical and chemical heterogeneity of the rocks and water in the SZ can affect groundwater flow and the transport of contaminants in the SZ. The principal forms of heterogeneity in the SZ site-scale model domain are physical and may be primary (i.e., related to the formation of the rocks) or secondary (i.e., related to events subsequent to their formation).

The most obvious form of primary heterogeneity is the mode of origin (i.e., volcanic rocks, clastic rocks, carbonate rocks, and alluvial deposits), which is the primary basis for subdividing the rocks into hydrogeologic units. Within each major category, further subdivisions are possible. Probably the major form of primary heterogeneity affecting groundwater flow in the SZ site-scale model domain results from the origin of the volcanic rocks (i.e., ash flow or air fall pyroclastic deposits, lava flows, and volcanic breccias). The pyroclastic rocks (termed tuffs) are primarily nonwelded to densely welded, vitric to devitrified ash flow deposits separated by nonwelded vitric air fall deposits. Thus, primary physical heterogeneity relates to whether the deposits resulted from massive eruptions of hot volcanic ash from volcanic centers that moved downslope, or whether they resulted from explosive eruptions that injected volcanic fragments into the air to fall out as bedded ash fall tuffs.

The thicker flow deposits, up to several hundred meters thick, were very hot, resulting in welding of the fragments into a dense mass. Thinner flows retained heat less effectively, resulting in partly welded to nonwelded ash flow tuffs. Ash fall tuffs, generally less than tens of meters thick, are cooled in the atmosphere and characteristically glassy (vitric) (Luckey et al. 1996 [DIRS 100465], p. 17).

The mode of origin controls the porosity and permeability of the volcanic rocks. The densely welded tuffs generally have minimal primary porosity and water-storage capacity, but commonly are highly fractured and function as aquifers (Luckey et al. 1996 [DIRS 100465], p. 17). Nonwelded ash flow tuffs, when unaltered, have moderate to low matrix permeability but high

porosity, and commonly constitute confining units. Ash fall tuffs have high primary porosity and moderate to low permeability, and they generally act as confining units.

As the tuff deposits cooled, they were subjected to secondary processes, including formation of cooling fractures, recrystallization or devitrification, and alteration of the initial glassy fragments to zeolite minerals and clay minerals, all of which affect the hydrologic properties of the rocks. Beginning with deposition and throughout their subsequent history, the rocks have been subjected to tectonic forces resulting in further fracturing and faulting. They also have been subject to changes in the position of the water table, which greatly affects the degree of alteration of the initially glassy deposits.

The forms of secondary heterogeneity most affecting the SZ are fracturing, faulting, and alteration of glassy materials to zeolites and clay minerals. Fractures, where interconnected, transmit water readily and account for the permeable character of the welded tuffs. Cooling fractures, which are pervasive in welded tuffs, tend to be strata-bound and confined to welded portions of flows, whereas tectonic fractures tend to cut through stratigraphic units, as do faults.

Nonwelded deposits are less subject to fracturing and more subject to alteration of the initial glassy deposits to zeolites and clay minerals, both of which reduce permeability. The presence of perched-water bodies in the UZ is attributed to the ubiquitous presence of a smectite-zeolite interval at the base of the Topopah Spring tuff, which, in the absence of through-going fractures, essentially stops the vertical movement of water (Luckey et al. 1996 [DIRS 100465], p. 46).

The heterogeneity in permeability of different types of deposits led to the subdivision of the Yucca Mountain geologic section into five basic SZ hydrologic units: upper volcanic aquifer, upper volcanic confining unit, lower volcanic aquifer, lower volcanic confining unit, and lower carbonate aquifer. To accommodate the more extensive area of the SZ flow model, HFM2006 (SNL 2007 [DIRS 174109], Table 6-5) includes 22 additional units above and below these basic five units. Near Yucca Mountain, volcanic deposits generally form laterally extensive stratigraphic units; however, due to physical heterogeneity, porosity and permeability are highly variable both laterally and vertically.

In the southern part of the SZ site-scale flow model domain, the volcanic deposits thin and inter-finger with valley fill deposits. The latter are heterogeneous (sand and gravel) because of their mode of deposition (Walker and Eakin 1963 [DIRS 103022], p. 14), but are not subject to the fracturing, faulting, and alteration types of heterogeneity that affect the volcanic rocks.

Within the SZ site-scale model area, little specific information is available on the lower carbonate aquifer. However, information from nearby areas (D'Agnese et al. 1997 [DIRS 100131], p. 90, Figures 46 and 47) suggests that the lower carbonate aquifer is minimally heterogeneous with reasonably high permeability attributed to pervasive solution-enlarged fractures.

Heterogeneity in material properties is a common characteristic of hydrogeologic units at the Yucca Mountain site and it exists at scales ranging from pore scale to regional scale. The larger-scale heterogeneity, at scales of kilometers to tens of kilometers, is effectively addressed via the different units within HFM2006, incorporation of specific hydrogeologic features

(e.g., faults and structural zones), and anisotropy. The pore scale heterogeneities are averaged via the concept of macroscopic parameters defined on the basis of a representative elementary volume (Freeze and Cherry 1979 [DIRS 101173], pp. 69 to 70). Groundwater flow equations use parameters defined on the basis of the representative elementary volume. For predominantly porous units such as bedded tuffs and alluvia, the size of the representative elementary volume may be on the order of a few cubic centimeters (de Marsily 1986 [DIRS 100439], p. 15). For fractured rocks (volcanics and carbonates), the size of the representative elementary volume is less well defined, but is typically related to the density of fracturing and is generally much larger than for granular material (Freeze and Cherry 1979 [DIRS 101173], p. 73). The 250-m grid spacing used for the flow model is sufficiently large to allow the use of representative-elementary-volume-defined parameters for groundwater flow. In fact, the grid spacing is large enough that subgrid scale heterogeneity needs to be considered with regard to radionuclide transport. Subgrid heterogeneity leads to enhanced dispersion with increasing scales of transport (de Marsily 1986 [DIRS 100439], pp. 247 to 248). Additionally, the uncertainty in the density of fracturing at the subgrid scale leads to uncertainty in the groundwater velocity and matrix diffusion. Flow modeling accounts for subgrid heterogeneity by defining scaled dispersivities and flowing interval spacing (BSC 2004 [DIRS 170014]) in the transport abstraction modeling (SNL 2007 [DIRS 177390], Section 6.5.2) as random variables characterized by probability density functions.

Heterogeneity at intermediate scales between the grid size of 250 m and the large-scale features of the HFM are addressed using uncertainty in the anisotropy of hydraulic conductivity. A primary concern related to intermediate scale heterogeneity is the possibility of a fast pathway (Freifeld et al. 2006 [DIRS 178611], Table 4) along a relatively continuous path. In the fractured volcanic aquifers beneath Yucca Mountain, the fast path, if it exists, is likely to be related to a fracture or structural feature. The hydraulic testing at the C-wells complex (SNL 2007 [DIRS 177394], Section 6.2) suggest that at a large scale (about 1 km²), hydraulic conductivity can be characterized as homogeneous, but anisotropic. The direction of anisotropy is primarily related to the dominant direction of fractures and faulting. The impact of possible fast paths at an intermediate scale of heterogeneity is incorporated in the transport simulations through probability distributions of specific discharge, horizontal anisotropy in permeability, and flowing interval spacing (SNL 2007 [DIRS 177390], Section 6.5.2). The aggregate uncertainty in these and other parameters related to radionuclide transport yield simulated SZ transport times for nonsorbing species on the order of 100 years in some Latin Hypercube Sampled realizations of the SZ system (SNL 2007 [DIRS 177390], Figure 6-28).

As noted previously, the properties of each hydrogeologic unit in the model are assumed uniform, but uncertain, with the value assigned during the calibration process. Nevertheless, heterogeneity of material properties at a variety of scales is included in the model via several different mechanisms. First, large-scale heterogeneity is defined by the distribution of units in HFM2006 and the discrete hydrogeologic features incorporated in the SZ site-scale flow model (Table 6-7). Subgrid heterogeneity is included in the transport simulations through the probability distributions for flowing interval spacing and dispersivity. Finally, intermediate scale heterogeneity, which is most likely to be reflected in possible fast paths at scales up to several kilometers, is included as uncertainty in anisotropy. Uncertainty in the HFM is discussed in Section 6.4.3.1.

6.3.1.10 Role of Faults

Faults and fault zones are hydrogeologic features that require special treatment in the SZ site-scale flow and transport models. Faulting and fracturing are pervasive at Yucca Mountain and they affect groundwater flow patterns because they may act as preferred conduits or barriers to groundwater flow. The role that faults play in facilitating or inhibiting groundwater flow depends on the nature of the fault (i.e., whether the faults are in tension, compression, or shear) and other factors such as the juxtaposition of varying geologic units along the fault plane, the rock types involved, fault zone materials, secondary mineralization, and depth below land surface.

Faunt (1997 [DIRS 100146]) investigated the effect of faulting on groundwater movement in the Death Valley region and developed a map of fault traces (Faunt 1997 [DIRS 100146], Figure 10) including diagrams (Faunt 1997 [DIRS 100146], Figure 11) showing the orientation of faults within the principal structural provinces of the region. Faunt (1997 [DIRS 100146], p. 38) grouped the faults into three categories depending on their orientations relative to the present-day stress field (i.e., those in relative tension, compression, or shear).

Faults in relative tension are more likely to be preferential conduits for groundwater, and faults in shear or compression are more likely to impede groundwater movements. Faults modeled to have the most evident effects on groundwater movement, such as effects on potentiometric contours, include the Solitario Canyon, U.S. Highway 95, Crater Flat, and Bare Mountain Faults (see Figure 6-4), all of which appear to act as barriers to groundwater flow. The following features are afforded special consideration in the SZ site-scale flow model: the Crater Flat Fault, the Solitario Canyon (with Windy Wash and Stage Coach splays), the U.S. Highway 95, the Bare Mountain, and Sever Wash Faults. In addition, zones are developed for the Fortymile Wash Structure and Lower Fortymile Wash alluvial regions that appear to act as conduits that focus flow. Other than the Fortymile Wash faults, these features are assigned anisotropic permeabilities that are 10 times more permeable in both directions parallel to the fault (x - z or y - z directions).

6.3.1.11 Altered Northern Region

The Claim Canyon caldera is an area of extensive alteration that seems to have resulted in a generalized reduction in permeability in many of the hydrogeologic units in this area (this area is hereinafter referred to as the altered northern region). The concept of the altered northern region allows different permeabilities to be assigned to the same geologic unit depending on whether or not a unit resides within the altered northern region (see Section 6.4.3.7). Deeper units (including the intrusive, crystalline, and lower clastic confining units and the lower carbonate aquifer) are excluded from this alteration because the caldera complex was not present during their genesis. Conceptually, this facilitates modeling of the LHG and it also makes intuitive sense because it is unlikely that permeabilities even within the same geologic unit would have identical values when they are separated by many kilometers (across the model domain from north to south). In the SZ site-scale model formulation, faults that fall within the altered northern region may have diminished impact on the model and could reasonably be removed from consideration here. A notable exception is Sever Wash Fault that retains a distinct permeability

from the underlying geologic units despite residing within the altered northern region. Sever Wash appears to be important in facilitating southeasterly flow near the repository area.

6.3.2 Groundwater Flow Processes

Simplifications used in modeling the groundwater flow process include those inherent to the SZ regional- and site-scale flow models (modeling assumptions), and those made in estimating parameters that are used as input to these models. The effective-continuum representation of fracture permeability is used because on the scale represented by the SZ site-scale flow model, the site is well represented by a continuum flow model. Aquifer hydraulic tests show evidence of fracture flow near Yucca Mountain (Geldon et al. 1997 [DIRS 100397]). Numerical modeling of fracture properties is done in one of three ways: discrete-fracture models, effective-continuum models, or dual-continuum models. Dual-continuum models are not needed because transient simulations are not performed. For steady-state SZ flow calculations, dual-continuum formulations are equivalent to single-continuum formulations. Discrete-fracture models represent each fracture as a distinct object within the modeling domain. Although a discrete-fracture model might reproduce the flow system more accurately, flow modeling is adequately conducted using a continuum model because:

- At Yucca Mountain, studies of the density and spacing of flowing intervals generally indicate that flow occurs through fracture zones (BSC 2004 [DIRS 170014], Figure 6-2). The fractures or fracture zones are located in various geological units, and in most cases, no single zone dominates groundwater flow. Geochemical studies (see Figure A6-62) independently confirm a south-southeasterly trace of the particle flowpath. For the limited set of wells examined by Luckey et al. (1996 [DIRS 100465], Figure 11), flow appears to be carried through fracture zones separated by a few tens of meters rather than through a few individual fractures.
- Significant portions of the geology comprise alluvial units through which flow and transport are appropriately modeled using a continuum model.
- The drawdown response to pumping at wells surrounding the C-wells complex in multi-well pump tests indicates a well-connected fracture network in the Miocene tuffaceous rocks in this area (Geldon et al. 1998 [DIRS 129721], p. 31).

The following assumptions also apply to the continuum modeling approach used in the SZ site-scale flow model:

- Estimates of discharge from the volcanic aquifer, developed from the SZ Expert Elicitation Panel (CRWMS M&O 1998 [DIRS 100353], p. 3-8) are applicable to the flowpath from below the repository to a distance of approximately 5-km down gradient in the volcanic units and were primarily based on data from hydraulic testing in wells in volcanic units and the hydraulic gradient inferred from water-level measurements. The relative values of groundwater flux in the volcanic aquifer and along the flowpath farther to the south are constrained by the calibration of the SZ site-scale flow model (reasonable extrema bound the calibration process).

- Horizontal anisotropy in permeability is adequately represented by a permeability tensor that is oriented in the north-south and east-west directions. In support of the TSPA-LA, horizontal anisotropy is considered for radionuclide transport in the SZ (SNL 2007 [DIRS 177394], Section 6.2.6). The numerical grid of the SZ site-scale flow model is aligned north-south and east-west, and values of permeability are specified in directions parallel to the grid. One analysis of the probable direction of horizontal anisotropy shows that the direction of maximum transmissivity is N 33°E (Winterle and La Femina 1999 [DIRS 129796], p. iii), indicating that the anisotropy applied on the SZ site-scale model grid is within approximately 30° of the inferred anisotropy. A detailed description of the horizontal anisotropy calculations is found in *Saturated Zone In-Situ Testing* (BSC 2006 [DIRS 177394], Appendix C6). Sensitivity analyses were performed to assess the impact of uncertainty in the anisotropy and are presented in *Saturated Zone Flow and Transport Model Abstraction* (SNL 2007 [DIRS 177390], Section 6.5.2.10).
- Horizontal anisotropy in permeability may apply to the fractured and faulted volcanic units of the SZ system along the groundwater flowpaths that run from the repository to points south and east of Yucca Mountain. The inferred flowpath from beneath the repository extends to the south and east. This is the area in which potential anisotropy could have an impact on radionuclide transport in the SZ. Given the conceptual basis for the anisotropy model, it is appropriate to apply anisotropy only to those hydrogeologic units that are dominated by groundwater flow in fractures. A more detailed discussion of anisotropy is provided in Section 6.4.3.11.
- Changes in the water-table elevation (due to future climate changes) will have negligible effect on the direction of the groundwater flow near Yucca Mountain although the magnitude of the groundwater flux will change. This supposition has been studied at regional (D'Agnese et al. 1999 [DIRS 120425]; Winterle 2003 [DIRS 178404]; Winterle 2005 [DIRS 178405]) and subregional scales (Czarnecki 1984 [DIRS 101043]). These studies found that the flow direction did not change significantly under increased recharge scenarios. The studies were based on confined aquifer models that did not take into account the free surface boundary at the water table or the saturation of geological units that currently are in the UZ overlying the present-day SZ. These UZ tuffs generally have a lower permeability than those in the SZ, and as such, UZ units that become saturated are not likely to yield faster fluxes in the SZ (BSC 2004 [DIRS 169861], Appendix A).
- Future water supply wells that might be drilled near Yucca Mountain (including outside the regulatory boundary) will have a negligible effect on the hydraulic gradient. Water levels at the southern boundary of the SZ site-scale flow and transport models (in the Amargosa Valley) currently reflect the effect of well pumpage (Luckey et al. 1996 [DIRS 100465], p. 41).
- In the analysis presented in this report, temperature is modeled to be proportional to the depth below the ground surface. Modeling a uniform temperature gradient with depth is equivalent to a model of uniform geothermal heat flux through a medium of homogeneous thermal conductivity. In addition, the temperature at the ground surface is held constant. Data indicate that the temperature gradients generally become more

linear with increasing depth below the water table. The goal of assigning temperature variations with depth in the SZ site-scale flow model is to account for resulting variations in fluid viscosity at different depths in the SZ.

- A confined-aquifer solution is used in the SZ site-scale flow model. The approach treats the upper boundary as if there is no UZ and, therefore, solves a simplified and more computationally efficient numerical model. In the numerical model, the top surface has boundary conditions of recharge flux (infiltration). The confined aquifer solution is enforced by assigning negative porosity to all nodes above the water table. This forces FEHM to model the system as fully saturated. If this procedure were not adopted, small variations in head around the water table would result in FEHM testing for an air phase, thus decreasing efficiency. The drawback of this approach is that the top surface of the numerical model corresponds to the measured water table and may be inconsistent with the model-derived water table. This discrepancy could affect flux through the model domain, but errors would be minimal because changes in the water-table elevation would be small in comparison to the saturated thickness of the model. Care was taken during the calibration process to model the small-head gradient area to the south and east of Yucca Mountain accurately. Specified-head boundary conditions on the lateral boundaries were set with no vertical gradient; however, it should be noted that the model allows for vertical flows that arise from recharge and heterogeneity. The numerical approach used is similar to the classical Dupuit-Forcheimer method (Bear 1979 [DIRS 105038]).

6.4 FORMULATION OF THE CONCEPTUAL MODEL

6.4.1 Mathematical Description of the Conceptual Model

An effective continuum approach is adopted for simulating groundwater flow through the fractured rock and alluvial materials within the domain of the SZ site-scale flow model. Based on this conceptualization, the equations governing groundwater flow can be derived by combining the equations describing the conservation of fluid mass and Darcy's Law. The equation for conservation of fluid mass (Bear 1972 [DIRS 156269], Equation 4.3.7) expressed in the notation given by (Tseng and Zyvoloski 2000 [DIRS 179068]) is:

$$\frac{\partial A_{mass}}{\partial t} + \bar{\nabla} \cdot \bar{f}_{mass} + q_{mass} = 0, \quad (\text{Eq. 6-1})$$

where $\bar{\nabla}$ is gradient operator, A_{mass} is the fluid mass per unit volume (kg/m^3) given by:

$$A_{mass} = \phi \rho_l, \quad (\text{Eq. 6-2})$$

\bar{f}_{mass} is the fluid mass flux vector ($\text{kg}/\text{m}^2/\text{s}$) given by:

$$\bar{f}_{mass} = \rho_l \bar{v}, \quad (\text{Eq. 6-3})$$

ϕ is the porosity in the system (dimensionless), ρ_l is the fluid density (kg/m^3), \bar{v} is the fluid velocity vector (m/s) (or, more specifically, areal flux or specific discharge (volume fluid/unit area/s), pore velocity is \bar{v}/ϕ), and q_{mass} is the fluid mass source ($\text{kg/m}^3/\text{s}$).

The velocity of the fluid can be expressed by the generalized Darcy's Law for an anisotropic medium (Bear 1972 [DIRS 156269], Equations 5.2.6 and 5.6.1) as:

$$\bar{v} = \frac{k}{\mu} \cdot (\bar{\nabla}P - \rho_l g \hat{z}), \quad (\text{Eq. 6-4})$$

where μ is the dynamic viscosity of the fluid (kg/m/s), P is the fluid pressure (Pa), k is the permeability tensor (m^2), g is the acceleration due to gravity (m/s^2), and \hat{z} is the unit vector in the direction of gravity (downward). In the case where flow is aligned in the direction of the principal axes of permeability (Bear 1972 [DIRS 156269], Equation 5.6.1), k may be expressed

$$\text{as } k = \begin{bmatrix} k_1 & 0 & 0 \\ 0 & k_2 & 0 \\ 0 & 0 & k_3 \end{bmatrix}.$$

Equations 6-1 and 6-4 can be combined to yield the fundamental equation describing groundwater flow (see Tseng and Zyvoloski 2000 [DIRS 179068], Equation 1 for isotropic case):

$$\frac{\partial A_{mass}}{\partial t} - \bar{\nabla} \cdot (\underline{D}_{mass} \bar{\nabla}P) + \frac{\partial(k_3 \rho_l^2 g / \mu)}{\partial z} + q_{mass} = 0 \quad (\text{Eq. 6-5})$$

where \underline{D}_{mass} is the hydraulic conductivity (m/s) tensor calculated as:

$$\underline{D}_{mass} = \frac{\rho_l}{\mu} k. \quad (\text{Eq. 6-6})$$

Groundwater flow is simulated in the SZ site-scale flow model by obtaining a numerical solution to this equation. Solution of this equation for pressure requires the specification of the pressure at the boundaries of the solution domain. For steady-state calculations, solution of this equation does not require specification of initial conditions (initial pressure distribution throughout the solution domain), because Equation 6-5 (at very large times for constant boundary conditions) represents steady-state flow, which is independent of initial conditions. Fluxes are determined using Equation 6-4 with pressure gradients obtained through "post-processing" of the pressure solution to Equation 6-5.

It is assumed that a steady-state model is sufficient to be used during calibration and also sufficient for the intended use of the SZ site-scale flow model. There are two potential causes of transient flow that are relevant to this assumption: (1) changes in climate over the past 15,000 years, and (2) pumping from wells within and south of the model domain during approximately the last 50 years. Use of the steady-state assumption requires that the modern-day flow system has had sufficient time to equilibrate to both of these perturbations to the natural system. It is noted that transient tests (C-wells and Alluvial Testing Complex) were performed

and that permeability values derived from those tests were considered in the validation of the numerical model. It is not expected that the model can reproduce the transient tests, largely due to the 250-m-gridblock sizes. Because transient pumping is not used in any Yucca Mountain radionuclide migration simulations and steady-state gradients are modeled accurately with the model, this does not invalidate the steady-state assumption. Climate change and other transient impacts are incorporated in the SZ flow and transport abstractions (SNL 2007 [DIRS 177390], Section 6.5). Furthermore, the effects of water table rise on flowpaths are investigated here in Section 6.6.4.

The conceptual model of the long-term groundwater flow in this region includes the hypothesis that recharge rates and, consequently, the elevation of the water table and groundwater flow rates, were larger during the last glacial pluvial period. The time required for the flow system to equilibrate to a more arid climate depends primarily on the hydraulic conductivity of the rocks and the amount of water that must be drained from storage to lower the water table.

It is likely that equilibration to the drier climate has occurred given: (1) the long time (thousands of years) since the climate change was completed, (2) the relatively small amount of water stored (small specific yield) in fractured volcanic rocks that make up much of the model domain near the water table, and (3) the relatively large hydraulic conductivity of the fractured volcanic rocks.

The time required for the flow field to arrive at steady-state with respect to pumping from wells is much shorter than the time required for equilibration to climate change. It depends primarily upon the time required for changes in water level to be transmitted through the SZ. Fast transmittal is expected in fractured volcanic rock because of their relatively large hydraulic conductivity and small specific storage. The fact that the modern-day flow system on the scale of this model domain has equilibrated to pumping is supported by the lack of consistent, large-magnitude variations in water levels observed in wells near Yucca Mountain (Luckey et al. 1996 [DIRS 100465], pp. 29 to 32). A transient response to pumping would be expected, instead, to result in a continued decrease in water levels. Overall, pumping rates are typically negligible compared to the total mass of fluid in the system, which is on the order of 10^{16} kg.

6.4.2 Computational Model

The FEHM V2.24 (STN: 10086-2.24-02; [DIRS 179539]) software code is used for SZ site-scale modeling to obtain a numerical solution to the mathematical equation describing groundwater flow, Equation (6-5). FEHM is a nonisothermal, multiphase flow and transport code that simulates the flow of water and air and the transport of heat and solutes in two- and three-dimensional saturated or partially saturated heterogeneous porous media. The code includes comprehensive reactive geochemistry and transport modules and a particle-tracking capability. Fractured media can be simulated using equivalent-continuum, discrete-fracture, dual-porosity, or dual-permeability approaches. A subset of the FEHM code capabilities was used in the SZ site-scale flow model because only a single-phase, isothermal flow model is solved.

Particle tracking is a numerical technique that simulates the transport of fluid “particles.” Particle-tracking techniques have a long history of use in similar applications (e.g., Pollock 1988

[DIRS 101466]; Tompson and Gelhar 1990 [DIRS 101490]; Wen and Gomez-Hernandez 1996 [DIRS 130510]). Particle tracks can be used to represent and estimate flowpaths.

The control-volume finite element (CVFE) method is used in FEHM to obtain a numerical solution to the groundwater flow equation over the model domain. Finite-element methods are based on the assumption that a continuum may be modeled as a series of discrete elements. For each element, equations based on a discretized form of the groundwater flow equation are written that describe the interaction of that element with its neighbors. These equations describe the hydrologic behavior of the elements. This discretization leads to a set of equations that must be solved numerically to estimate groundwater pressure at each node throughout the model domain.

The CVFE method has been used extensively in petroleum-reservoir engineering (Forsyth 1989 [DIRS 144110]). The CVFE method solves for the potentials using a finite-element technique while the control-volume aspect establishes local mass conservation and upstream weighting (Verma and Aziz 1997 [DIRS 143606]). Quadrilaterals and triangles in two dimensions and hexahedra and tetrahedra in three dimensions are divided into volumes associated with gridblocks and areas associated with interblock distances. Gridblock volumes are the Voronoi volumes (Forsyth 1989 [DIRS 144110]) associated with each gridblock. Voronoi volumes are also called perpendicular bisector volumes. A Voronoi volume is formed by boundaries that are orthogonal to the lines joining adjacent gridblocks and that intersect the midpoints of the lines (Verma and Aziz 1997 [DIRS 143606]). Any point within a Voronoi volume is closer to its associated gridblock than to any other node in the grid. Implementing the CVFE method on simple elements with constant properties is equivalent to the traditional finite-element method.

The stiffness coefficients (e.g., elements of the stiffness matrix) of the traditional finite-element method can be interpreted as linear functions of the area through which the fluid passes while traveling from one node to its neighbor. A stiffness coefficient uses the area of the boundary of the Voronoi volume that intersects the line joining adjacent nodes. LaGriT V1.0 (STN: 10212-1.1-00; [DIRS 173140]) produced this CVFE grid. These coefficients are used to form control-volume difference equations for the conservation equations. This method is not traditional because equation parameters are defined by node, not element, but this method leads to an intuitive understanding of the numerical method.

In FEHM, the nodal definition of equation parameters leads naturally to a separation of the nonlinear and purely geometric parts. This separation is detailed by Zyvoloski (1983 [DIRS 101171]) and is valid over lower-order elements. The nonlinear part uses average inverse kinematic viscosity, which is ρ/μ , between two nodes, although the average is usually taken to be the upstream nodal value. The result is a much more stable code for solving nonlinear problems that retains much of the geometric flexibility of finite elements. This method has been used in FEHM since 1983 (Zyvoloski 1983 [DIRS 101171]) and has been extensively verified. Harmonic weighting of the intrinsic permeability is used. It is noted that the SZ site-scale flow model has a spatially varying viscosity term (due to spatially varying temperature) and interblock fluid fluxes are modeled by upwinding the viscosity terms. Newton-Raphson iteration is applied to the system of equations, which is solved with a multidegree of freedom and preconditioned, conjugate gradient method using either the

generalized minimum residual method or the biconjugate gradient-squared acceleration technique.

6.4.3 SZ Site-Scale Flow Model Inputs

The development of the SZ site-scale flow model involves the input of data from a number of sources, including water-level and head distributions, definitions of the hydrogeologic units, distributions of recharge flux and lateral fluxes into the model domain, feature and fault distributions, temperature profiles in wells, and boundary conditions. The data sources for these inputs are identified in Table 4-1.

Incorporation of these inputs into the SZ site-scale flow model first requires the generation of a hydrogeologic framework conceptualization and a computational grid. The HFM conceptualization and known features of the site were used to design a geologically-zoned grid for flow modeling. Once a computational grid is formulated, HFM data inputs were used to assign hydrogeologic units and features, recharge fluxes, hydrogeologic properties, and boundary conditions at nodes throughout the model domain.

6.4.3.1 Hydrogeologic Framework Model (HFM) Overview

The HFM (SNL 2007 [DIRS 174109]) is a conceptual model providing a three-dimensional interpretation of the hydrostratigraphic unit locations and structure within the SZ site-scale flow and transport model domain. It was developed using standard geologic methods and software based on all appropriate data from the Yucca Mountain area. The geometry of geologic units is defined with EARTHVISION V5.1 (STN: 10174-5.1-00; [DIRS 167994]) framework files, hereafter referred to as HFM2006 (DTN: MO0610MWDHFM06.002 [DIRS 179352]), which characterize a three-dimensional geocellular model of the base HFM for the SZ. HFM2006 extends from the land surface to the base of the 2004 regional groundwater flow model at -4,000 m elevation (Belcher 2004 [DIRS 173179], Figure B-2) and has a top surface coincident with the topographic surface. Horizontally, the HFM2006 is constructed with boundaries coincident with finite difference cells in DVRFS (Belcher 2004 [DIRS 173179]). HFM2006 is constructed by combining a set of structural contour maps representing the tops of hydrogeologic units using EARTHVISION and it includes data from geologic maps and sections, borehole data, geophysical data, and existing geologic models. This representation enables the computational grid to be populated with an initial set of hydrologic properties for the calibration of the SZ site-scale flow model. HFM2006 and its development are documented in *Hydrogeologic Framework Model for the Saturated-Zone Site-Scale Flow and Transport Model* (SNL 2007 [DIRS 174109]). The updated HFM (DTN: MO0610MWDHFM06.002 [DIRS 179352]) is a three-dimensional representation of the hydrogeologic units surrounding the location of the Yucca Mountain geologic repository and is developed specifically for use in the SZ site-scale flow model. HFM2006 is updated with information collected since development of the recent update to the DVRFS (Belcher 2004 [DIRS 173179]) and with the new NC-EWDP data through Phase IV. These boreholes provide new stratigraphic information south of Yucca Mountain and mostly north of U.S. Highway 95. The hydrogeologic layers of the HFM2006 form a series of alternating aquifers and confining units and alluvium above the regional carbonate aquifer that comprise one or more contiguous geologically defined stratigraphic units that can be grouped according to measured or inferred common hydrologic properties. These

units (Table 6-2) provide a geometric representation of hydrogeology and structure and are used as a basis for assigning hydrologic properties within the SZ site-scale flow model domain.

The DVRFS HFM consists of 28 surfaces representing the top elevation of each of the 27 hydrogeologic units plus the base at $-4,000\text{-m}$ elevation, and a horizontal grid consisting of a rectangular array of nodes with 125-m spacing (SNL 2007 [DIRS 174109], Section 6). HFM2006 consists of 24 surfaces because unit IDs 10, 13, 22, and 25 are not present in its model area (SNL 2007 [DIRS 174109], Tables 6-2 and 6-3). An important goal of the HFM2006 was to match geologic units with the regional DVRFS HFM. This match allows more direct comparisons with the regional conditions and parameters, without a transition at the site-scale model boundary, and facilitates use of boundary volumetric/mass flow rates extracted from the regional-scale model for use as target boundary conditions during site-scale model calibration. Permeabilities (hydraulic conductivities for the regional model) may not match across model boundaries because these parameters are calibrated independently. The HFM2006 surface grids exactly reproduce the DVRFS Model grid nodes except where more detailed data are available, primarily within the domain of the Geologic Framework Model (GFM) (DTN: MO0012MWDGFM02.002 [DIRS 153777]) and near NC-EWDP boreholes area. These more detailed areas are important considerations in understanding the SZ flow system and they help define the boundaries of the fractured tuff aquifers immediately beneath and down gradient from Yucca Mountain, and the alluvial aquifer from which groundwater discharges in the Amargosa Valley. Data from the NC-EWDP investigations better constrain the location of the tuff-alluvium contact at the water table and better characterize the thickness and lateral extent of the alluvial aquifer north of U.S. Highway 95 (SNL 2007 [DIRS 177390], Section 6.5.2.2).

Recent NC-EWDP drilling revealed a larger formation of alluvial material (Unit 26) in HFM2006 replacing volcanic and sedimentary unit previously thought to be present. It also revealed more of Unit 20 (Timber Mountain Volcanics) to the south of the GFM area than was previously indicated.

This report describes SZ flow modeling using HFM2006, which incorporates the newer DVRFS HFM (Belcher 2004 [DIRS 173179]), GFM2000 (DTN: MO0012MWDGFM02.002 [DIRS 153777]), and all NC-EWDP data through Phase IV.

Table 6-2. Hydrogeologic Units for the Hydrogeologic Framework Model

| Hydrogeologic Units in HFM2006 | | | | |
|--------------------------------|--------------|---------------------------------|---|----------------|
| Unit ID | Abbreviation | Unit Name | Description | Stacking Order |
| 28 | YAA | Younger alluvial aquifer | Pliocene to Holocene coarse-grained basin-fill deposits | 27 |
| 27 | YACU | Younger alluvial confining unit | Pliocene to Holocene playa and fine-grained basin-fill deposits | 26 |
| 26 | OAA | Older alluvial aquifer | Pliocene to Holocene coarse-grained basin-fill deposits | 25 |
| 25 | OACU | Older alluvial confining unit | Pliocene to Holocene playa and fine-grained basin-fill deposits (not in HFM2006 domain) | 24 |
| 24 | LA | Limestone aquifer | Cenozoic limestone, undivided | 23 |

Table 6-2. Hydrogeologic Units for Hydrogeologic Framework Model (Continued)

| Hydrogeologic Units in HFM2006 | | | | |
|--------------------------------|--------------|--|--|----------------|
| Unit ID | Abbreviation | Name | Description | Stacking Order |
| 23 | LFU | Lava-flow unit | Cenozoic basalt cones and flows and surface outcrops of rhyolite-lava flows | 22 |
| 22 | YVU | Younger volcanic-rock unit | Cenozoic volcanic rocks that overlie the Thirsty Canyon Group (not in HFM2006 domain) | 21 |
| 21 | Upper VSU | Volcanic- and sedimentary-rock unit | Cenozoic volcanic and sedimentary rocks, undivided, that overlie volcanic rocks of SWNVF | 20 |
| 20 | TMVA | Thirsty Canyon-Timber Mountain volcanic-rock aquifer | Miocene Thirsty Canyon and Timber Mountain Groups, plus Stonewall Mountain Tuff, undivided | 19 |
| 19 | PVA | Paintbrush volcanic-rock aquifer | Miocene Paintbrush Group | 18 |
| 18 | CHVU | Calico Hills volcanic-rock unit | Miocene Calico Hills Formation | 17 |
| 17 | WVU | Wahmonie volcanic-rock unit | Miocene Wahmonie and Salyer Formations | 16 |
| 16 | CFPPA | Crater Flat-Prow Pass aquifer | Miocene Crater Flat Group, Prow Pass Tuff | 15 |
| 15 | CFBCU | Crater Flat-Bullfrog confining unit | Miocene Crater Flat Group, Bullfrog Tuff | 14 |
| 14 | CFTA | Crater Flat-Tram aquifer | Miocene Crater Flat Group, Tram Tuff | 13 |
| 13 | BRU | Belted Range unit | Miocene Belted Range Group (not in HFM2006 domain) | 12 |
| 12 | OVU | Older volcanic-rock unit | Oligocene to Miocene; near the NTS consists of all volcanic rocks older than the Belted Range Group. Elsewhere, consists of all tuffs that originated outside of the SWNVF | 11 |
| 11 | Lower VSU | Volcanic- and sedimentary-rock unit | Cenozoic volcanic and sedimentary rocks, undivided; where named Cenozoic volcanic rocks exist, lower VSU underlies them | 10 |
| 10 | SCU | Sedimentary-rock confining unit | Paleozoic and Mesozoic sedimentary and volcanic rocks (not in HFM2006 domain) | 9 |
| 7 | UCA | Upper carbonate-rock aquifer | Paleozoic carbonate rocks (UCA only used where UCCU exists, otherwise UCA is lumped with LCA) | 8 |
| 6 | UCCU | Upper clastic-rock confining unit | Upper Devonian to Mississippian Eleana Formation and Chainman Shale | 7 |
| 9 | LCA_T1 | Lower carbonate-rock aquifer (thrust) | Cambrian through Devonian predominantly carbonate rocks – thrust | 6 |
| 8 | LCCU_T1 | Lower clastic-rock confining unit (thrust) | Late Proterozoic through Lower Cambrian primarily siliciclastic rocks (including the Pahrump Group and Noonday dolomite) – thrust | 5 |
| 5 | LCA | Lower carbonate-rock aquifer | Cambrian through Devonian predominantly carbonate rocks | 4 |
| 4 | LCCU | Lower clastic-rock confining unit | Late Proterozoic through Lower Cambrian primarily siliciclastic rocks (including the Pahrump Group and Noonday dolomite) | 3 |

Table 6-2. Hydrogeologic Units for Hydrogeologic Framework Model (Continued)

| Hydrogeologic Units in HFM2006 | | | | |
|--------------------------------|--------------|---------------------------------|--|----------------|
| Unit ID | Abbreviation | Name | Description | Stacking Order |
| 3 | XCU | Crystalline-rock confining unit | Middle Proterozoic metamorphic and igneous rocks | 2 |
| 2 | ICU | Intrusive-rock confining unit | All intrusive rocks, regardless of age | 1 |

Source: HFM2006 (SNL 2007 [DIRS 174109], Table 6-2) and from Belcher (2004 [DIRS 173179], Table E-1).

NOTE: The hydrogeologic names, descriptions, and stacking order are from Belcher (2004 [DIRS 173179]) and are used for the HFM2006 and SZ computational grid to maintain consistency across models.

HFM2006 was constructed to represent faults and other hydrogeologic features (such as zones of alteration) that affect SZ flow. Fault trace maps show faults on cross sections and the locations where faults intersect the land surface. Faults in the model area dip at multiple angles, but most are high-angle faults. Given fault dip uncertainty and grid resolution constraints, these features were simplified and implemented as vertical features. Faults deemed important to flow near Yucca Mountain were explicitly considered in the model and are identified separately and discussed in Section 6.4.3.7. These features are included in the SZ numerical model as distinct permeability zones in FEHM.

Important thrust faults were represented by repeating hydrogeologic units in HFM2006. When geologic, structural, or stratigraphic surfaces are stored as arrays, they cannot have multiple *z*-values at one location. This limitation means that thrust faults and mushroom-shaped intrusions cannot be represented by an array. To deal with these problems, simplifying techniques were used. Where units were repeated by thrust faults, two different grids were created for the same hydrogeologic unit. A unit boundary map was then added to define an outline for the perimeter of the thrust sheet. Within this boundary, hydrogeologic structural altitude values were treated as defining unique additional hydrogeologic unit(s). Where units were continuous across this boundary, altitudes of surfaces are the same on each side of the boundary, making the boundary “invisible.” Because of significant uncertainty in orientation, extent, and hydrogeologic properties for many of the faults in the SZ site-scale model domain, only those faults and other features of hydrologic importance were constructed in HFM2006 (SNL 2007 [DIRS 174109], Figures 6-2 and 6-3).

The top of HFM2006 is truncated by the 2006 potentiometric surface as described in Appendix E. The surface contour map was constructed using potentiometric data from various borehole locations (BSC 2004 [DIRS 170009], Figure 6-2) supplemented with new data from NC-EWDP. Data from the uppermost-completed borehole intervals were used and elevations were derived from USGS 3-arc-second 1-by-1 degree digital elevation model files.

6.4.3.2 Grid Generation

The computational grid for the SZ site-scale flow model was developed using LaGriT V1.1 (STN: 10212-1.1-00; [DIRS 173140]), which is a software tool for generating, editing, and optimizing multi-material unstructured finite element grids (triangles and tetrahedra). LaGriT maintains the geometric integrity of complex input volumes, surfaces, and geologic data and produces an optimal grid (Delaunay, Voronoi) elements. The computational grid figures in the

following sections are created with General Mesh Viewer (GMV), a grid-visualization software product that enables accurate and detailed analyses of LaGriT grid properties. GMV is distributed through the LANL web site at: <http://laws.lanl.gov/XCM/gmv/GMVHome.html>.

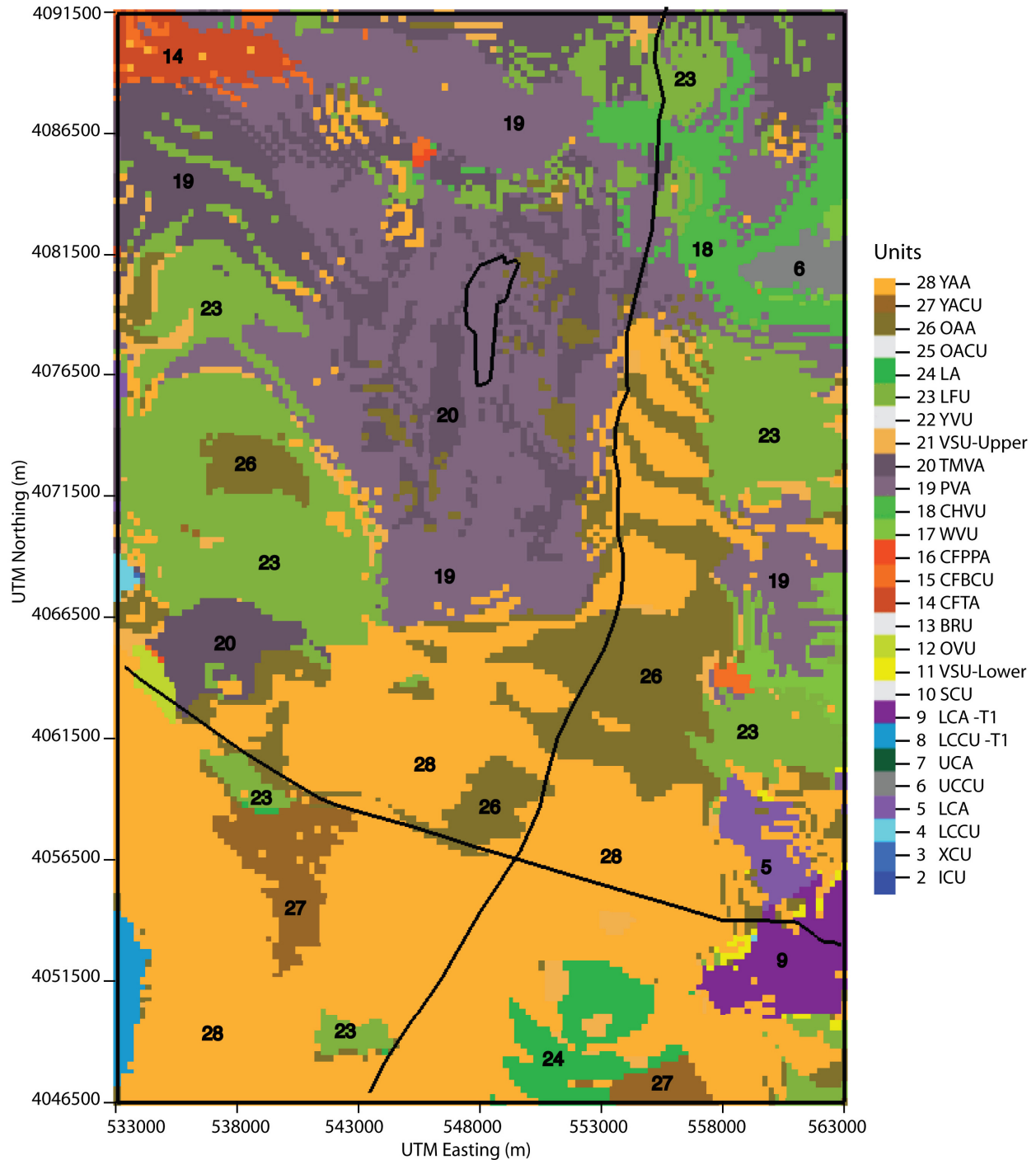
The grid was designed so that in the horizontal, its nodes are coincident with the grid cell corners of the 2004 DVRFS (Belcher 2004 [DIRS 173179]), with even multiples of 125 m in the UTM coordinate system. The grid for the flow model extends upward along the vertical coordinate to the ground surface, although those nodes located above the water table are computationally inactive. A confined aquifer solution using the water-table elevation to define the top of the flow system is implemented and described in Section 6.4.1. The extension of the grid to the ground surface allows, if desired, the simulation of a dynamic water table. The depth of the flow-model grid drops to 4,000 m (9,020 ft) below sea level to match the depth of HFM2006 and it includes more of the regional carbonate aquifer than previous model versions. The extent of the computational grid is shown in Table 6-3 and Figure 6-5.

Table 6-3. Coordinates of the Base-Case SZ Site-Scale Model Domain

| Location | HFM Surfaces (m) | Grid Extents (m) | Grid Total Distance (m) |
|--------------------------|-----------------------------|-----------------------------|------------------------------------|
| UTM Easting, meters | 530,750 to 565,250 | 533,000 to 563,000 | 30,000 |
| UTM Northing, meters | 4,044,250 to 4,093,750 | 4,046,500 to 4,091,500 | 45,000 |
| Bottom to ground surface | -4,000 to 2,018.5 | -4,000 to 2,200 | 5,950 at highest point |

Sources: DTN: MO0610MWDHFM06.002 [DIRS 179352] (HFM2006).

Output DTN: SN0612T0510106.004 (SZ site-scale flow model).



Source: DTN: MO0610MWDHFM06.002 [DIRS 179352].

NOTES: Source for the repository outline, which is for illustration purposes only is from SNL 2007 [DIRS 179466]. This view shows the top of the 250-m computational grid, which is coincident with the domain topology. The different colors in the figure indicate the material units as defined by hydrogeologic surfaces described in Table 6-2. Black lines show the repository outline, U.S. Highway 95, and a line tracing north-south along Fortymile Wash.

UTM = Universal Transverse Mercator.

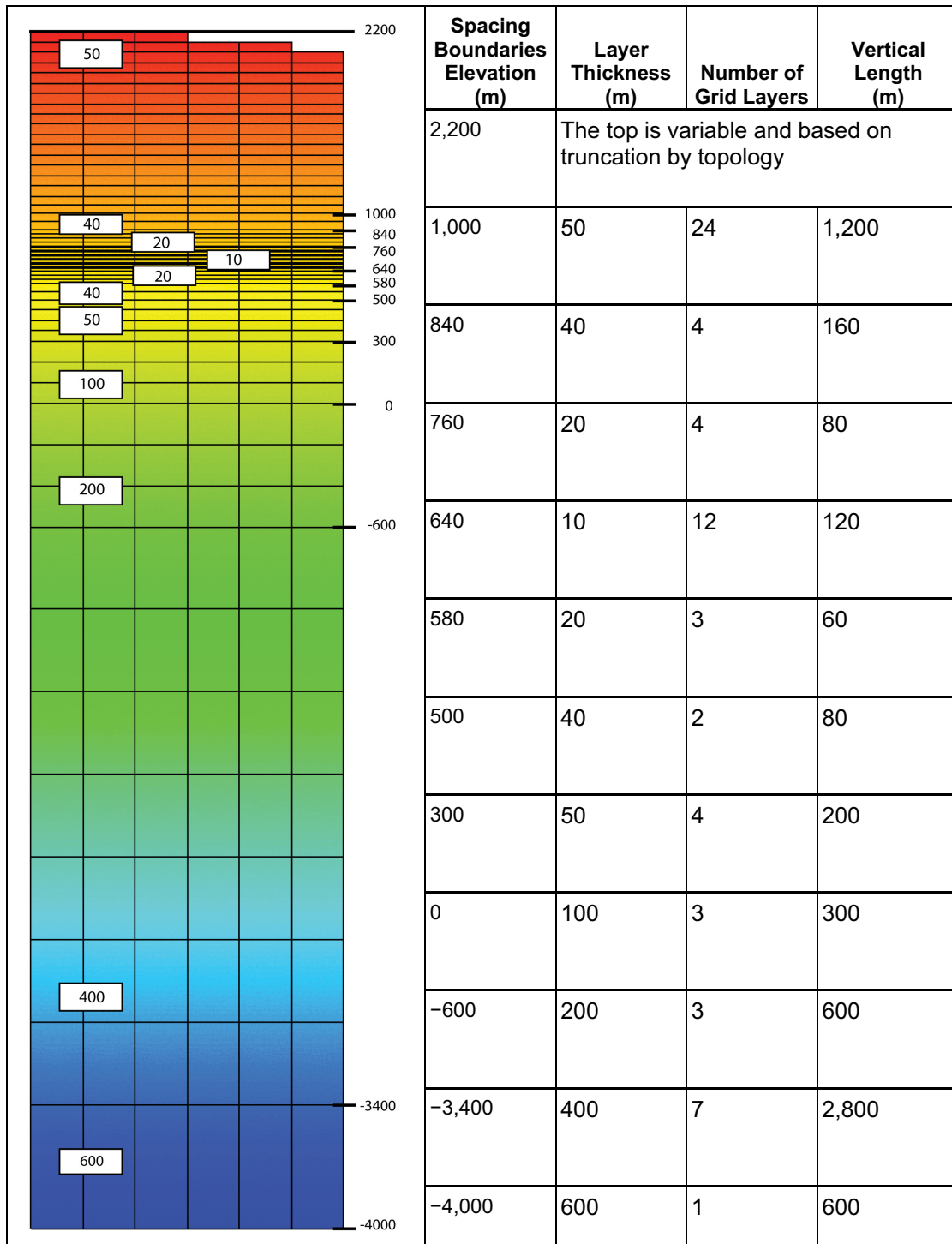
Figure 6-5. Top of the 250-m SZ Site-Scale Computational Grid

A structural grid using orthogonal hexahedral elements comprises the SZ site-scale flow model. Previous models of Yucca Mountain SZ flow and transport (Czarnecki et al. 1997 [DIRS 100377]) have used both unstructured (finite-element) meshes and structured orthogonal grids. However, the principal reason structured grids are used for this work is to facilitate the use of streamline particle-tracking capabilities in FEHM. Although structured meshes are not as flexible as unstructured meshes in fitting complex geometry, tests have shown that they provide accurate solutions so long as there is adequate resolution to represent the geometry of the different materials in each hydrogeologic layer. Moreover, there must be enough resolution to account for any large gradients. The sufficiency of grid resolution is usually investigated by running a flow model using various grids of differing resolutions. If little difference is found among model results using grids of increasing resolution, those resolutions at which the model differences become minimal can be used to identify suitable grid resolutions. A study of the accuracy of both the flow and transport solution was performed on 10 grids with horizontal resolutions ranging from 500 to 10,000 m to determine the appropriate horizontal grid resolution for the SZ site-scale flow model (Bower et al. 2000 [DIRS 149161]). Though 500-m spacing is sufficient for these models, higher resolution can better capture the interface between materials. But as resolution increases, so do the number of grid nodes. For FEHM simulations, the final grid must stay under 2 million nodes, additional restrictions due to operating system and LaGriT QA controls, further constrain the grid to under 1 million nodes. The 250-m grid spacing used for this model provides improved accuracy over older 500-m spacing, improving the representation of the material interfaces.

More important than the horizontal spacing, high grid resolution in the vertical dimension is needed for capturing material units that are thin, or that pinch out into other materials. Each grid layer in the structured grid is horizontal, but the layers of the physical hydrogeologic units are gently sloping with approximately 7% dip to the east. Therefore, a finer and nonuniform grid resolution is used in the vertical dimension to capture the geometry of the sloping hydrogeologic units. The vertical grid spacing is selected to provide sufficient resolution to accurately represent flow along critical flow and transport pathways in the SZ. A finer resolution is used near the water table in the vicinity of the repository (~700 m) and progressively coarser resolution is used for the deeper portions of the aquifer. The vertical grid spacing ranges from 10 m (33 ft) near the water table to 600 m (1,969 ft) at the bottom of the model domain. The vertical dimension of the model domain is divided into 12 zones, and constant vertical grid spacing is adopted in each of these zones. The computational grid starts as a rectangular shape with 121 nodes along the x -axis and 181 nodes along y -axis and 67 along z -axis. Grid nodes above the ground surface are identified and removed resulting in a variable total number of nodes along the z -axis for any given x, y location. In total, 67 layers are included in the vertical dimension that extends from +2,200 m (7,218 ft) to -4,000 m (-13,1230 ft) elevation. The structure of the vertical layering used in the SZ site-scale flow and transport model grid is summarized in Table 6-4 and are shown in the three-dimensional views in Figures 6-6 and 6-7. The material properties were assigned to the intersections of the grid layers. At the locations where the grid is coarse, some of the HFM layers were not represented. However, in the areas of greatest interest, the grid is sufficiently fine and the resolution of the HFM is on the same level as the resolution of the grid.

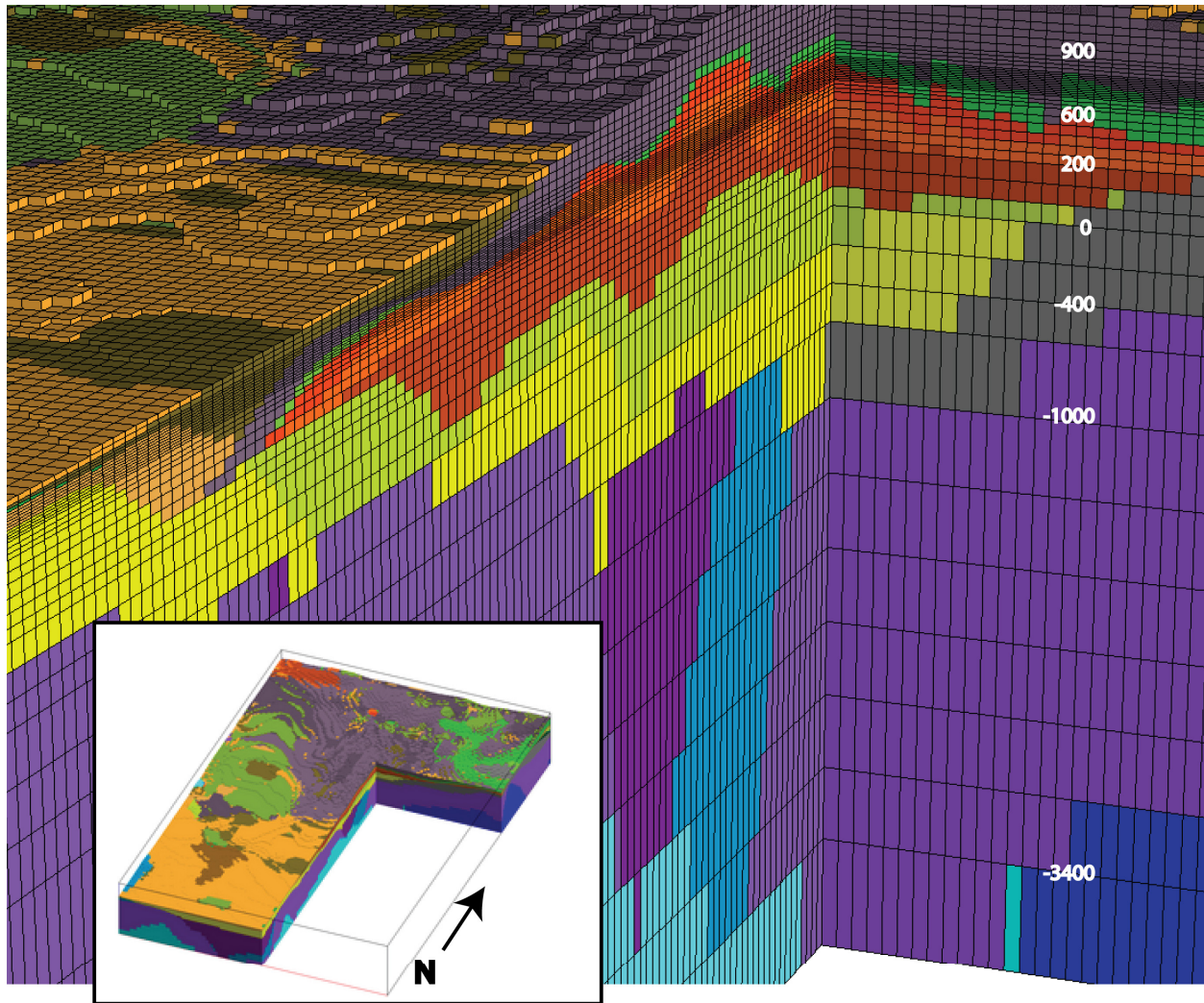
The top surface of the mesh is an irregular stair stepped surface created by removing any element above a digital elevation model (DEM). Because the top surface will not exactly match the DEM, a decision is made to use the following criteria. If the centroid (average value of the eight corner nodes of a hexahedral element) is above the DEM the element is removed. The final truncated grid has a stair stepped top surface with some associated grid nodes above the DEM. Figure 6-7 is an image of the full computational grid showing the top surface to illustrate how topography is represented. The inset shows a close-up at the top of the grid showing the vertical changes in grid resolution. The image is a view of the northwest corner where water table surface is located about 150 m below the ground surface. These figures show how grid resolution approximates the units defined by the HFM2006 surfaces.

Table 6-4. Vertical Grid Spacing Used in the SZ Site-Scale Flow Model



Source: Output DTN: LA0612TM831231.002.

NOTE: The image shows the vertical distribution of the grid layers. Boxed numbers are the layer thicknesses and numbers along image right are elevation (MASL) where layer thicknesses change. The top of this grid is truncated by the ground surface resulting in a variable top elevation.

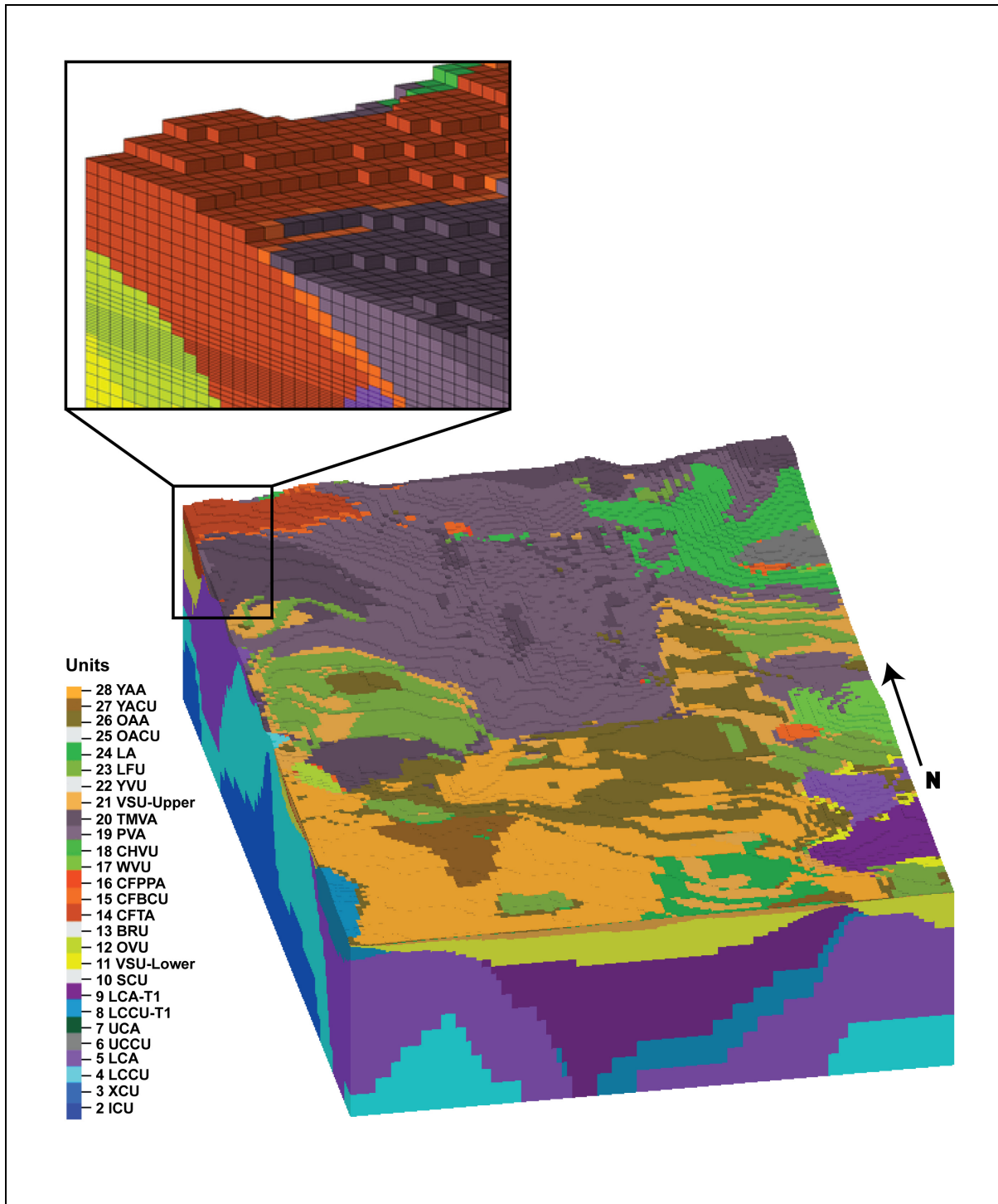


Source: Output DTN: LA0612TM831231.002.

NOTES: For illustration purposes only, view shows a cut away of the computational grid with 3× vertical exaggeration. Grid spacing at the bottom of the grid is at 600 m, then 400, 200, 100, 50, 40, 20, with 10 m near an elevation of 700 m. Spacing then increases with elevation from 10 to 20 and 40 m, with 50-m spacing near the higher elevations in the north. The inset at the bottom of the image shows the location of the cut out in relation to the full grid. The grid points are colored with the values of the hydrogeologic Units 2 through 28 as described in Table 6-2.

UTM = Universal Transverse Mercator.

Figure 6-6. Close-Up View of Computational Grid (3× Vertical Exaggeration) Showing Cut Away at UTM Easting = 549,000 m and UTM Northing = 4,078,000 m Through the Yucca Mountain Repository



Source: Output DTN: LA0612TM831231.001.

NOTE: The grid extends 533,000 to 563,000 m from west to east, and 4,046,500 to 4,091,500 m south to north (Coordinates UTM North American Datum 27). Detail shows the grid blocks and ground surface at the northwest top corner of the grid.

UTM = Universal Transverse Mercator.

Figure 6-7. View of the 250-m Computational Grid (2× Vertical Exaggeration) Showing Node Points Colored by Hydrogeologic Units Values from HFM2006

6.4.3.3 Hydrogeologic Properties

HFM2006 provides the hydrogeologically-defined geometry for SZ flow and transport process models and is used to assign geologic properties to the nodes of the computational grid. The physical hydrogeologic unit present at each node in the computational grid was established during the computational grid construction. The HFM2006 surface files represent the top surface of each hydrogeologic layer in the model framework and were imported into LaGriT to identify the hydrogeologic layer designation for each node and cell of the computational grid. Cells above the ground surface were identified using the HFM2006 surfaces, then they were removed from the grid. Quality checks were performed to ensure that the final grid is correct. These include histograms of element volume and element aspect ratio as described by Bower et al. (2000 [DIRS 149161]). Once the grid geometry was evaluated and the material units conform as needed to the input HFM, FEHM modeling input files are generated. These files include the mesh geometry, lists of nodes on external boundaries, and node lists sorted by material property.

All nodes were automatically and visually checked to ensure that they were assigned the correct material identification corresponding to the input HFM. Lists of the number of nodes associated with each material were compared to the volume of each material in the EARTHVISION framework to confirm that the hydrogeologic units are identified correctly.

When evaluating the computational grid for SZ flow and transport, the hydrogeologic properties of the grid are compared to the hydrogeologic framework used as input. It is expected that the grid units will differ slightly from the HFM due to differences in grid spacing (i.e., 250 versus 125 m). The grid units should still resemble the input HFM and areas of importance should be replicated accurately. The flow pathways are expected to leave the repository and travel in a south-southeasterly direction towards Fortymile Wash and the 18-km compliance boundary. From the 18-km boundary to the end of the model, the flowpaths should trend to the south-southwest and generally follow Fortymile Wash. Outlines of the repository, Fortymile Wash, and U.S. Highway 95 are included on Figure 6-5 as reference to these areas.

6.4.3.4 Evaluation of Hydrogeology represented in the SZ Computational Grid

All nodes were automatically and visually checked to ensure that they were assigned the correct material. The number of nodes assigned to each hydrogeologic unit and their associated element volumes are presented in Table 6-5. Lists of the number of nodes associated with each material were compared to the volume of each material in the HFM2006 to confirm that the hydrogeologic units are identified correctly. To check that hydrogeologic properties are being assigned in accord with the HFM2006, relative unit volumes are compared. Differences will occur between the HFM and grid units due to variations in grid element sizes in the computational grid. Volumes represented by the HFM2006 surfaces are included for comparison. Large grid elements less accurately capture thin layers as shown when comparing unit volumes. Figures showing the grid units are supplied in Appendix G to confirm that differences are reasonable and acceptable.

Table 6-5. SZ Computational Grid and HFM2006 Volume Comparisons by Unit

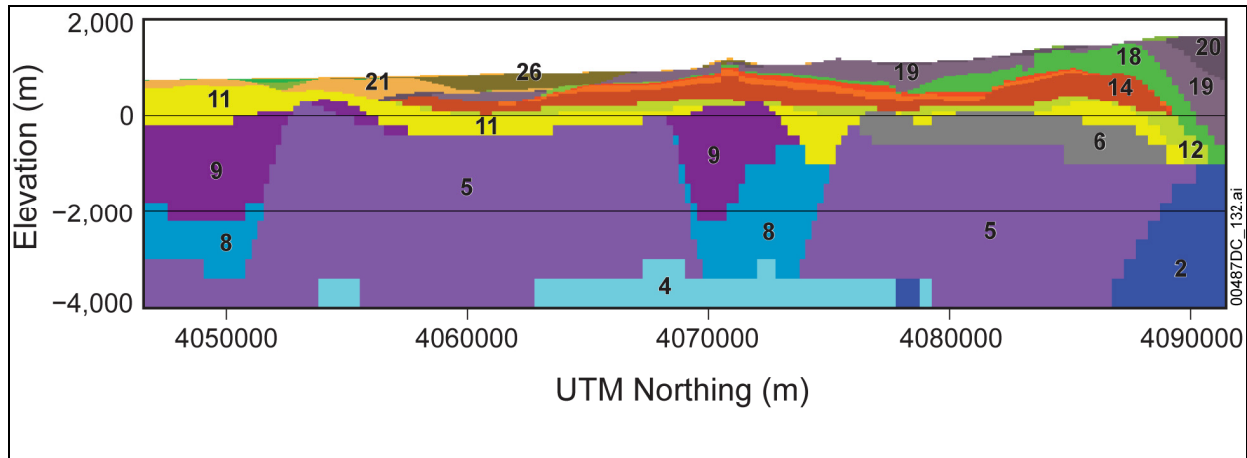
| Unit | Names | SZ Computational Grid | | | HFM2006 Surfaces | |
|--------|-----------|-----------------------------|--------------------------------------|---------------------|----------------------------------|---------------------|
| | | Tetrahedral Elements Number | Volume of Elements per Unit (m) | % Fractional Volume | Volume between surfaces (m) | % Fractional Volume |
| 28 | YAA | 32,106 | 4.75×10^9 | 0.07 | 1.15×10^{10} | 0.17 |
| 27 | YACU | 7,788 | 8.11×10^8 | 0.01 | 9.89×10^8 | 0.01 |
| 26 | OAA | 137,772 | 2.09×10^{10} | 0.31 | 2.35×10^{10} | 0.34 |
| 24 | LA | 18,834 | 2.08×10^9 | 0.03 | 2.18×10^9 | 0.03 |
| 23 | LFU | 38,208 | 8.56×10^9 | 0.13 | 1.48×10^{10} | 0.22 |
| 21 | Upper VSU | 316,716 | 5.53×10^{10} | 0.81 | 5.58×10^{10} | 0.82 |
| 20 | TMVA | 152,586 | 3.77×10^{10} | 0.56 | 4.38×10^{10} | 0.64 |
| 19 | PVA | 838,668 | 2.35×10^{11} | 3.47 | 2.45×10^{11} | 3.59 |
| 18 | CHVU | 280,368 | 9.29×10^{10} | 1.37 | 9.45×10^{10} | 1.38 |
| 17 | WVU | 122,802 | 2.52×10^{10} | 0.37 | 2.57×10^{10} | 0.38 |
| 16 | CFPPA | 140,064 | 3.38×10^{10} | 0.56 | 3.78×10^{10} | 0.55 |
| 15 | CFBCU | 439,698 | 1.35×10^{11} | 1.98 | 1.35×10^{11} | 1.98 |
| 14 | CFTA | 584,232 | 2.85×10^{11} | 4.20 | 2.85×10^{11} | 4.17 |
| 12 | OVU | 158,982 | 1.68×10^{11} | 2.47 | 1.69×10^{11} | 2.48 |
| 11 | Lower VSU | 461,478 | 5.97×10^{11} | 8.78 | 5.96×10^{11} | 8.72 |
| 9 | LCA T1 | 185,736 | 3.00×10^{11} | 4.42 | 3.00×10^{11} | 4.39 |
| 8 | LCCU T1 | 101,550 | 2.63×10^{11} | 3.87 | 2.64×10^{11} | 3.86 |
| 7 | UCA | 24,900 | 8.33×10^9 | 0.12 | 8.83×10^9 | 0.12 |
| 6 | UCCU | 238,248 | 2.18×10^{11} | 3.21 | 2.21×10^{11} | 3.24 |
| 5 | LCA | 793,620 | 2.55×10^{12} | 37.59 | 2.54×10^{12} | 37.13 |
| 4 | LCCU | 275,532 | 1.07×10^{12} | 15.77 | 1.08×10^{12} | 15.79 |
| 3 | XCU | 47,490 | 2.23×10^{11} | 3.28 | 2.26×10^{11} | 3.30 |
| 2 | ICU | 106,974 | 4.50×10^{11} | 6.62 | 4.55×10^{11} | 6.67 |
| Totals | | 5,504,352 | Element Volume 6.79×10^{12} | | Sum Volume 6.83×10^{12} | |

Source: Output DTN: LA0612TM831231.001.

NOTES: HFM2006 volumes represent the best achievable volumes when matching surface resolutions. The computational grid lengths are 250 m in the horizontal and depths range from 10 to 600 m in the vertical. Units 10, 13, 22, and 25 are not found within the domain of the SZ site-scale flow model.

Figures 6-8 through 6-10 represent sections cut through the computational grid and can be compared to matching sections cut through HFM2006 (SNL 2007 [DIRS 174109], Figures 6-5 and 6-6). The first figure is a north-to-south vertical section cut at an easting of 552,500 m. This section was selected because it is located approximately along the flowpath from Yucca Mountain to the south. The second figure is a west-to-east vertical section cut at a northing of 4,064,000 m and it is located within the area of the newest NC-EWDP well data used in HFM2006. This section cuts across most of the faulting in the area and demonstrates where the faulting is represented in the more widely spaced data of the regional model, which served as the basis for HFM2006. As can be seen in this figure, some of the offsets on the faults are preserved through changes in altitude of a given hydrogeologic unit. Given the depth to which the model extends and the lack of information in most of the modeled volume, this seems to be a rational simplification (SNL 2007 [DIRS 174109], Section 6).

Figure 6-10 is a 5× vertical exaggeration detail of the west-east cross section. The spacing is shown with the grid lines and the accuracy imposed by grid resolution is apparent. Units at the lower levels and with large 200- to 600-m edge lengths capture only a coarse representation of the deeper units. Vertical spacing of 10 to 20 m in the shallower units do a much better job of capturing the hydrogeologic unit shapes where increased accuracy is needed.

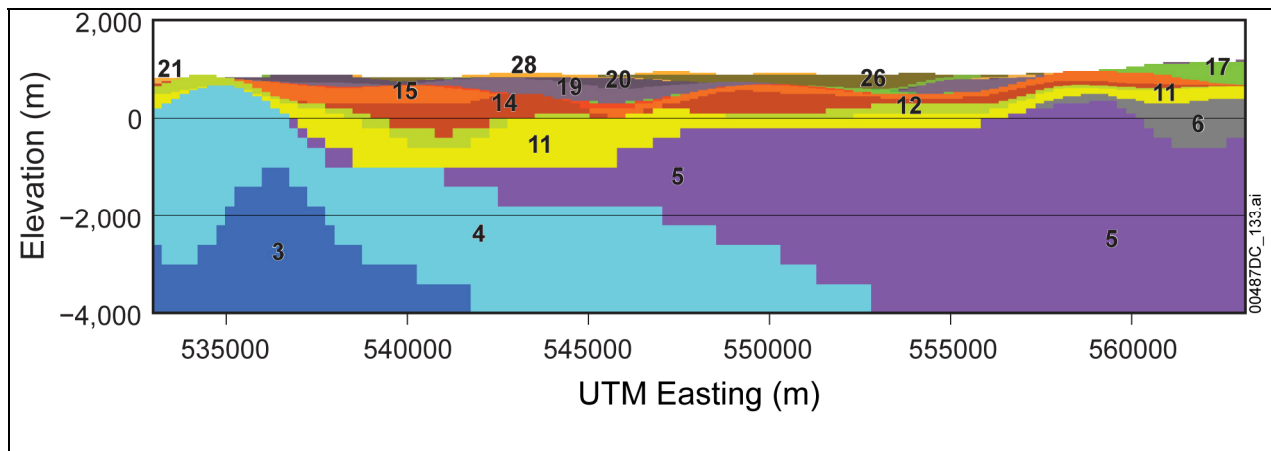


Source: Output DTN: LA0612TM831231.001.

NOTE: Coordinates in UTM, Zone 11, NAD27 meters, 2 × vertical exaggeration. Unit numbers are the hydrogeologic numbers defined by HFM2006 in Table 6-2. The colors correspond to those in the legend for Figure 6-7.

UTM = Universal Transverse Mercator.

Figure 6-8. Hydrogeologic Units Present at North-South Cross Section in the SZ Computational Grid at UTM Easting = 552,500 m

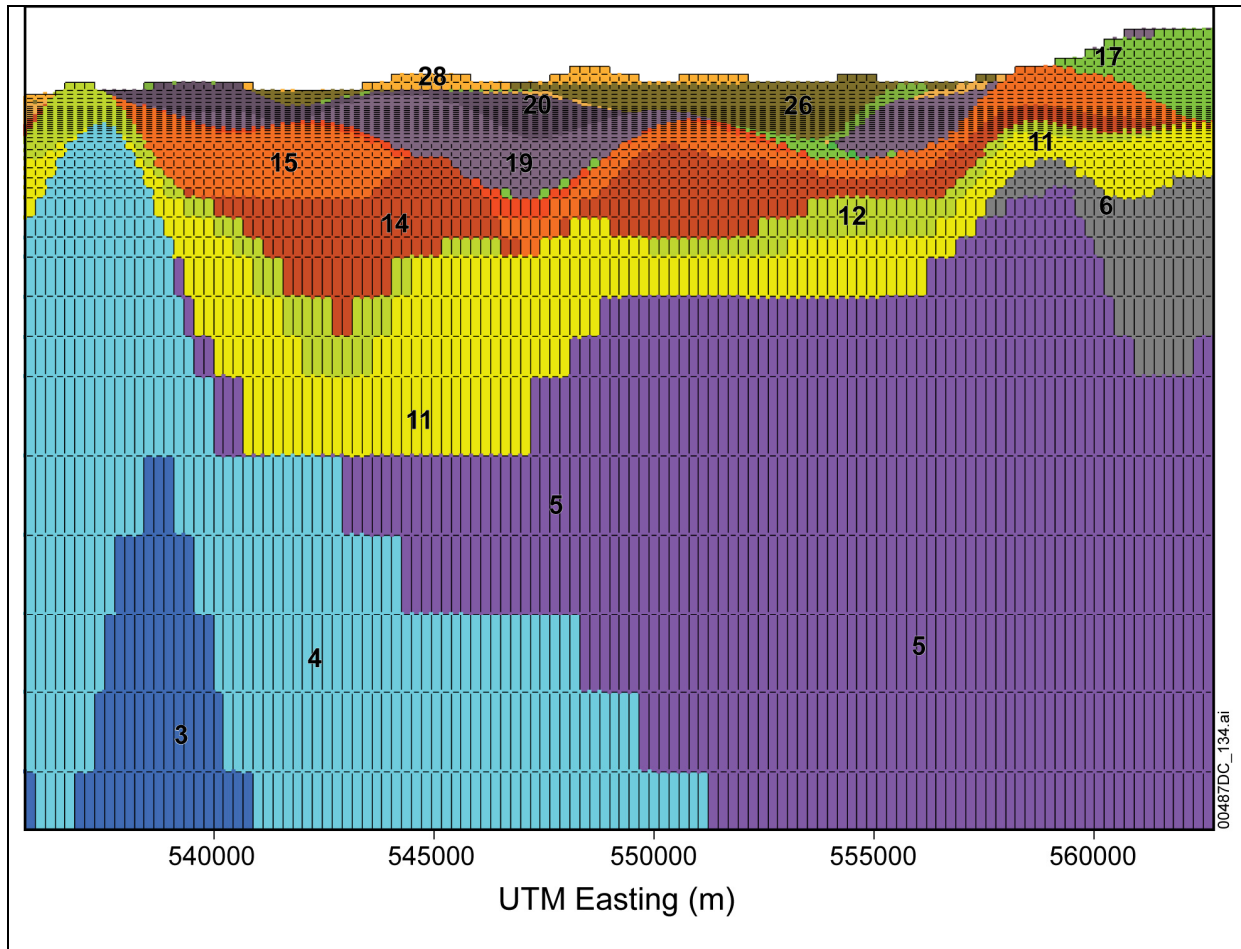


Source: Output DTN: LA0612TM831231.001.

NOTE: Coordinates in UTM, Zone 11, NAD27 meters, 2 × vertical exaggeration. Unit numbers are the hydrogeologic numbers defined by HFM2006 in Table 6-2. The colors correspond to those in the legend for Figure 6-7.

UTM = Universal Transverse Mercator.

Figure 6-9. Hydrogeologic Units Present at West-East Cross Section in the SZ Computational Grid at UTM Northing = 4,064,000 m



Source: Output DTN: LA0612TM831231.001.

NOTE: Coordinates in UTM, Zone 11, NAD27 meters, 5 × vertical exaggeration. Unit numbers are the hydrogeologic numbers defined by HFM2006 in Table 6-2. This image shows the spacing of the grid in the vertical direction. The grid nodes used in FEHM flow modeling are shown here at the vertices of each grid block. Grid nodes and volumes are colored according to HFM2006 hydrogeology. The colors correspond to those in the legend for Figure 6-7.

UTM = Universal Transverse Mercator.

Figure 6-10. Hydrogeologic Grid Nodes and Spacing at West-East Cross Section in the SZ Computational Grid at UTM Northing = 4,064,000 m

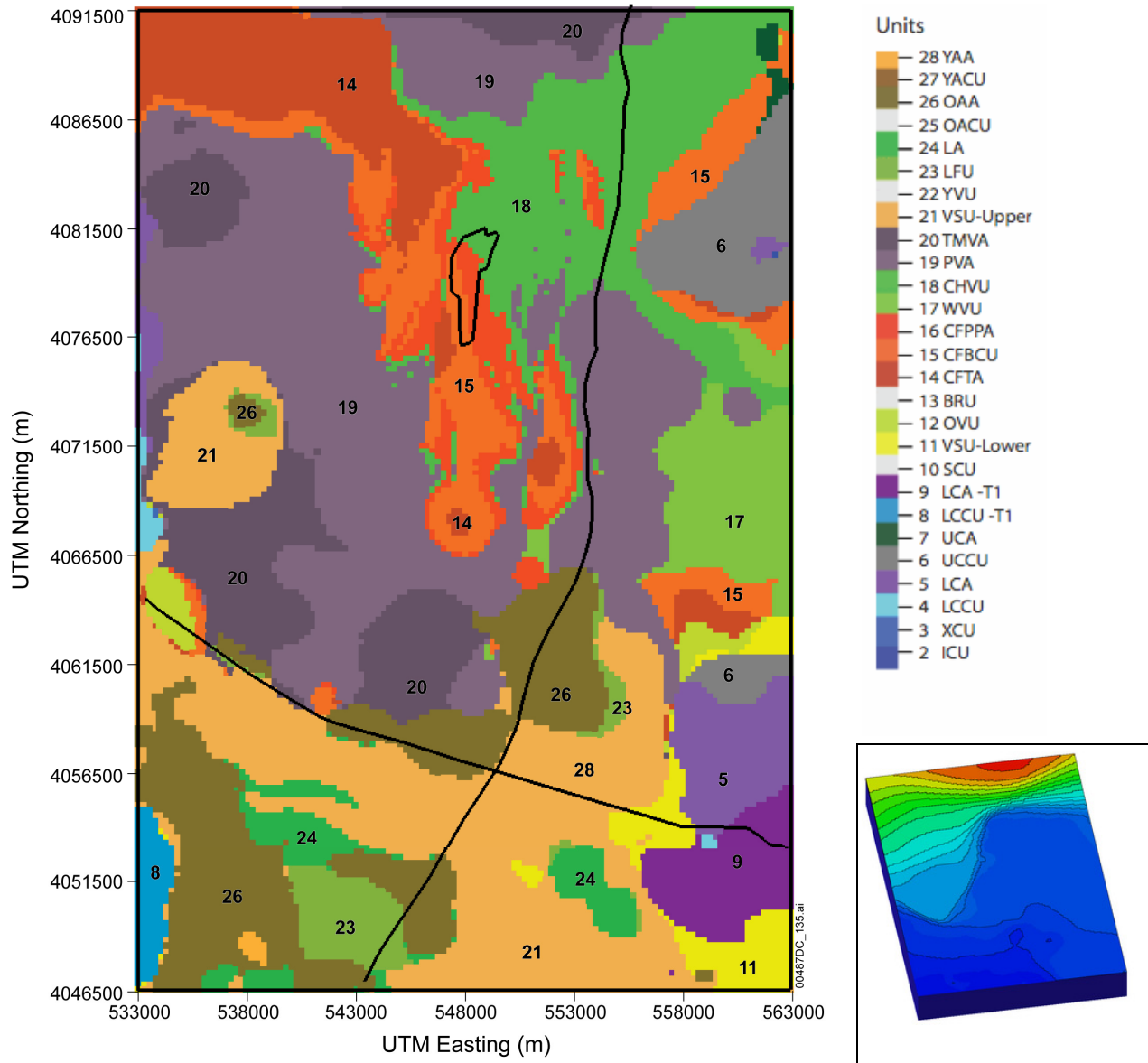
6.4.3.5 Hydrogeology at the Water Table

A new water-table surface is used in conjunction with HFM2006 and is discussed in Appendix E. The water-table surface defines which grid nodes are below and above the water table, those that are above the water table are inactivated in the FEHM flow model. This results in node elevations at the top of the flow model that range from ~1,200 m in the north to ~700 m in the south. The hydrogeologic units at the water table top are shown in Figure 6-11, which compares well with HFM2006 view at the water table (SNL 2007 [DIRS 174109], Figure 6-7c).

Table 6-6. SZ Computational Grid Nodes by Unit

| Unit | Abbreviation | Nodes per Unit Under Top Surface | Nodes per Unit Under Water Table Surface |
|-------------|---------------------|---|---|
| 28 | YAA | 9,965 | 197 |
| 27 | YACU | 1,580 | 247 |
| 26 | OAA | 24,148 | 10,637 |
| 24 | LA | 3,289 | 1,387 |
| 23 | LFU | 8,608 | 2,751 |
| 21 | Upper VSU | 53,911 | 42,717 |
| 20 | TMVA | 27,940 | 18,131 |
| 19 | PVA | 143,658 | 94,149 |
| 18 | CHVU | 47,905 | 29,189 |
| 17 | WVU | 21,116 | 14,576 |
| 16 | CFPPA | 23,461 | 20,242 |
| 15 | CFBCU | 73,939 | 67,436 |
| 14 | CFTA | 98,162 | 93,327 |
| 12 | OVU | 27,152 | 26,691 |
| 11 | Lower VSU | 78,182 | 76,856 |
| 9 | LCA_T1 | 31,608 | 28,588 |
| 8 | LCCU_T1 | 17,848 | 17,053 |
| 7 | UCA | 4,228 | 4,201 |
| 6 | UCCU | 40,842 | 33,533 |
| 5 | LCA | 135,186 | 131,312 |
| 4 | LCCU | 52,891 | 52,745 |
| 3 | XCU | 10,018 | 10,015 |
| 2 | ICU | 20,708 | 20,708 |
| Totals | | 956,345 | 774,177 |

Source: Output DTN: LA0612TM831231.001.



Source: Output DTN: LA0612TM831231.001.

NOTE: For illustration purposes only. The figure depicts grid points at the water-table surface. The black lines are used for reference and are the repository outline (SNL 2007 [DIRS 179466]), U.S. Highway 95, and Fortymile Wash. The inset shows the computational grid colored by the water table elevations ranging from 680 m in the south to 1,230 m in the north.

UTM = Universal Transverse Mercator.

Figure 6-11. Hydrogeologic Units Present at the Water-Table Surface in the SZ Computational Grid

The resolution of the computational grid was designed to have the smallest vertical spacing in the vicinity of the water-table below the repository surface and below. Therefore, the computational grid honors the hydrogeology of the HFM2006 as can be seen in these figures. Updates to the HFM2006 show differences most evident in the southern part of the model where the volcanic and sedimentary unit replaces the valley-fill aquifer as the most pervasive unit. Updates to the HFM2006 also include increased abundance of the Crater Flat group to the west

of Yucca Mountain and the occurrence of Lava Flow unit to the east of Fortymile Wash and to the north of U.S. Highway 95. These changes may have influence on the calibration and specific discharge simulations of the flow model.

Further comparisons can be made across each unit by comparing HFM2006 layer thickness and distribution maps (SNL 2007 [DIRS 174109], Appendix C) to the distribution of grid nodes for each hydrogeologic unit (SNL 2007 [DIRS 174109], Appendix A) and are presented in Appendix G. Figures for each grid unit include the distribution of each unit for the full model domain, and a second figure showing the grid units truncated by the water table surface. The truncated grid units show the active grid nodes for the FEHM modeling domain. Both sets of images are views looking directly down at the top, with south toward the page bottom and showing the horizontal distribution for each unit 1 through 28. The shapes of the HFM2006 maps (SNL 2007 [DIRS 174109], Appendix C) and the grid units (SNL 2007 [DIRS 174109], Appendix A) compare reasonably given that the grid resolution is 250 m and the HFM2006 is 125 m and that vertical grid resolution varies from 10 to 600 m.

6.4.3.6 Uncertainty

Uncertainty in the SZ computational grid is a function of HFM2006 and the resolution of the grid in relation to the flowpaths. Large grid spacing and associated loss of hydrogeologic unit shape accuracy are chosen to correspond with areas deep in the model and beyond the flowpath regions. Areas of highest resolution were chosen in the shallow units and in the area of the water table below the repository. Uncertainties in the HFM2006 relate most importantly to the quantity and location of available qualified data, and secondly to the interpretation of surfaces and the representation of important faults and structures. Uncertainties due to the definition of the hydrogeologic units are propagated through the flow and transport model abstraction (SNL 2007 [DIRS 177390]).

Model uncertainties in the HFM2006 can be attributed to interpretations and simplifications driven largely by the distribution and availability of data. The data distribution over the SZ area is uneven, much of the volume is unsampled, and many of the inputs are interpretations. As a result, the expected error in the HFM2006 varies significantly over the model area. Some of the surfaces, such as that of the upper volcanic aquifer in the area of the repository, are relatively well defined by more than one data set (derived from the surface hydrogeologic unit map and borehole lithologic logs). Others, especially the units that crop out less commonly, are less well defined and are extrapolated from sparse data. In the area of the repository, the unit locations are relatively well known. Even in this area, however, only one borehole penetrates the Paleozoic rocks. Data uncertainty increases with depth and distance from the repository as data become sparse and the effects of faults deeper in the system become unknown. As a result, the model contains an inherent level of uncertainty that is a function of data distribution and geologic complexity. Additional limitations include data-poor regions in the deeper Paleozoic carbonate region (SNL 2007 [DIRS 174109], Section 6.4.3).

HFM2006 is constructed with a horizontal grid spacing of 125 m, but most of the model domain does not contain sufficient geologic detail to support this resolution. This results in smoothly interpreted or interpolated surfaces at a resolution finer than justified by the geologic data. This finer resolution does not add any additional error. Specific borehole data and other measured

data were incorporated where available. The site-scale flow model indicates that as long as the horizontal spatial ambiguity in the location of hydrogeologic contacts is less than 250 m (the horizontal grid cell size), there is insignificant impact on model specific discharge or flux calculations (Section 6.7.3). Because flow leaving the repository area is confined to a few of the most permeable units, the vertical dimension of the computational flow grid deserves special consideration (vertical resolution is variable with the smallest spacing of 10 m located between 640 and 760 m). The vertical uncertainty of the input data is variable with borehole contacts at approximately plus or minus 3 m (10 ft). Uncertainty in relatively less complex areas of the GFM with some geologic constraints has been described as plus or minus 23.8 m (78 ft) at a distance of about 1,000 m from a known data point (BSC 2004 [DIRS 170029], Section 6.6.3). The depth from the top of the upper layer of the HFM2006 model to the water table (Output DTN: MO0611SCALEFLW.000) is less than 1,000 m and averages 255 m over the model area. This distance constraint provides confidence that the uncertainty is less than that described for some of the GFM (SNL 2007 [DIRS 174109], Section 6.4.3).

As with HFM2006, the upper portion of the grid, less than 1,000 m deep and close to the surface provides less uncertainty than the deeper portions of the model.

6.4.3.7 Features

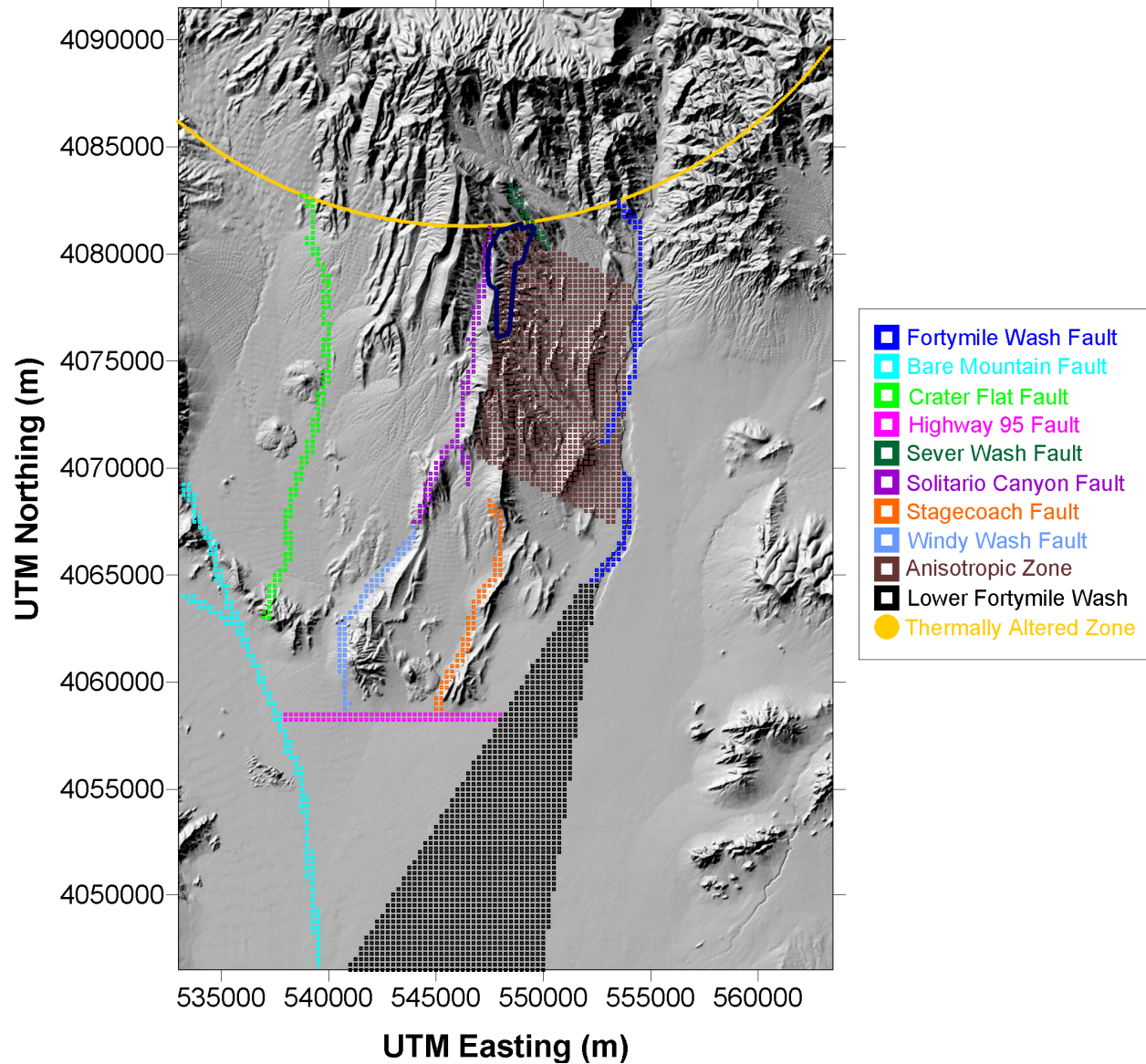
To represent discrete features and regions having distinct hydrological properties within the model domain, a set of ten hydrogeologic features were identified and incorporated into the flow model. The hydrogeologic features included in the SZ site-scale flow model primarily represent faults, areas of mineralogical alteration, and areas of alluvial deposition. The features described here are typically defined as vertical in nature (faults) although some are defined areally (zones of altered permeability). Features are distinct from the subhorizontal geological formations, which form zones with distinct geometry and material properties and are described in Section 6.3.1.10. Each of the features described in this report comprises multiple geologic formations and represents a zone of altered (enhanced, reduced, and/or anisotropic) permeability within the individual formations. Each feature has an impact on the SZ site-scale flow model. The geometric definition, description, nature of permeability alteration, and impact on the model for each of these features are described in Table 6-7. In the table, the numbers in the parentheses refer to zone numbers in the input file for FEHM. The features are shown in Figure 6-12, which is based on the Yucca Mountain area geologic map (DTN: GS010908314221.001 [DIRS 162874]) and shows feature representation in the SZ site-scale flow model. The permeability values associated with the features described in Table 6-7 are presented and discussed in Section 6.5.1.3.

The Lower Fortymile Wash alluvial zone was added because of the distinct character of the Fortymile Wash in the southern part of the model. Field observations indicate possible channelization with attendant textural contrasts with surrounding alluvial material (Oatfield and Czarnecki 1989 [DIRS 149438]). This zone of increased permeability was constrained by a quadrilateral with vertices listed in Table 6-7 and included only members of alluvial units (surfaces 24 and 26 to 28 in Table 6-2).

A zone was defined near Yucca Mountain with a quadrilateral whose vertices are listed in Table 6-7. This zone serves two purposes: to define the extent of the anisotropic region in the

volcanic units (Units 12, 14, 15, 16, 17, 18, 19, 20, and 25), and to provide boundaries for a zone of enhanced permeability in the Crater Flat tuffs to better approximate the small hydraulic gradient in the region. The zone was defined based on responses of USW H-4, UE-25 C#1, UE-25 WT#14, and UE-25 WT#3 to pumping at the C-holes from May 1996 to November 1997. Furthermore, this zone did not include wells USW H-5, G-1, and UZ-14 because, although these wells are located east of the Solitario Canyon Fault, they showed anomalous heads closer to those observed in wells located west of Solitario Canyon Fault (USW H-6, WT-7, and WT-14). This indicates that some non-characterized feature or process is impacting the water levels just to the east of Solitario Canyon Fault and the newly defined zone allows the model to better represent these data. The quadrilateral is defined to encompass the small-gradient area southeast of the repository between Solitario Canyon and Fortymile Wash Faults without including wells USW H-5, G-1, and UZ-14, but including wells USW H-4, UE-25 C#1, UE-25 WT#14, and UE-25 WT#3.

Most hydrogeologic units (the 19 units with areal extents that reach into the north of the model including all units except the lower clastic confining unit thrust, lower carbonate aquifer thrust, Wahmonie volcanic unit, limestone aquifer, and the young alluvial confining unit) have been divided into northern and southern zones near the Claim Canyon caldera boundary to represent the altered northern zone (see Section 6.3.1.11). This zone of decreased permeability with geometry described in Table 6-7 facilitates model representation of the LHG north of Yucca Mountain. Except for Sever Wash Fault, fault nodes do not reside in this region. The altered northern region is defined with an arc that intersects the model domain and it is defined by a circle with center 546,500; 4,102,400 (UTM easting and northing) and radius 21,100 m. This designation was selected such that the defining circle roughly corresponds to the center of the caldera complex and the radial extent includes wells: GEXA Well #4, UE-29 a#2, UE-29 UNZ#91, UE-25 WT#6, USW G-2, and USW WT-24. Breaking the hydrogeologic units into independent northern and southern zones yields 19 additional calibration parameters. Figure 6-13 illustrates the radial extent of the altered northern region.

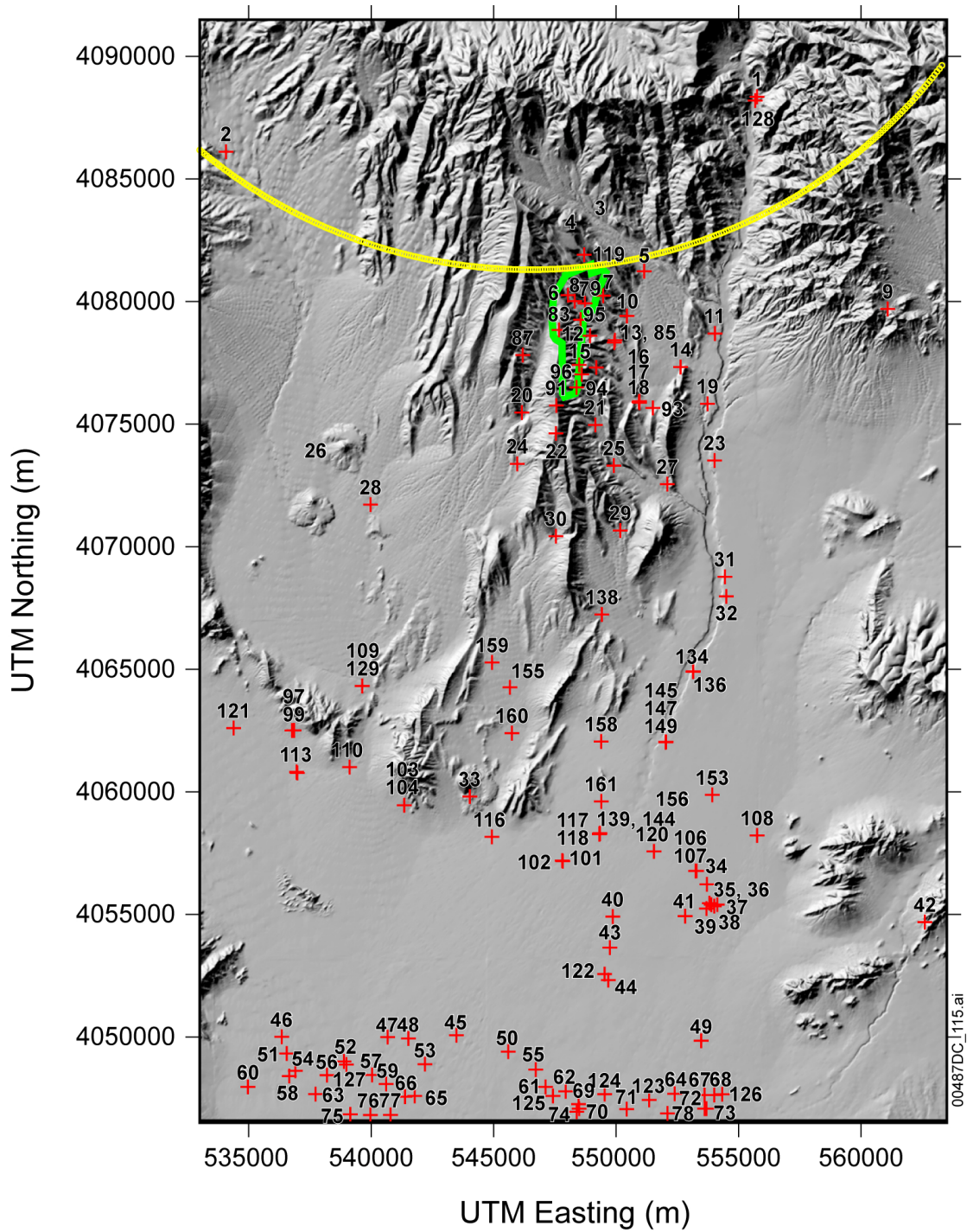


Source: Output DTN: SN0612T0510106.004, *feature_set.zonn* and *aniso.zonn*).

NOTE: Source for repository outline: SNL 2007 [DIRS 179466]. Fault traces are labeled in the legend. FEHM zone number correspond to the following regions: 39 – Anisotropic zone; 40 – Fortymile Wash Fault; 41 – Bare Mountain Fault; 42 – Crater Flat Fault; 43 – U.S. Highway 95 Fault; 44 – the Solitario Canyon Fault; 45 – Sever Wash Fault; 46 – Stagecoach Fault; 47 – Windy Wash Fault; 50 – Lower Fortymile Wash.

UTM = Universal Transverse Mercator.

Figure 6-12. Geologic Features Included in the SZ Site-Scale Flow Model



Source: Output DTN: SN0612T0510106.004, *north_zones.zonn*.

NOTE: Source for repository outline: SNL (2007 [DIRS 179466]). The altered northern region is delineated by the yellow arc. Calibration wells are shown on the plot with numbers corresponding to Table 6-8.

UTM = Universal Transverse Mercator.

Figure 6-13. The Altered Northern Region and Well Locations

Table 6-7. Hydrological Features in the SZ Site-Scale Flow Model

| Feature Name and Description | Number of Nodes | Hydrogeological Characteristics | Impact on Model |
|--|-----------------|---|--|
| 1. Fortymile Wash Fault (#401 and #402) – This is a north-south trending feature east of Yucca Mountain. Vertically, it extends from top to bottom of the model. | 3,317 and 2,028 | Possible control of fluid pathways near Yucca Mountain. Because this fault is likely a conducting feature, it is defined isotropically. | The fault is a possible preferential flow path |
| 2. Bare Mountain Fault (#41) – This is a northwest- to southeast-trending feature in the southwestern corner of the model. Vertically, it extends from top to bottom of the model. | 7,939 | This fault has a vertical permeability anisotropy factor of 10. | The fault directs flow from Crater Flat to the Amargosa Desert |
| 3. Crater Flat Fault (#42) – This is a north-south trending feature in the western half of the model, starting south of the Claim Canyon and terminating near U.S. Highway 95, almost halfway between the western boundary of the model and the Solitario Canyon Fault. Vertically, it extends from top to bottom of the model. | 7,095 | This fault has plane parallel permeability anisotropy factor of 10. | The fault generates a higher head in the western half of the model thereby limiting the influx from the western boundary (it restricts the flow to the east) |
| 4. U.S. Highway 95 Fault (#43) – This is an east-west trending feature in the lower half of the western portion of the model. Vertically, it extends from top to bottom of the model, but it does not continue through the alluvial units defining the Lower Fortymile Wash zone. | 3,633 | This fault has plane parallel permeability anisotropy factor of 10. | This fault restricts flow in the north-south direction and supports high heads to its north |
| 5. Sever Wash Fault (#46) – This is a northwest-southeast trending feature. Vertically, it extends from top to bottom of the model. | 2,437 | This fault has a vertical permeability anisotropy factor of 10. | This fault may serve to divert southerly flow around the repository to the east thereby facilitating southeast flowpaths from the repository |
| 6. Solitario Canyon Fault (#44) – This is a north-south trending feature just to the west of Yucca Mountain. Vertically, it extends from top to bottom of the model. | 7,041 | This fault has plane parallel permeability anisotropy factor of 10. | This fault generates a higher head to the west of Yucca Mountain and impedes flow from Crater Flat to Yucca Mountain |
| 7. Stage Coach Fault (#45) – This fault forms the eastern splay starting at the southerly end of the Solitario Canyon Fault. Vertically, it extends from top to bottom of the model. | 1,182 | This fault has plane parallel permeability anisotropy factor of 10. | This fault generates a higher head to the west and impedes flow from the east |
| 8. Windy Wash Fault (#47) – This fault forms the eastern splay starting at the southerly end of the Solitario Canyon Fault. Vertically, it extends from top to bottom of the model. Only that portion of the fault south of its connection to the Solitario Canyon Fault is used in the model. | 2,437 | This fault has plane parallel permeability anisotropy factor of 10. | This fault generates a higher head to the west and impedes flow from the east |

Table 6 7. Hydrological Features in the SZ Site-Scale Flow Model (Continued)

| Feature Name and Description | Number of Nodes | Hydrogeological Characteristics | Impact on Model |
|---|-----------------|--|--|
| 9. Lower Fortymile Wash Alluvial Zone (#50)^a – This is a region to the south of Yucca Mountain in the southern half of the model that connects to the southern end of Fortymile Wash Fault. Vertically, it extends from top to bottom of the model, but it only comprises alluvial units. | a | This zone represents the possible increased permeability due to Fortymile Wash | This zone influences the SZ site-scale flow model and it is expected to be important to TSPA due to its effect on solute transport |
| 10. Anisotropic/Crater Flat Zone (#39/#60)^b – This is a region east of the Solitario Canyon Fault and west of Fortymile Wash Fault. It is included in the model to facilitate representation of the small-gradient area southeast of the repository and also to allow the model to better represent the heads in wells USW H-5, G-1, and UZ-14. Vertically, it extends from top to bottom of the model, but it comprises only Crater Flat tuffs. This zone also defines the horizontally anisotropic region, but in this instance, it includes all volcanic units within this quadrilateral (Units 12, 14, 15, 16, 17, 18, 19, 20, and 25). | b | This zone represents a possible permeability increase in the Yucca Mountain region for the Crater Flat units. Also, this zone defines the horizontally anisotropic volcanic units. | This zone may affect the gradient near the repository and also the specific discharge |

Source: DTN: GS010908314221.001 [DIRS 162874].

Output DTN: SN0612T0510106.004.

NOTES: Faults are defined as nodes that fall within 180 m of the coordinates defining the fault as listed in DTN: GS010608312332.001 [DIRS 155307] with the location of the U.S. Highway 95 fault updated in DTN: GS010908314421.001 [DIRS 162874]. Linear interpolation was used to specify fault location coordinates to ensure that spacing between data points defining the fault was never more than 125 m from its neighbors. This guarantees that the fault will be defined with a stair-stepping appearance when viewed from above (each fault node is connected to at least two other fault nodes in the horizontal. Fortymile Wash fault was defined as all nodes within 250 m of the specified fault coordinates.

^aThis zone is defined by a bounding quadrilateral (UTM): $(x_1, y_1) = 540,000; 4,046,500; (x_2, y_2) = 550,000; 4,046,500; (x_3, y_3) = 552,100; 4,062,400; (x_4, y_4) = 550,840; 4,062,400.$

^bThis zone defined by a bounding quadrilateral (UTM): $(x_1, y_1) = 548,500; 4,081,288; (x_1, y_1) = 554,100; 4,078,462; (x_1, y_1) = 553,445; 4,067,200; (x_1, y_1) = 546,800; 4,070,549.$

Anisotropy in the horizontal hydraulic conductivity was based on responses of USW H-4, UE-25 C#1, UE-25 WT#14, and UE-25 WT#3 to pumping at the C-holes from May 1996 to November 1997. The range of anisotropies and their directions were calculated by SNL (2007 [DIRS 177394], Appendix C6.2). The calculated directions of anisotropy from this effort (derived from the shape of the cone of depression from the C-wells test) support the principally north-south anisotropy direction between the C-holes and USW H-4 along Antler Wash. The zone must be large enough to include wells USW H-4 on the west, UE-25 WT#14 on the east, and UE-25 WT#3 in the south. Overall, the zone of anisotropy is defined to include all volcanics (Units 12, 14, 16, 17, 18, 19, 20, and 25) that fall within a generalized region east of the Solitario Canyon Fault and west of Fortymile Wash Fault.

SZ = saturated zone; TSPA = total system performance assessment; UTM = Universal Transverse Mercator.

6.4.3.8 Boundary and Initial Conditions

The lateral boundary conditions are described in Section 6.3.1.6. Historically, groundwater has been extracted from wells in the Amargosa Valley south of Yucca Mountain. Drawdown from the wells is represented in the potentiometric surface map that was used to establish southern boundary head conditions derived from the potentiometric surface. Consequently, the effect of pumping on flow within the model domain is accounted for by the head values specified along the southern boundary and the truncation by the water table. A small amount of pumping also has occurred from within the southern portion of the site-scale model domain, but ignoring this pumping is assumed to have little effect on the calculated flowpaths and flow times to compliance boundaries. No explicit representation of pumping is included in this model.

The initial conditions (initial pressure or head distribution) are not relevant because the SZ site-scale flow model is formulated for steady-state flow.

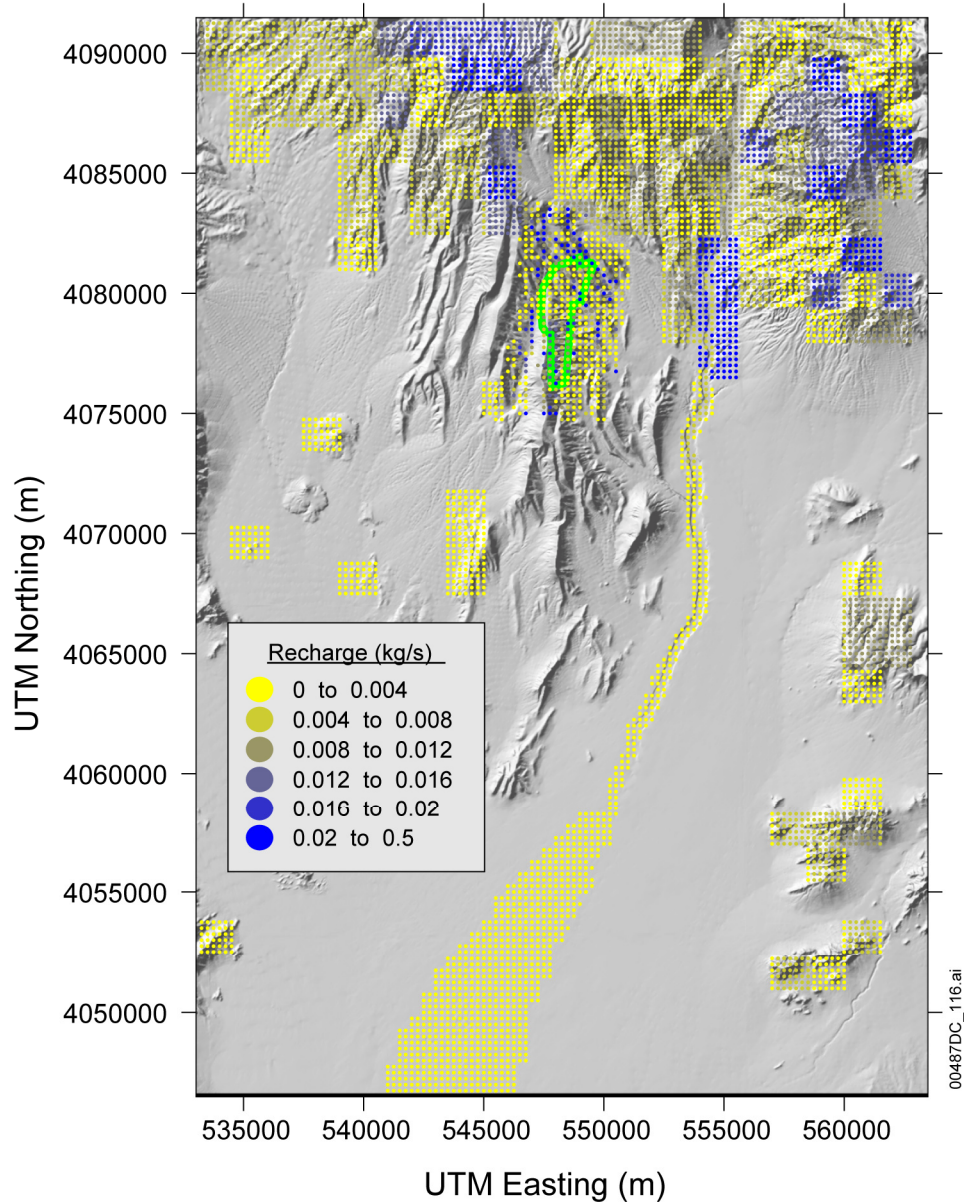
6.4.3.9 Recharge

Nodes above the water table were inactivated by specifying a negative porosity. Recharge (infiltration) was applied to the top surface of the active computational grid (at the water table) as a flux boundary condition by distributing an infiltration map onto the computational mesh (Figure 6-14). The process used to specify the recharge for the SZ site-scale flow model is outlined in *Recharge and Lateral Groundwater Flow Boundary Conditions for the Saturated Zone Site-Scale Flow and Transport Model* (BSC 2004 [DIRS 170015], Section 6.2). The recharge data were developed with some correlation to the landscape and geology at ground surface based on data from the 2004 DVRFS (Belcher 2004 [DIRS 173179], Figure C-8), the 2003 UZ flow model (BSC 2004 [DIRS 169861]), and data from Savard (1998 [DIRS 102213]) for the Fortymile Wash Fault and the Lower Fortymile Wash alluvial zone. Although redistribution of infiltration in the UZ is likely to change the pattern of recharge, these data are considered sufficient for the flow model. The data used from the 2004 DVRFS are qualified for one time use in this report in Appendix C. It is worth noting that the data reported by Savard (1998 [DIRS 102213]) for infiltration along the Fortymile Wash Fault actually indicate less infiltration than the surrounding nodes as interpreted from the 2004 DVRFS (Belcher 2004 [DIRS 173179]) (see Figure 6-14).

Total recharge was about 61.3 kg/s (1.93×10^6 m³/yr or 1,570 acre-ft/yr). Of this total, about 5.6 kg/s (1.76×10^5 m³/yr or 143 acre-ft/yr) was attributed to flux from the UZ flow model area and about 2.0 kg/s (6.20×10^4 m³/yr (50 acre-ft/yr) was attributed to infiltration along Fortymile Wash, leaving a remainder of about 53.7 kg/s (1.707×10^6 m³/yr or 1,375 acre-ft/yr) from distributed recharge. The recharge in each node of the regional model was extracted and the corresponding recharge to the SZ site-scale model node was calculated (the regional model grid has a resolution of 1,500 m, which is six times coarser than the site-scale model grid resolution).

Target groundwater inflows approximately along the eastern, northern, and western boundaries of the SZ site-scale flow model total 337.8 kg/s (10.7×10^6 m³/yr or 8,650 acre-ft/yr), 158.9 kg/s (5.0×10^6 m³/yr or 4,065 acre-ft/yr), and 120.3 kg/s (3.8×10^6 m³/yr or 3,080 acre-ft/yr), respectively (Appendix D). These inflows, totaling 617.2 kg/s (19.5×10^6 m³/yr or 15,790 acre-ft/yr), represent 10 times the estimated recharge applied at the water table due to

infiltration. Of the total inflow across the eastern boundary, 273.1 kg/s (8.6×10^6 m³/yr or 6,970 acre-ft/yr), or 81%, occurs across the southern 6 km, nearest the Amargosa Desert, and nearly all of that occurs in bottom layers of the regional-scale flow model and represents flows in the lower carbonate aquifer (D'Agnese et al. 1997 [DIRS 100131], p. 90, Figures 46 and 47; Belcher 2004 [DIRS 173179]). Much of the inflow to the SZ site-scale flow model from the 2004 DVRFS (Belcher 2004 [DIRS 173179]) is through the bottom layer of that model, which largely comprises the lower carbonate aquifer and may be up to 3-km thick. However, because the 2004 DRFS (Belcher 2004 [DIRS 173179]) uses the HUF package, it cannot be assumed that model layers correspond to hydrogeologic unit contacts (as is the case for the SZ site-scale flow model). Thus, it is difficult to estimate how large a fraction of the total flow through the volcanics can be attributed to infiltration. Across all 16 layers of the 2004 DVRFS (Belcher 2004 [DIRS 173179]), 61.3 kg/s represents about 10% of the total inflow while across the top 15 layers, it represents approximately 19% of the total inflow. A recent update to infiltration estimates in the region immediately surrounding Yucca Mountain (SNL 2007 [DIRS 174294]) was used to supply new percolation fluxes to the UZ flow model, which yielded a weighted flow through its footprint of 8.4 kg/s under present-day climatic conditions (SNL 2007 [DIRS 175177], Table 6.2-7). While this is a 49% increase over the previous net infiltration through the UZ footprint (5.6 kg/s), it remains a small portion of the infiltration budget, 13%, and a correspondingly smaller portion of the entire flow budget through the lateral boundaries, equal to about 1%.



Source: Repository outline (green curve) (SNL 2007 [DIRS 179466])
 Infiltration data: Output DTN: SN0612T0510106.003 (*wt_250_04.dat*).

NOTE: Recharge map combines the components of recharge from the 2004 DVRFS, recharge below the UZ site-scale model domain and focused recharge along Fortymile Wash using a 250-m grid resolution.

UTM = Universal Transverse Mercator.

Figure 6-14. Recharge Applied to the SZ Site-Scale Flow Model

6.4.3.10 Nodal Hydrogeologic Properties

Hydrogeologic properties must be specified for each node in the computational grid. Using the grouping definitions generated during the grid-building process, permeabilities are assigned to each node. Temperatures (hence viscosities) are also applied and porosities can be defined for transport simulations if desired.

The parameter values for viscosity depend on the temperature at each node and a uniform vertical temperature gradient is assumed. The assumption of a uniform temperature gradient with depth is equivalent to assuming uniform geothermal heat flux through a medium of homogeneous thermal conductivity. In addition, the temperature at the ground surface is assumed constant. The data on temperature in boreholes presented by Sass et al. (1988 [DIRS 100644]; DTN: MO0102DQRBTEMP.001 [DIRS 154733], Figures 4, 5, 6, 7, 8, and 10) indicate that there is significant variability in the temperature gradient at different locations and within individual wells, presumably from advective redistribution of heat from infiltration and vertical groundwater flow. The data were used to estimate an approximate average temperature gradient and representative surface temperature for the site. As noted by Sass et al. (1988 [DIRS 100644], p. 2), there is considerable variability in the temperature gradients among the wells from about 15°C/km to nearly 60°C/km. The approximate average value of the temperature gradient in the wells is 25°C/km, and the average surface temperature is about 19°C (yielding maximum temperatures of 167.75°C at the bottom of the model domain). However, these data also indicate that the temperature gradients become increasingly linear with depth below the water table. It is important to note that the goal of assigning temperature variations with depth in the SZ site-scale flow model is to account for resulting variations in fluid viscosity at different depths in the SZ. The linear approximation of the temperature gradient is adequate to capture the general effects of variations in groundwater viscosity with depth in the SZ site-scale flow model.

The density also varies with temperature, but the effect is much smaller than that of viscosity, and therefore density is treated as a constant. Using a variable viscosity allows the calibration of intrinsic permeability to be made instead of hydraulic conductivity. The former is a rock property, whereas the latter is both a rock and fluid property. This approach, in turn, allows for more accurate flux calculations at the boundaries of the model.

The approach taken to incorporate groundwater temperature in the SZ site-scale model was to assign the average temperature gradient (25°C/km) multiplied by depth below surface plus the average surface temperature (19°C) to all nodes in the model domain. All temperatures remain fixed, and the heat-transport equations are not solved in the simulation. Thus, the specified values of temperatures were used to calculate the local groundwater viscosity, but temperature variations do not yield variable-density flow processes because density was treated as a constant in all calculations.

6.4.3.11 Vertical Anisotropy

A fractured or porous media exhibits anisotropy when hydraulic properties are not uniform in all directions. For Yucca Mountain, anisotropic permeability potentially affects the specific discharge, the flowpaths, and the flowpath lengths in the volcanic tuffs and alluvium. During calibration of the SZ site-scale flow model, anisotropy ratios were held constant. The SZ site-scale flow model includes a horizontal to vertical anisotropy ratio of 10:1, a typical value, in most alluvial units, particularly younger units (CRWMS M&O 1998 [DIRS 100353], Table 3-2). Non-alluvial units (i.e., the intrusive confining unit, crystalline confining unit, lower clastic confining unit, lower carbonate aquifer, upper clastic confining unit, upper carbonate aquifer, lower clastic confining unit thrust, and lower carbonate aquifer thrust) were modeled with isotropic permeability because the geology indicates this is a reasonable assumption. Faults may be modeled with anisotropic permeability; often with permeabilities in plane of the fault (strike

and vertical) multiplied by 10 (e.g., Solitario Canyon fault permeabilities in the y - and z -directions are 10 times that in the cross-fault direction). The permeabilities of major faults are used as calibration parameters; however, the anisotropy ratios were constant during the calibration process. A 10:1 horizontal to vertical anisotropy was also assigned in the Lower Fortymile Wash Alluvial Zone.

6.5 SZ SITE-SCALE FLOW MODEL RESULTS

6.5.1 Model Calibration

Calibration is the process by which values of important model parameters are estimated and optimized to produce the best fit between model output and observed data. Calibration is generally accomplished by adjusting model input parameters (e.g., permeabilities) to minimize the difference between observed and simulated conditions (in this case, comparing simulated and observed head values and lateral boundary volumetric/mass flow rates). Model calibration may be performed manually or through automated optimization procedures. Automated optimization procedures generally employ a carefully prescribed mathematical process that selects the optimal set of parameters based on minimizing an objective function describing the difference between observed and simulated conditions. These procedures typically provide the most structured and thorough means of calibrating a model, and, frequently, they provide useful additional information regarding model sensitivity to parameters and other useful statistical measures. Consequently, an automated optimization procedure is used to calibrate the SZ site-scale flow model. However, manual adjustments to the calibration are also performed to ensure accurate representation of the small hydraulic gradient region southeast of the repository by ensuring that simulated particle pathlines do not contradict flow directions inferred from the potentiometric map.

A description of the calibration technique includes discussions of: optimization procedures; model outputs, whose differences between observed values (calibration targets) were minimized; and parameters that were varied during calibration.

6.5.1.1 Calibration Criteria

Proper calibration of the SZ site-scale flow model requires consideration of the full range of available data, which include field data for water levels and hydraulic heads, permeability data from field and laboratory tests, locations of known faults and other geologic data, and hydrochemical data. Opinions expressed by the Expert Elicitation Panel (CRWMS M&O 1998 [DIRS 100353]) must also be considered. The goal during development of the SZ site-scale flow model was to deliver to performance assessment a model that, given data sparseness, is as realistic as possible.

6.5.1.2 Parameter Optimization Procedure

The SZ site-scale flow model was calibrated with the commercial parameter estimation code, PEST (Watermark Computing 2002 [DIRS 161564]). PEST is a Levenberg-Marquardt (LM)-based optimization algorithm. The LM package is a well-established algorithm (Press et al. 1992 [DIRS 103316], pp. 678 to 683), it is robust, and widely applicable. It will search for the minima of a multidimensional function. In this case, the “function” is a weighted

sum-of-squares difference (SSD) between a set of observations (the heads in 161 wells in the Yucca Mountain region plus lateral boundary volumetric/mass flow rates from the regional flow model) and the solution to the partial differential equation that describes saturated flow. PEST computes the derivatives of the SSD function with respect to the various parameters. As discussed, those parameters optimized during calibration are the intrinsic permeability or permeability multiplier of each of the various hydrogeologic units, faults, and features. To estimate optimized permeabilities:

1. An initial estimate or guess for each unknown parameter is specified at the beginning of the fitting process
2. FEHM computes the resulting heads for the initial estimate of parameters
3. The results are returned to the PEST code
4. Through a series of FEHM simulations with perturbations in the parameters, the PEST LM package computes the derivative of the SSD function with respect to each of the parameters
5. The LM package then determines the amount to change each parameter's current value to improve the fit to the data through a mathematical process that combines gradient information and second derivative (approximated) information
6. This process is repeated until the fit to data is within a prescribed tolerance or until no further improvement is possible.

This coupling between PEST and FEHM allows any variable in FEHM to be used as a fitting parameter, regardless of whether it is a flow- or transport-related parameter. PEST simply finds the local minima of the target function. To enable PEST to search for the global minimum, a procedure is attached to the code that carries out a simulated annealing process, which specifies how PEST moves from one local minimum to another, better local minimum. This process is repeated until no further improvement occurs. The simulated annealing process (Press et al. 1992 [DIRS 103316], pp. 436 to 448) is simple in principle: the approach is to reject an improved solution occasionally, move to a new location in parameter space, and continue the search. Theory indicates that this technique will eventually find the global or a near-global minimum. In the flow model, the procedure includes resetting the value of the LM step-size parameter after each local minimum is found.

The SZ site-scale flow model was calibrated to achieve a minimum difference between observed water levels and simulated water levels, and also between volumetric/mass flow rates along specific boundary segments simulated by the SZ regional- and site-scale models. For calibration targets, 161 water level and head measurements were used. This was the complete set of wells available at the time of calibration. Measurements (DTN: GS010908314221.001 [DIRS 162874]; BSC 2004 [DIRS 170009], Table A-1; this report, Appendix E) represent either water levels or deeper head measurements. The deeper measurements represent average values over "open" or "packed-off" intervals, and the coordinates of the observations represent midpoints of the open interval, midpoint of the bottom of the open interval and the average water level, or the depth of the node at the water table, whichever is smallest. The calibration targets

represent steady-state values and where pumping is taking place, as in the Amargosa Valley, current water levels are used. When comparing simulated water levels to target water levels, the model represents water levels at the target locations by assigning the target head value to the nearest FEHM node. Refer to Appendix E of *Water-Level Data Analysis for the Saturated Zone Site-scale Flow and Transport Model* (BSC 2004 [DIRS 170009]) for a complete description of many water levels, well locations, and measurement depths. Nye County data used in the calibration are qualified for intended use in Appendix D and presented in Output DTN: SN0702T0510106.007.

Well NC-EWDP-19-IM2 was completed with five well screens, although no packers were installed. Hence, water level measurements were assumed to be taken at the weighted midpoint of the five intervals yielding a weighted measurement location of 599.2 m (the midpoint between the bottom of the bottom interval and the top of the top interval is 612.0 m and the water level is 813.24 m).

It should be noted that two probes from Nye County wells were not used in the calibration process: NC-EWDP-3S probe 1 and NC-EWDP-9SX probe 3. Originally well NC-EWDP-3S had a Westbay casing installation that included three zones. Nye County geologists encountered some undisclosed problems with the well and had to reinstall the Westbay casing. On March 31, 2001, the reinstallation was completed, but it eliminated probe 1, leaving just probes 2 and 3 (Gilmore 2006 [DIRS 179104]). Only a single data point was ever taken from probe 1 and hence this datum was not used in calibrating the model. Regarding NC-EWDP-9SX probe 3, Tucci (2001 [DIRS 155410], pp. 21, 24, 27, and 48 of 80) states that the data from this probe were not reliable because of potential probe or packer malfunction.

During the calibration process, emphasis was placed on minimizing the difference between observed and simulated water levels at selected target locations based on probable flow pathways. This was accomplished by multiplying the squared differences at that location by a weighting factor. A weighting factor of 1 (i.e., standard importance) was applied to most calibration targets. However, a preferential weighting factor ($\Sigma = 20$) was applied to 22 calibration targets in the small-gradient region to the south and east of Yucca Mountain. These calibration targets were given high weighting because they are in the likely groundwater pathway leaving the repository site and because small changes in head in this area often yield a large effect on the flow direction. Six calibration targets are north of Yucca Mountain in the high head region. These are either assigned a low weighting (0.1, which implies little importance) if they were thought to represent perched conditions, or a weight of 10 to help ensure that no unphysical “mounding” of water occurs. Four additional water levels that are assumed to represent perched conditions are assigned weights of 0.1. Three wells in the moderately high head area just west of the Solitario Canyon Fault are assigned weights of 20 because their accuracy ensures proper representation of this fault as a hydraulic barrier. Because Crater Flat tuffs are important to estimated flowpaths, those wells completed in these units (and not already assigned a high weight for being in the flowpath), are given a weight of 5. Two wells, USW UZ-14 and USW H-5, were deweighted because of anomalously high heads. The high potentiometric heads in these two boreholes is attributed to the presence of a splay of the Solitario Canyon Fault penetrated by the boreholes (Ervin et al. 1994 [DIRS 100633], pp. 9 to 10). This splay is believed to be an extension of the hydrologic barrier to west-to-east groundwater flow from Crater Flat (related to the Solitario Canyon Fault). The high heads in USW H-5 (about 775 m)

are related to heads in Crater Flat (ranging from 775 to 780 m), and this borehole defines part of the moderate hydraulic gradient along the western edge of Yucca Mountain. Borehole USW UZ-14 is in a transition zone between the large and moderate hydraulic areas, and the high potentiometric level (about 779 m) is related to either of these areas. Rousseau et al. (1999 [DIRS 102097], p. 172) hypothesized that perched water in USW UZ-14 could be caused by a nearby projected growth fault that impedes percolation of water from the surface. The high heads in USW UZ-14 also could be caused by the low permeability rocks in the upper part of the SZ at that borehole. These hypotheses, in combination with the lack of a corresponding feature or process in the qualified DTN used to specify faults, supports the dewatering of USW UZ-14 and USW H-5 (essentially, without an explicit feature, the model should not be asked to match anomalous heads). Wells showing an upward gradient are assigned a weight of 10 because it is important to reproduce this phenomenon. If multiple calibration targets (head measurements) are available from a single well, the sum of weights from each well sum to the specified value (e.g., four measurements from USW H-1 each have weights of 7, 1, 1, and 1). Well names including a complete listing of all target water-level values, target locations, and the weighting applied to each target are provided in Table 6-8. In addition to water levels, volumetric/mass flow rates through three of the four lateral boundary segments were used as calibration targets (west, north, and east). Each of the three lateral boundaries was supplied with a cumulative weight of 5 (see Table 6-11).

Table 6-8. Comparison of Observed Hydraulic Heads from the SZ Site-Scale Flow Model and Model Computed Head Data

| Site Name | Fig. 6-16 | Node Number | x (UTM) (m) | y (UTM) (m) | z (elevation) (m) | Measured Water Level (Head Data) ^a (m) | Modeled Head | Weight |
|--------------|-----------|-------------|-------------|-------------|--------------------|---|--------------|--------|
| UE-29 a #2 | 1 | 897244 | 555753 | 4088351 | 990.8 | 1,187.7 | 1,150.46 | 10 |
| GEXA Well 4 | 2 | 847393 | 534069 | 4086110 | 859.2 | 1,009.0 | 1,006.01 | 10 |
| UE-25 WT#6 | 3 | 846002 | 549352 | 4083103 | 840 ^b | 1,034.6 | 870.93 | 0.1 |
| USW G-2 | 4 | 845756 | 548143 | 4082542 | 840 ^b | 1,020.2 | 880.16 | 0.1 |
| UE-25 WT #16 | 5 | 673914 | 551146 | 4081234 | 714.1 | 738.3 | 734.93 | 1 |
| USW UZ-14 | 6 | 695253 | 548032 | 4080260 | 725.0 ^c | 779.0 | 734.71 | 0.1 |
| UE-25 WT #18 | 7 | 695259 | 549468 | 4080238 | 722.1 | 730.8 | 734.60 | 20 |
| USW G-1 | 8 | 279088 | 548306 | 4080016 | 125.7 | 754.2 | 745.78 | 1 |
| UE-25 a #3 | 9 | 607533 | 561084 | 4079697 | 681.4 | 748.3 | 773.84 | 20 |
| UE-25 WT #4 | 10 | 673064 | 550439 | 4079412 | 709.0 | 730.8 | 734.56 | 20 |
| UE-25 WT #15 | 11 | 650823 | 554034 | 4078694 | 698.7 | 729.2 | 735.80 | 20 |
| USW G-4 | 12 | 431672 | 548933 | 4078602 | 542.2 | 730.6 | 734.58 | 20 |
| UE-25 a #1 | 13 | 453456 | 549925 | 4078330 | 584.0 | 731.0 | 734.54 | 20 |
| UE-25 WT #14 | 14 | 650092 | 552630 | 4077330 | 703.6 | 729.7 | 734.36 | 20 |
| USW WT-2 | 15 | 649954 | 548595 | 4077028 | 702.0 | 730.6 | 734.57 | 20 |

Table 6 8. Comparison of Observed Hydraulic Heads from the SZ Site Scale Flow Model and Model Computed Head Data (Continued)

| Site Name | Fig. 6-16 | Node Number | x (UTM) (m) | y (UTM) (m) | z (elevation) (m) | Measured Water Level (Head Data) ^a (m) | Modeled Head | Weight |
|-------------------------|-----------|-------------|-------------|-------------|-------------------|---|--------------|--------|
| UE-25 c #3 | 17 | 386668 | 550930 | 4075902 | 474.3 | 730.2 | 734.44 | 20 |
| UE-25 c #2 | 18 | 430349 | 550955 | 4075871 | 553.2 | 730.2 | 734.43 | 20 |
| UE-25 WT #13 | 19 | 649370 | 553730 | 4075827 | 703.8 | 729.1 | 734.28 | 20 |
| USW WT-7 | 20 | 735215 | 546151 | 4075474 | 740.9 | 775.8 | 783.67 | 20 |
| USW WT-1 | 21 | 670881 | 549152 | 4074967 | 708.4 | 730.4 | 734.50 | 20 |
| USW G-3 | 22 | 320225 | 547543 | 4074619 | 318.1 | 730.5 | 735.52 | 1 |
| UE-25 J-13 | 23 | 341668 | 554017 | 4073517 | 354.8 | 728.4 | 734.24 | 20 |
| USW WT-10 | 24 | 713413 | 545964 | 4073378 | 734.2 | 776.0 | 781.34 | 20 |
| UE-25 WT #17 | 25 | 670037 | 549905 | 4073307 | 705.4 | 729.7 | 734.41 | 1 |
| USW VH-2 | 26 | 319581 | 537738 | 4073214 | 282.8 | 810.4 | 915.89 | 1 |
| UE-25 WT #3 | 27 | 669682 | 552090 | 4072550 | 705.8 | 729.6 | 734.24 | 20 |
| USW VH-1 | 28 | 406468 | 539976 | 4071714 | 490.5 | 779.4 | 779.16 | 1 |
| UE-25 WT #12 | 29 | 646936 | 550168 | 4070659 | 702.6 | 729.5 | 734.31 | 1 |
| USW WT-11 | 30 | 624903 | 547542 | 4070428 | 691.9 | 730.7 | 734.55 | 1 |
| UE-25 J-12 | 31 | 558381 | 554444 | 4068774 | 659.6 | 727.9 | 733.52 | 20 |
| UE-25 JF #3 | 32 | 558018 | 554498 | 4067974 | 662.7 | 727.8 | 733.33 | 20 |
| Cind-R-Lite Well | 33 | 663479 | 544027 | 4059809 | 710.2 | 729.8 | 737.29 | 1 |
| Ben Bossingham | 34 | 639932 | 553704 | 4056228 | 697.4 | 718.4 | 718.57 | 1 |
| Fred Cobb | 35 | 595767 | 553808 | 4055459 | 675.6 | 702.8 | 717.89 | 1 |
| Bob Whellock | 36 | 595768 | 553883 | 4055398 | 682.0 | 704.1 | 718.08 | 1 |
| Louise Pereidra | 37 | 639571 | 554131 | 4055399 | 698.0 | 705.6 | 718.30 | 1 |
| Joe Richards | 38 | 595647 | 554008 | 4055337 | 679.3 | 701.6 | 717.80 | 1 |
| NDOT Well | 39 | 595646 | 553685 | 4055242 | 682.1 | 705.4 | 717.61 | 1 |
| James H. Shaw | 40 | 551707 | 549863 | 4054911 | 664.3 | 706.7 | 716.24 | 1 |
| Airport Well | 41 | 507917 | 552818 | 4054929 | 636.5 | 705.3 | 716.85 | 1 |
| TW-5 | 42 | 617340 | 562604 | 4054686 | 688.7 | 725.1 | 724.32 | 1 |
| Richard Washburn | 43 | 573003 | 549746 | 4053647 | 669.9 | 707.7 | 713.55 | 1 |
| Richard Washburn | 44 | 594178 | 549679 | 4052322 | 675.3 | 704.4 | 703.36 | 1 |
| Nye County Develop. Co. | 45 | 505460 | 543481 | 4050069 | 638.6 | 694.3 | 698.58 | 1 |
| Fred Wooldridge | 46 | 571134 | 536350 | 4050006 | 673.8 | 691.9 | 696.21 | 1 |
| Fred J. Keefe | 47 | 593053 | 540673 | 4049994 | 676.7 | 694.3 | 702.57 | 1 |
| Leslie Nickels | 48 | 527353 | 541518 | 4049937 | 654.7 | 694.3 | 701.66 | 1 |
| L. Mason | 49 | 636785 | 553471 | 4049848 | 699.2 | 722.1 | 709.95 | 1 |
| Unknown | 50 | 570929 | 545596 | 4049403 | 667.6 | 697.8 | 694.28 | 1 |
| Davidson Well | 51 | 570772 | 536552 | 4049329 | 672.0 | 690.1 | 694.41 | 1 |

Table 6 8. Comparison of Observed Hydraulic Heads from the SZ Site Scale Flow Model and Model Computed Head Data (Continued)

| Site Name | Fig. 6-16 | Node Number | x (UTM) (m) | y (UTM) (m) | z (elevation) (m) | Measured Water Level (Head Data) ^a (m) | Modeled Head | Weight |
|-------------------------|-----------|-------------|-------------|-------------|--------------------|---|--------------|--------|
| Eugene J. Mankinen | 52 | 592562 | 538889 | 4049000 | 678.6 | 707.4 | 694.95 | 1 |
| Donald O. Heath | 53 | 526872 | 542194 | 4048892 | 651.6 | 694.1 | 693.54 | 1 |
| Elvis Kelley | 54 | 614213 | 536903 | 4048621 | 685.1 | 691.0 | 692.66 | 1 |
| Manuel Rodela | 55 | 614373 | 546718 | 4048669 | 686.7 | 693.6 | 693.32 | 1 |
| Charles C. DeFir Jr. | 56 | 614218 | 538196 | 4048442 | 685.7 | 706.9 | 693.77 | 1 |
| William R. Monroe | 57 | 570423 | 540035 | 4048450 | 669.5 | 693.7 | 699.29 | 1 |
| DeFir Well | 58 | 570410 | 536655 | 4048405 | 671.1 | 690.2 | 692.51 | 1 |
| Edwin H. Mankinen | 59 | 548282 | 540608 | 4048083 | 662.8 | 695.2 | 696.00 | 1 |
| Bill Strickland | 60 | 592062 | 534967 | 4047966 | 677.0 | 689.2 | 690.31 | 1 |
| M. Meese | 61 | 548308 | 547120 | 4047963 | 664.6 | 686.4 | 692.57 | 1 |
| Theo E. Selbach | 62 | 570092 | 547941 | 4047782 | 673.3 | 696.2 | 693.08 | 1 |
| C.L. Caldwell | 63 | 526249 | 537727 | 4047670 | 654.5 | 691.4 | 691.66 | 1 |
| Leonard Siegel | 64 | 570110 | 552390 | 4047685 | 667.2 | 709.0 | 705.40 | 1 |
| James K. Pierce | 65 | 548045 | 541778 | 4047596 | 664.0 | 690.4 | 690.90 | 1 |
| James K. Pierce | 66 | 591846 | 541381 | 4047563 | 677.1 | 705.6 | 691.02 | 1 |
| Cooks West Well | 67 | 613916 | 553609 | 4047631 | 690.2 | 720.1 | 709.67 | 1 |
| Cooks East Well | 68 | 613918 | 554006 | 4047633 | 693.4 | 718.9 | 711.52 | 1 |
| Nye County Land Co. | 69 | 591753 | 548466 | 4047261 | 680.0 ^c | 690.1 | 693.27 | 1 |
| Amargosa Town Complex | 70 | 569731 | 548492 | 4047077 | 668.3 | 688.8 | 693.45 | 1 |
| Nye County Develop. Co. | 71 | 482135 | 550431 | 4047057 | 615.4 | 691.2 | 692.53 | 1 |
| Lewis C. Cook | 72 | 635454 | 553612 | 4047076 | 702.5 | 717.4 | 709.89 | 1 |
| Lewis C. Cook | 73 | 613554 | 553687 | 4047077 | 688.7 | 714.8 | 711.25 | 1 |
| Amargosa Valley Water | 74 | 569731 | 548393 | 4046953 | 673.9 | 701.3 | 693.45 | 1 |
| Earl N. Selbach | 75 | 569573 | 539147 | 4046844 | 672.1 | 696.5 | 693.59 | 1 |
| Lewis N. Dansby | 76 | 547675 | 539968 | 4046817 | 664.7 | 694.2 | 693.52 | 1 |
| Edwin H. Mankinen | 77 | 613381 | 540788 | 4046821 | 686.2 | 694.0 | 692.81 | 1 |
| Willard Johns | 78 | 591646 | 552097 | 4046882 | 678.9 | 699.5 | 699.93 | 1 |
| USW H-1 tube 1 | 79 | 213387 | 548727 | 4079926 | -495.5 | 785.5 | 756.57 | 7 |

Table 6 8. Comparison of Observed Hydraulic Heads from the SZ Site Scale Flow Model and Model Computed Head Data (Continued)

| Site Name | Fig. 6-16 | Node Number | x (UTM) (m) | y (UTM) (m) | z (elevation) (m) | Measured Water Level (Head Data) ^a (m) | Modeled Head | Weight |
|-------------------------|-----------|-------------|-------------|-------------|--------------------|---|--------------|--------|
| USW H-1 tube 2 | 80 | 300991 | 548727 | 4079926 | 193.0 | 736.0 | 734.60 | 1 |
| USW H-1 tube 3 | 81 | 454298 | 548727 | 4079926 | 562.5 | 730.6 | 734.61 | 1 |
| USW H-1 tube 4 | 82 | 607605 | 548727 | 4079926 | 680.5 | 730.8 | 734.61 | 1 |
| USW H-5 upper | 83 | 650798 | 547668 | 4078841 | 704.2 | 775.5 | 734.91 | 0.1 |
| USW H-5 lower | 84 | 387986 | 547668 | 4078841 | 446.4 | 775.6 | 734.72 | 0.1 |
| UE-25 b #1 lower | 85 | 256468 | 549949 | 4078423 | -8.8 | 729.7 | 734.58 | 10 |
| UE-25 b #1 upper | 86 | 344072 | 549949 | 4078423 | 366.2 | 730.6 | 734.54 | 10 |
| USW H-6 upper | 87 | 562704 | 546188 | 4077816 | 662.9 | 776.0 | 786.21 | 10 |
| USW H-6 lower | 88 | 321793 | 546188 | 4077816 | 315.8 | 775.9 | 781.82 | 10 |
| USW H-4 upper | 89 | 365365 | 549188 | 4077309 | 395.5 | 730.4 | 734.55 | 10 |
| USW H-4 lower | 90 | 255860 | 549188 | 4077309 | 45.0 | 730.5 | 739.48 | 10 |
| USW H-3 upper | 91 | 452236 | 547562 | 4075759 | 576.9 | 731.5 | 734.60 | 5 |
| USW H-3 lower | 92 | 342731 | 547562 | 4075759 | 343.2 | 755.9 | 736.09 | 5 |
| UE-25 p #1 (Lwr Intrvl) | 93 | 211341 | 551501 | 4075659 | -410.3 | 752.4 | 740.54 | 20 |
| USW SD-7 | 94 | 518306 | 548384 | 4076499 | 637.7 | 727.6 | 734.56 | 20 |
| USW SD-9 | 95 | 607241 | 548550 | 4079256 | 678.3 | 731.1 | 734.61 | 20 |
| USW SD-12 | 96 | 650196 | 548492 | 4077415 | 696.7 | 730.0 | 734.58 | 20 |
| NC-EWDP-1DX, shallow | 97 | 768353 | 536848 | 4062509 | 784.1 ^b | 787.2 | 782.97 | 1 |
| NC-EWDP-1DX, deep | 98 | 270572 | 536848 | 4062509 | 133.1 | 749.1.8 | 772.59 | 1 |
| NC-EWDP-1S probe 1 | 99 | 749061 | 536851 | 4062504 | 751.8 | 787.4 | 782.95 | 1 |
| NC-EWDP-1S probe 2 | 100 | 708052 | 536851 | 4062504 | 730.8 | 787.5 | 782.83 | 1 |
| NC-EWDP-2D ^d | 101 | 399481 | 547823 | 4057170 | 507.1 | 706.1 | 716.64 | 1 |
| NC-EWDP-2DB | 102 | 246174 | 547800 | 4057196 | -77.0 | 712.6 | 717.93 | 1 |
| NC-EWDP-3D | 103 | 334841 | 541352 | 4059450 | 337.8 | 719.2 | 736.39 | 5 |
| NC-EWDP-3S probe 2 | 104 | 597653 | 541349 | 4059450 | 682.8 | 719.9 | 737.17 | 2.5 |

Table 6 8. Comparison of Observed Hydraulic Heads from the SZ Site Scale Flow Model and Model Computed Head Data (Continued)

| Site Name | Fig. 6-16 | Node Number | x (UTM) (m) | y (UTM) (m) | z (elevation) (m) | Measured Water Level (Head Data) ^a (m) | Modeled Head | Weight |
|---------------------|-----------|-------------|-------------|-------------|----------------------|---|--------------|--------|
| NC-EWDP-3S probe 3 | 105 | 510049 | 541349 | 4059450 | 642.3 | 719.9 | 737.17 | 2.5 |
| NC-EWDP-4PA | 106 | 618271 | 553246 | 4056772 | 687.0 | 718.0 | 718.65 | 1 |
| NC-EWDP-4PB | 107 | 443063 | 553281 | 4056774 | 582.5 | 723.5 | 718.66 | 1 |
| NC-EWDP-5SB | 108 | 662800 | 555756 | 4058222 | 707.8 | 723.6 | 720.97 | 1 |
| NC-EWDP-7S | 109 | 769212 | 539638 | 4064323 | 760 ^b | 830.3 | 767.21 | 0.1 |
| NC-EWDP-9SX probe 1 | 110 | 767636 | 539118 | 4061010 | 765.3 | 766.4 | 757.59 | 1 |
| NC-EWDP-9SX probe 2 | 111 | 748344 | 539118 | 4061010 | 751.3 | 767.2 | 757.56 | 1 |
| NC-EWDP-9SX probe 4 | 112 | 620271 | 539118 | 4061010 | 694.8 | 767.3 | 757.45 | 1 |
| NC-EWDP-12PA | 113 | 576340 | 536985 | 4060772 | 666.7 | 722.9 | 755.86 | 1 |
| NC-EWDP-12PB | 114 | 576340 | 536952 | 4060799 | 666.7 | 723.0 | 755.86 | 1 |
| NC-EWDP-12PC | 115 | 663935 | 536951 | 4060814 | 713.7 | 720.8 | 755.67 | 1 |
| NC-EWDP-15P | 116 | 684593 | 544927 | 4058163 | 716.9 | 722.4 | 720.59 | 1 |
| NC-EWDP-19P | 117 | 618981 | 549329 | 4058292 | 694.7 | 707.3 | 717.66 | 1 |
| NC-EWDP-19D | 118 | 421872 | 549317 | 4058271 | 549.7 | 711.8 | 717.65 | 1 |
| USW WT-24 | 119 | 717538 | 548697 | 4081909 | 734.8 | 840.1 | 836.46 | 10 |
| NC-Washburn-1X | 120 | 618627 | 551544 | 4057569 | 687.0 | 714.4 | 718.00 | 1 |
| BGMW-11 | 121 | 577177 | 534386 | 4062600 | 673.4 | 715.9 | 711.17 | 1 |
| Richard Washburn | 122 | 638100 | 549529 | 4052567 | 739.9 ^b | 703.9 | 703.74 | 1 |
| L. Cook | 123 | 613786 | 551348 | 4047432 | 690.0 ^b | 713.2 | 698.36 | 1 |
| Unknown | 124 | 591999 | 549532 | 4047668 | 680.0 ^b | 689.5 | 693.04 | 1 |
| Amargosa Water | 125 | 613771 | 547420 | 4047594 | 690.3 ^b | 690.4 | 692.58 | 1 |
| Lewis C. Cook | 126 | 635820 | 554329 | 4047666 | 700.0 ^b | 715.7 | 712.36 | 1 |
| Unknown | 127 | 614463 | 538989 | 4048877 | 690.7 ^b | 690.8 | 694.95 | 1 |
| USW UZ-N91 | 128 | 921140 | 555680 | 4088196 | 1,150.0 ^b | 1,186.7 | 1,184.03 | 10 |
| NC-EWDP-7SC | 129 | 687476 | 539632 | 4064317 | 724.1 ^c | 828.5 | 767.18 | 0.1 |
| NC-EWDP-7SC-Z1 | 130 | 769212 | 539632 | 4064317 | 760.0 ^b | 830.3 | 767.21 | 0.1 |
| NC-EWDP-7SC-Z2 | 131 | 769212 | 539632 | 4064317 | 760.0 ^b | 830.4 | 767.21 | 0.1 |

Table 6 8. Comparison of Observed Hydraulic Heads from the SZ Site Scale Flow Model and Model Computed Head Data (Continued)

| Site Name | Fig. 6-16 | Node Number | x (UTM) (m) | y (UTM) (m) | z (elevation) (m) | Measured Water Level (Head Data) ^a (m) | Modeled Head | Weight |
|----------------------|-----------|-------------|-------------|-------------|-------------------|---|--------------|--------|
| NC-EWDP-7SC-Z3 | 132 | 729744 | 539632 | 4064317 | 741.0 | 821.7 | 767.20 | 1 |
| NC-EWDP-7SC-Z4 | 133 | 643748 | 539632 | 4064316 | 704.5 | 792.5 | 767.16 | 0.1 |
| NC-EWDP-10P Deep | 134 | 534660 | 553149 | 4064916 | 650.4 | 726.9 | 730.55 | 1 |
| NC-EWDP-10P Shallow | 135 | 644165 | 553149 | 4064916 | 696.4 | 726.9 | 730.54 | 1 |
| NC-EWDP-10S-Z1 | 136 | 644165 | 553140 | 4064899 | 696.0 | 727.0 | 730.54 | 1 |
| NC-EWDP-10S-Z2 | 137 | 534660 | 553140 | 4064899 | 650.3 | 727.5 | 730.55 | 1 |
| NC-EWDP-18P | 138 | 645239 | 549416 | 4067233 | 702.3 | 711.2 | 732.66 | 1 |
| NC-EWDP-19IM1-Z1 | 139 | 618981 | 549317 | 4058291 | 691.1 | 711.9 | 717.66 | 0.1 |
| NC-EWDP-19IM1-Z2 | 140 | 553278 | 549317 | 4058291 | 659.1 | 712.1 | 717.65 | 0.1 |
| NC_EWDP-19IM1-Z3 | 141 | 487575 | 549317 | 4058291 | 628.6 | 712.5 | 717.64 | 0.1 |
| NC_EWDP-19IM1-Z4 | 142 | 443773 | 549317 | 4058291 | 589.0 | 713.3 | 717.64 | 0.1 |
| NC_EWDP-19IM1-Z5 | 143 | 421872 | 549317 | 4058291 | 545.0 | 711.8 | 717.65 | 0.1 |
| NC_EWDP-19IM2 | 144 | 465674 | 549337 | 4058291 | 599.2 | 723.3 | 717.64 | 1 |
| NC_EWDP-22PA Deep | 145 | 533203 | 552020 | 4062038 | 652.0 | 724.8 | 724.55 | 1 |
| NC_EWDP-22PA Shallow | 146 | 642708 | 552020 | 4062038 | 700.9 | 724.8 | 724.54 | 1 |
| NC_EWDP-22PB Deep | 147 | 401797 | 552038 | 4062037 | 514.9 | 724.8 | 724.71 | 1 |
| NC_EWDP-22PB Shallow | 148 | 445599 | 552038 | 4062037 | 584.9 | 724.8 | 724.55 | 1 |
| NC_EWDP-22S-Z1 | 149 | 642708 | 552019 | 4062020 | 700.3 | 724.9 | 724.54 | 1 |
| NC_EWDP-22S-Z2 | 150 | 533203 | 552019 | 4062020 | 651.7 | 724.9 | 724.55 | 1 |
| NC_EWDP-22S-Z3 | 151 | 445599 | 552019 | 4062020 | 584.9 | 724.9 | 724.55 | 1 |
| NC_EWDP-22S-Z4 | 152 | 401797 | 552019 | 4062020 | 514.8 | 724.9 | 724.71 | 1 |
| NC_EWDP-23P Deep | 153 | 532122 | 553923 | 4059875 | 649.2 | 724.3 | 721.93 | 1 |
| NC_EWDP-23P Shallow | 154 | 641627 | 553923 | 4059875 | 704.0 | 724.2 | 721.93 | 1 |
| NC_EWDP-16P | 155 | 687500 | 545665 | 4064263 | 722.3 | 729.4 | 739.27 | 1 |
| NC_EWDP-19PB Deep | 156 | 553278 | 549337 | 4058316 | 659.5 | 707.9 | 717.65 | 1 |
| NC_EWDP-19PB Shallow | 157 | 640882 | 549337 | 4058316 | 702.1 | 707.4 | 717.66 | 1 |
| NC_EWDP-24P | 158 | 686426 | 549386 | 4062055 | 786.4 | 727.1 | 725.30 | 1 |

Table 6 8. Comparison of Observed Hydraulic Heads from the SZ Site Scale Flow Model and Model Computed Head Data (Continued)

| Site Name | Fig. 6-16 | Node Number | x (UTM) (m) | y (UTM) (m) | z (elevation) (m) | Measured Water Level (Head Data) ^a (m) | Modeled Head | Weight |
|-------------|-----------|-------------|-------------|-------------|--------------------|---|--------------|--------|
| NC_EWDP-27P | 159 | 687981 | 544935 | 4065276 | 728.2 | 728.6 | 739.53 | 1 |
| NC_EWDP-28P | 160 | 686653 | 545746 | 4062393 | 718.7 | 729.3 | 738.82 | 1 |
| NC_EWDP-29P | 161 | 663380 | 549396 | 4059606 | 719.2 ^b | 724.8 | 719.12 | 1 |

Source: DTN: GS010908312332.002 [DIRS 163555].

Output DTN: SN0612T0510106.004, *sz06.pest*.

^aHead data refer to the observed mean hydraulic head (m).

^bScreen midpoint is above the potentiometric surface, therefore the modeled hydraulic head for this well is taken to be the uppermost active cell immediately below the potentiometric surface.

^cAverage of lower interval and water level was calculated to specify the measurement location (ensures that measurement falls in an active cell).

^dWell location in DTN: GS010908312332.002 [DIRS 163555] is incorrectly stated as $x = 547744$, $y = 4057164$.

UTM = Universal Transverse Mercator.

NOTES: The "Fig. 6-16" label in the second column of the table refers to the well numbers given in Figure 6-16.

The information on well name, UTM coordinates easting and northing, and measured heads is from DTN: GS010908312332.002 [DIRS 163555] and Output DTN: SN0702T0510106.007. The measured heads in Table 6-8 correspond to the average hydraulic head or water-table altitude data. Mean hydrostatic heads were calculated as time averages over the period of available measurements and were rounded to the nearest tenth of a meter.

Appendix D qualifies Nye County data from Phases III and IV for use in this report. Note that well locations of NC-EWDP Phases III and IV wells have been recalculated with CORPSCON V5.11.08.00 (STN: 10547-5.11.08, [DIRS 155082]) and may differ from those found elsewhere (e.g., BSC 2004 [DIRS 170009], Table A-1) (see Appendix F).

The z elevation shown in Table 6-8 is from Output DTN: SN0612T0510106.004. These data are stored in file *well_locations.macro*. This file provides well UTM coordinates and measurement depths.

The model heads shown in Table 6-8 are from Output DTN: SN0612T0510106.004. The modeled heads are stored in file *sz06.pest*. This file provides initial, intermediate, and final values of calibrated heads. The final heads are located at the end of this file and correspond to the simulation time equal to 3.6525×10^{10} days. Each well is represented by its nearest node. The relationship between the wells and the nodes is provided in Table 6-8. There are 161 water levels in the output file.

6.5.1.3 Calibration Parameters

The model formulation and the FEHM code require a specified permeability at each node. Sets of nodes are grouped into specific permeability zones based on similar permeability characteristics as identified in HFM2006 (SNL 2007 [DIRS 174109]). A single permeability value is assigned to each zone, and these zonal permeabilities are the parameters optimized during model calibration. Permeability zones correspond to hydrogeologic units identified in the HFM2006 conceptual model or to specific hydrogeologic features (see Table 6-7). All of the nodes within a specific hydrogeologic unit were assigned a calibrated permeability unless this node was included in one of the permeability zones established for specific hydrogeologic

features or faults. The zone sizes were fixed based on data from HFM2006. Uncertainty associated with geologic contacts is discussed in Section 6.7.3.

Recall that vertical anisotropy is assigned a value of 10:1 (horizontal to vertical) in the volcanic and valley-fill units (above Unit 9). Lower permeability in the vertical direction than in the horizontal direction typically occurs in stratified media, and the ratio of 10:1 is in the generally accepted range (CRWMS M&O 1998 [DIRS 100353], Table 3-2). For a site-specific example, the relatively high vertical gradient observed in well UE-25 p#1 suggests that vertical permeability is lower than horizontal permeability (minimal hydraulic connectivity). Nine wells (see Section 6.3.1.5) exhibited vertical gradients (BSC 2004 [DIRS 170009], Table 6-4). The uncertainty associated with the vertical anisotropy is discussed in Section 6.7.2.

Specific hydrogeologic features thought to potentially impact groundwater flow are classified as distinct permeability zones. The permeability variable or permeability multiplication factor used for a specific feature was assigned to all of the nodes within that feature. The hydrogeologic features for which special permeability zones were established are primarily faults, fault zones, and areas of hydrogeologic alteration (Section 6.5.2). As previously discussed, these features are distinct from the subhorizontal hydrogeologic units identified in HFM2006. Each of the identified hydrogeologic features includes multiple geologic formations and represents a zone of altered permeability within individual formations.

Twenty-three permeability zones were established based on the geologic units within the SZ site-scale model domain from HFM2006 for model calibration. Additional (usually low) permeability zones reflecting altered northern region were added to the model to help establish known system characteristics (like the LHG). These were established by dividing existing (base) geologic units into altered northern regions with permeabilities defined by multipliers. These permeability multipliers are calibration parameters that modify the permeability values assigned to geologic units in the altered northern regions. Eight additional zone representing faults and the Lower Fortymile Wash alluvium were established because they were identified as important structural features (e.g., the Solitario Canyon Fault) or were necessary for some conceptual feature, such as the LHG north of Yucca Mountain (which is partially established in the model domain with help from the altered northern region).

As required by PEST, upper and lower bounds were placed on each permeability variable during parameter optimization with limits chosen to reflect maximum and minimum field values (permeability) or a realistic range of values (permeability multipliers). A list identifying permeability zones, its calibrated permeability parameter, and the upper and lower bounds specified for the parameter is provided in Table 6-9.

Table 6-9. Calibration Parameters Used in the SZ Site-Scale Flow Model

| Parameter Name (zone number) | Geologic Unit or Feature | Calibrated Value (m ²) | Minimum Value (m ²) | Maximum Value (m ²) |
|---------------------------------|--------------------------------------|---------------------------------------|------------------------------------|------------------------------------|
| ICU (2) | Intrusive Confining Unit (granite) | 9.9×10^{-17} | 1.0×10^{-19} | 1.0×10^{-10} |
| XCU (3) | Crystalline Confining Unit (granite) | 1.0×10^{-16} | 1.0×10^{-19} | 1.0×10^{-10} |
| LCCU (4) | Lower Clastic Confining Unit | 9.7×10^{-17} | 1.0×10^{-19} | 1.0×10^{-10} |
| LCA (5) | Lower Carbonate Aquifer | 9.7×10^{-15} | 2.0×10^{-15} | 1.0×10^{-10} |

Table 6-9. Calibration Parameters Used in the SZ Site-Scale Flow Model (Continued)

| Parameter Name (zone number) | Geologic Unit or Feature | Calibrated Value (m ²) | Minimum Value (m ²) | Maximum Value (m ²) |
|---------------------------------|--|---------------------------------------|------------------------------------|------------------------------------|
| UCCU (6) | Upper Clastic Confining Unit | 9.8×10^{-16} | 1.0×10^{-19} | 1.0×10^{-10} |
| UCA (7) | Upper Carbonate Aquifer | 1.1×10^{-12} | 1.0×10^{-19} | 1.0×10^{-10} |
| LCCUT1 (8) | Lower Clastic Confining Unit Thrust | 9.8×10^{-19} | 1.0×10^{-19} | 1.0×10^{-10} |
| LCAT1 (9) | Lower Carbonate Aquifer Thrust | 5.6×10^{-12} | 1.0×10^{-19} | 1.0×10^{-10} |
| VSUL (11) | Volcanic and Sedimentary Units (lower) | 1.1×10^{-14} | 1.0×10^{-19} | 1.0×10^{-10} |
| OVU (12) | Older Volcanic Unit | 9.8×10^{-16} | 1.0×10^{-19} | 1.0×10^{-10} |
| CFTA (14) | Crater Flat-Tram Aquifer | 9.4×10^{-13} | 1.0×10^{-19} | 1.0×10^{-10} |
| CFBCU (15) | Crater Flat-Bullfrog Confining Unit | 5.2×10^{-14} | 1.0×10^{-19} | 1.0×10^{-10} |
| CFPPA (16) | Crater Flat-Prow Pass Aquifer | 3.1×10^{-12} | 1.0×10^{-19} | 1.0×10^{-10} |
| WVU (17) | Wahmonie Volcanic Unit | 9.8×10^{-14} | 1.0×10^{-14} | 1.0×10^{-10} |
| CHVU (18) | Calico Hills Volcanic Unit | 2.4×10^{-13} | 1.0×10^{-19} | 1.0×10^{-10} |
| PVA (19) | Paintbrush Volcanic Aquifer | 6.5×10^{-14} | 1.0×10^{-19} | 1.0×10^{-10} |
| TMVA (20) | Timber Mountain Volcanic Aquifer | 9.5×10^{-14} | 1.0×10^{-19} | 1.0×10^{-10} |
| VSU (21) | Volcanic and Sedimentary Units (upper) | 8.7×10^{-13} | 1.0×10^{-19} | 1.0×10^{-10} |
| LFU (23) | Lava Flow Unit | 8.9×10^{-14} | 1.0×10^{-19} | 1.0×10^{-10} |
| LA (24) | Limestone Aquifer | 9.8×10^{-14} | 1.0×10^{-19} | 1.0×10^{-10} |
| OAA (26) | Older Alluvial Aquifer | 1.5×10^{-13} | 1.0×10^{-19} | 1.0×10^{-10} |
| YACU (27) | Young Alluvial Confining Unit | 9.9×10^{-15} | 1.0×10^{-19} | 1.0×10^{-10} |
| YAA (28) | Young Alluvial Aquifer | 9.8×10^{-13} | 1.0×10^{-19} | 1.0×10^{-10} |
| ICUm (102) | ICU multiplier | 0.3 | 1.0×10^{-6} | 1.0 |
| XCUm (103) | XCU multiplier | 0.2 | 1.0×10^{-6} | 1.0 |
| LCCUm (104) | LCCU multiplier | 0.2 | 1.0×10^{-6} | 1.0 |
| LCAm (105) | LCA multiplier | 0.2 | 1.0×10^{-6} | 1.0 |
| UCCUm (106) | UCCU multiplier | 9.7×10^{-3} | 1.0×10^{-6} | 1.0 |
| UCAm (107) | UCA multiplier | 2.0×10^{-2} | 1.0×10^{-6} | 1.0 |
| LCCUT1m (108) | LCCUT1 multiplier | 9.8×10^{-3} | 1.0×10^{-6} | 1.0 |
| VSULm (111) | VSUL multiplier | 1.0×10^{-2} | 1.0×10^{-6} | 1.0 |
| OVUm (112) | OVU multiplier | 9.9×10^{-3} | 1.0×10^{-6} | 1.0 |
| CFTAm (114) | CFTA multiplier | 1.0×10^{-2} | 1.0×10^{-3} | 1.0 |
| CFBCUm (115) | CFBCU multiplier | 9.1×10^{-3} | 1.0×10^{-6} | 1.0 |
| CFPPAm (116) | CFPPA multiplier | 1.4×10^{-3} | 1.0×10^{-6} | 1.0 |
| CHVUm (118) | CHVU multiplier | 2.3×10^{-3} | 1.0×10^{-6} | 1.0 |
| PVAm (119) | PVA multiplier | 9.6×10^{-3} | 1.0×10^{-3} | 1.0 |
| TMVAm (120) | TMVA multiplier | 9.8×10^{-3} | 1.0×10^{-6} | 1.0 |
| VSUm (121) | VSU multiplier | 1.0×10^{-2} | 1.0×10^{-6} | 1.0 |
| LFUm (123) | LFU multiplier | 1.0×10^{-2} | 1.0×10^{-6} | 1.0 |
| OAAm (126) | OAA multiplier | 1.0×10^{-2} | 1.0×10^{-6} | 1.0 |
| YAAm (128) | YAA multiplier | 1.0×10^{-2} | 1.0×10^{-6} | 1.0 |
| YMZm (39) | Yucca Mountain zone multiplier | 8.9 | 1.0 | 1.0×10^3 |
| 4wzf (40) | Fortymile Wash Fault Zone | 1.4×10^{-10} | 1.0×10^{-19} | 1.0×10^{-10} |
| bmfz (41) | Bare Mountain Zone | 9.9×10^{-16} | 1.0×10^{-19} | 1.0×10^{-10} |
| cffz (42) | Crater Flat Fault Zone | 9.7×10^{-17} | 1.0×10^{-19} | 1.0×10^{-10} |
| h95z (43) | Highway 95 Fault Zone | 1.0×10^{-14} | 1.0×10^{-19} | 1.0×10^{-10} |
| swfz (45) | Sever Wash Fault Zone | 9.8×10^{-18} | 1.0×10^{-19} | 1.0×10^{-10} |
| scfz (44) | Solitario Canyon Fault Zone | 5.0×10^{-16} | 1.0×10^{-19} | 1.0×10^{-10} |
| stfz (46) | Stage Coach Fault Zone | 4.7×10^{-16} | 1.0×10^{-19} | 1.0×10^{-10} |

Table 6-9. Calibration Parameters Used in the SZ Site-Scale Flow Model (Continued)

| Parameter Name (zone number) | Geologic Unit or Feature | Calibrated Value (m ²) | Minimum Value (m ²) | Maximum Value (m ²) |
|---------------------------------|-----------------------------|---------------------------------------|------------------------------------|------------------------------------|
| wwfz (47) | Windy Wash Fault Zone | 4.8×10^{-16} | 1.0×10^{-19} | 1.0×10^{-10} |
| wash (50) | Lower Fortymile Wash | 2.0×10^{-11} | 1.0×10^{-19} | 1.0×10^{-10} |

Output DTN: SN0612T0510106.004, sz_site_2006.pst.

In addition to the PEST optimization described above, several manual adjustments were made to improve the model in ways that were not possible during the PEST run. Specifically, during calibration, only water levels (and lateral volumetric/mass flows) were considered in the objective function and hence head gradients or important head differences between wells were not explicitly considered. Manual adjustments were made to ensure that the flow direction southeast of the repository (in the small-gradient, anisotropic region) matched the direction inferred from the range and distribution of head values in this area. These adjustments modified the direction of particle paths emanating from the repository (to match the direction inferred from differences in the measured water levels) while maintaining good calibration (low objective function and low weighted RMSE for heads). The specific discharge was adjusted by changing the permeability of several units as listed in Table 6-10. Specific discharges were manipulated without adversely affecting the heads or gradient in the small hydraulic gradient area near Yucca Mountain. Table 6-8 shows the units that were adjusted during hand calibration, their PEST optimized permeability values, and their hand calibrated values. It should be noted that an additional zone corresponding to the Bullfrog Tuff within the quadrilateral defined by the Yucca Mountain zone was added during hand calibration with a permeability of 5×10^{-13} m² to ensure that the small hydraulic gradient region observed southeast of the repository is honored by the model and the flow paths from below the repository did not terminate along the eastern model boundary.

Table 6-10. Hand Calibration Results used in the SZ Site-Scale Flow Model

| Parameter Name (unit/zone number) | Geologic Unit or Feature | Hand-Calibrated Value (m ²) | PEST-Calibrated Value (m ²) |
|--------------------------------------|---------------------------------------|--|--|
| LCAT1 (9) | Lower Carbonate Aquifer | 5.6×10^{-12} | 5.6×10^{-14} |
| CFBCU (15) | Bullfrog Tuff | 5.2×10^{-14} | 5.2×10^{-14} |
| CFPPA (16) | Prow Pass Tuff | 3.1×10^{-12} | 1.1×10^{-13} |
| PVA (19) | Paintbrush Volcanic Aquifer | 6.5×10^{-14} | 2.5×10^{-13} |
| VSU (21) | Volcanic and Sedimentary Unit | 8.7×10^{-13} | 8.7×10^{-16} |
| OAA (26) | Older Alluvial Aquifer | 1.5×10^{-13} | 8.8×10^{-13} |
| CFPPAm (116) | Prow Pass Tuff Multiplier | 1.4×10^{-3} | 9.4×10^{-3} |
| CHVUm (117) | Crater Hills Volcanic Unit Multiplier | 2.3×10^{-3} | 2.3×10^{-3} |
| 4wfz (40) | Fortymile Wash Fault Zone | 1.4×10^{-10} | 6.4×10^{-11} |
| wash (50) | Lower Fortymile Wash Alluvial Zone | 2.0×10^{-11} | 5.2×10^{-13} |

Output DTN: SN0612T0510106.004, sz_site_2006_calibrated.pst.

6.5.2 Calibration Results

A model of this complexity proved challenging to calibrate. One issue is that for broad ranges of parameter values the response surface of the objective function was quite flat; however, for certain parameter vectors, the objective function could quickly become sensitive. For example, when the permeability of a fault was higher than that of the surrounding unit, the fault would have no impact on flowpaths, but once its permeability drops below that of surrounding units, the fault significantly changed the flow field. Another issue related to an inability to include soft data in the calibration process due to software quality assurance constraints (hence the hand calibration measures). Some trade-off between minimum objective function had to be made to match soft data for flowpath direction particularly in the small hydraulic gradient region.

6.5.2.1 Water Levels

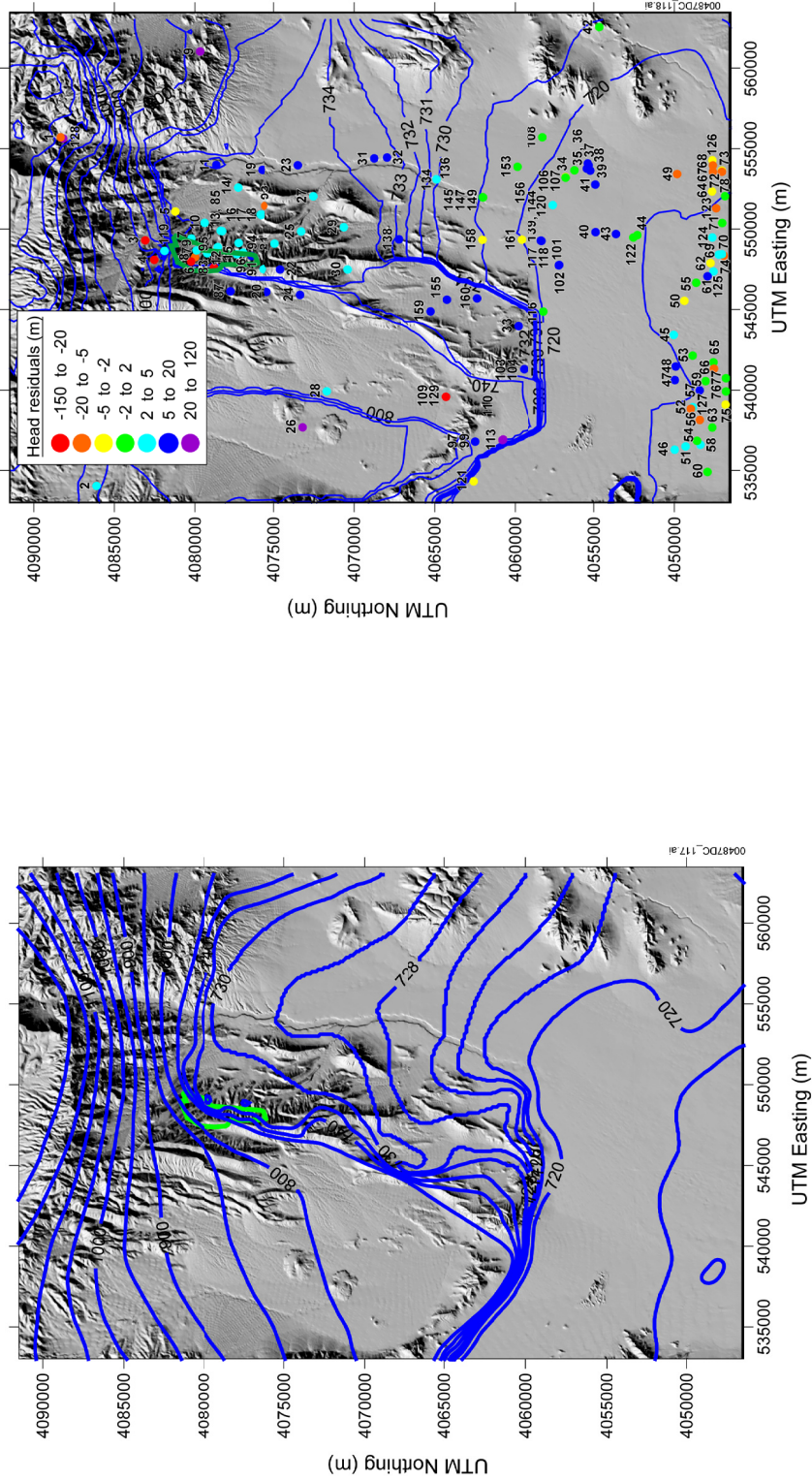
The water levels simulated by the calibrated SZ site-scale flow model are compared to the observed water level at each of the calibration target locations in Table 6-8. The location of each target observation well is shown in Figure 6-13. The calibration targets (water levels) are taken from *Water-Level Data Analysis for the Saturated Zone Site-Scale Flow and Transport Model* (BSC 2004 [DIRS 170009], Attachment I; DTN: GS010908312332.002 [DIRS 163555]) and NC-EWDP (Appendix D and also Output DTN: SN0702T0510106.007). The updated potentiometric surface (Appendix E) was used to truncate the top of the flow model grid and to provide the boundary conditions around the perimeter of the model. Of the 161 water-level calibration targets presented in Table 6-8, 105 values were obtained from *Water-Level Data Analysis for the Saturated Zone Site-Scale Flow and Transport Model* (BSC 2004 [DIRS 170009], Attachment I), ten values were obtained from DTN: GS010908312332.002 [DIRS 163555], and the rest can be found in Output DTN: SN0702T0510106.007. The distribution of residuals (the differences between measured and modeled heads), along with the potentiometric (left) and simulated water-level (right) surfaces, is provided in Figure 6-15. The actual water levels (not the interpolated potentiometric surface) in each well are used for comparison.

The weighting scheme (Table 6-8) used with PEST focused the calibration in high-confidence areas (i.e., the small-gradient area) or areas important to TSPA calculations (i.e., along the flow path). A low-weight target value instructs PEST to essentially ignore the value while a high value forces PEST to respect the target value at the expense of other observations. Alternate weighting schemes were investigated (e.g., uniform weighting or weights inversely proportional to the variance in observation data) but were discarded when they yielded physically inconsistent flowpaths (e.g., pathlines that terminate along the eastern model boundary).

The calibrated SZ site-scale flow model has a weighted (see Table 6-8) root-mean-square error (RMSE) of 0.82 m when considering only differences between observed and modeled heads (lateral flux calibration targets were not included). The modeled head at the node nearest to the well location was used for the comparison (no interpolation was needed because of the 250-m grid size). Without weighting, the RMSE is 24.39 m. Compared to the overall head drop of approximately 500 m in the model domain, the 24.39-m average residual corresponds to a 5% error. As shown in Figure 6-16, a comparison between measured water-level data and the potentiometric surface yielded an RMSE of 20.7 m (weighted RMSE of 8.8 m). Thus, the

RMSE for calibrated model is only 18% worse than the best-fit potentiometric surface (24.39 m compared to 20.70 m). Moreover, the weighted RMSE of the calibrated model is an order of magnitude better than the best-fit potentiometric surface and this indicates excellent model agreement in high weight areas of the model domain—areas felt to be the most important to get accurate model simulations (i.e., downgradient from the repository). Because of the 10-m minimum layer thickness, head differences of less than this magnitude are within the uncertainty range of the model.

As can be seen in Figure 6-15, the largest head residuals (~100 m) are in the northern part of the model in the altered northern region and in the vicinity of the moderate hydraulic gradient. These residuals are largely the result of the low weighting factor of (0.1) and the possibility that they reflect perched conditions (see Section 6.5.2.1 for a description and Section 6.7.7 for a discussion of perched water effects). In the figure, a negative residual means that the calibrated value was lower than the target data (note that the PEST record file shows opposite signs; a negative residual means that the calibrated value was higher than observed). The next highest head residuals border the Crater Flat and Solitario Canyon Faults. These residuals (~25 m) are most likely the result of 250-m grid blocks not being able to resolve the 780-m to 730-m drop in head in the short distance just east of the above-mentioned features. There may be additional complicating factors such as varied hydrologic characteristics in the Solitario Canyon Fault along its north-south transect. In the model, the fault acts as a barrier, but is defined with only one calibration parameter. This may not be adequate to represent the local behavior of such a long feature. For example, well USW G-1, about 1,000 m from the Solitario Canyon fault, shows an 8-m difference between measured and simulated heads. The measured head for this well (754 m), located on the east side of the fault, is closer to measured head values on the west side of the fault. Because the majority of wells on the east side have heads of approximately 745 m, the simulated head for USW G-1 has a calibrated result close to that value. Overall results indicate that the model adequately represents the water table near Yucca Mountain. In the vicinity of the 18-km compliance boundary and south, the modeled potentiometric surface is typically on the order of 5 m higher than the observed water levels although the estimated gradients match well (see Section 7.2.1).



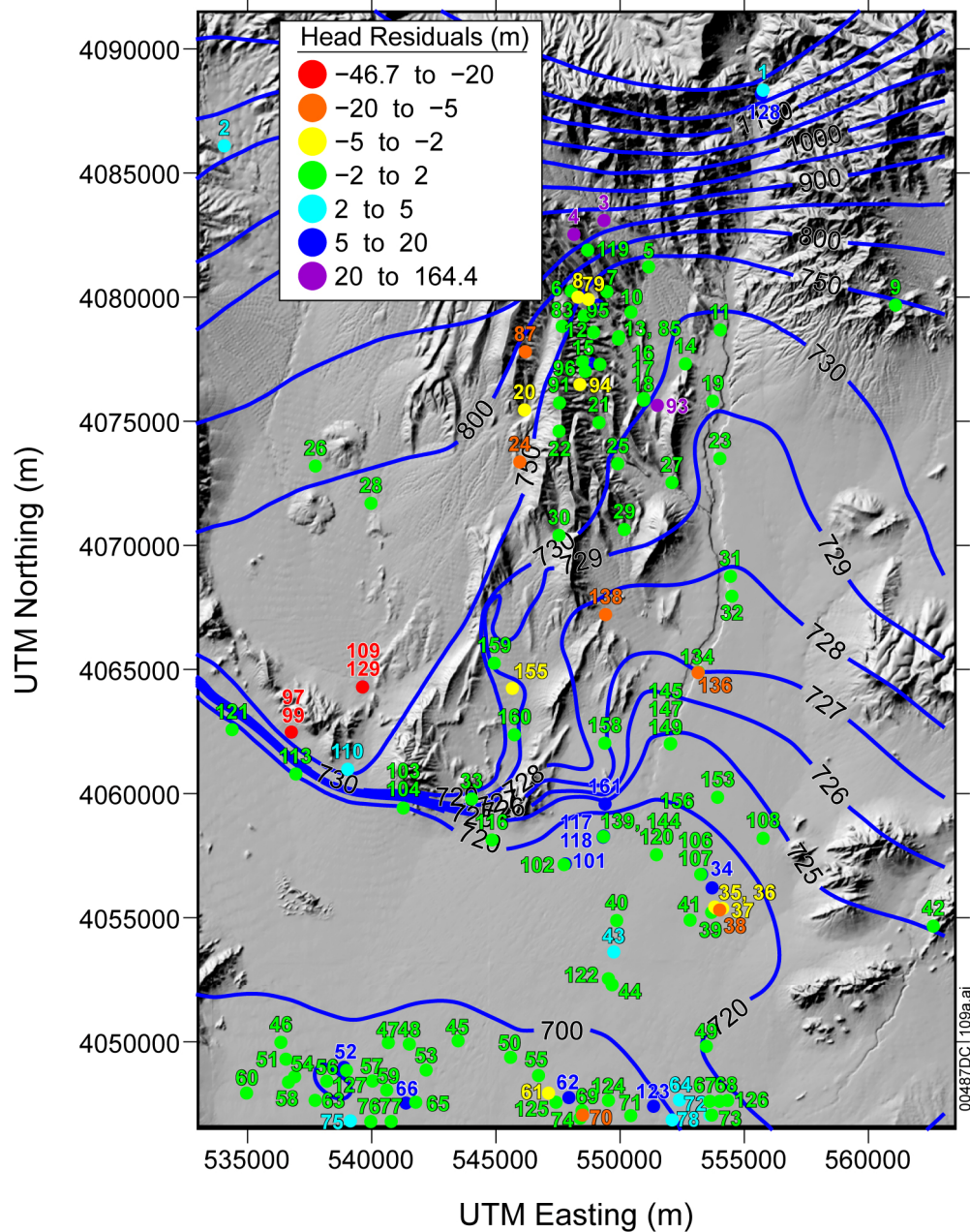
Sources: SNL 2007 [DIRS 179466] (repository outline); DTN: GS010908312332.002 [DIRS 163555] (well locations and water levels).

Output DTNs: SN0610T0510106.001, and SN0702T0510106.007 (well locations and water levels); MO0611SCALEFLW.000 (potentiometric surface), left panel; SN0612T0510106.004 (model potentiometric surface), right panel.

NOTES: Symbols in right panel represent well locations. Head residual is the simulated value minus the observed value. The wells are numbered to correspond to the second column of Table 6-8 (multiple-depth wells only show the heads corresponding to the highest screened interval altitude).

UTM = Universal Transverse Mercator.

Figure 6-15. Contour Plot of Potentiometric Surface (Left Panel) and Simulated Water-Level Data with Residual Heads (Right Panel)



Source: DTN: GS010908312332.002 [DIRS 163555]

Output DTNs: MO0611SCALEFLW.000 (potentiometric surface); SN0610T0510106.001, and SN0702T0510106.006 (well locations and water levels).

NOTE: The wells are numbered to correspond to the second column of Table 6-8 (multiple-depth wells only show the number corresponding to the highest screened interval altitude). Color of the symbol indicates the head residual which is the simulated value minus the observed value. The contours represent the potentiometric surface.

UTM = Universal Transverse Mercator.

Figure 6-16. Well Locations and Head Residuals between Measured Water-Level Data and the Potentiometric Surface Used to Construct Model Boundary Conditions

6.5.2.2 Comparing Volumetric/Mass Flow Rates from the Regional-Scale Model with Volumetric/Mass Flow Rates from the Calibrated Site-Scale Model

The SZ site-scale flow model corresponds to only a small part of the DVRFS, which is used to supply target lateral volumetric/mass flow rates. A comparison between the two models was suggested by the Expert Elicitation Panel (CRWMS M&O 1998 [DIRS 100353]). The regional flow model simulates a closed system and uses data from spring discharges to calibrate the water flux through the system (Belcher 2004 [DIRS 173179]). Thus, this model provides a rough estimate of volumetric/mass flow rates expected through the SZ site-scale model domain.

The regional model HFM is described by Belcher (2004 [DIRS 173179], Chapter E). The SZ site-scale flow model uses an equivalent HFM, which is described in *Hydrogeologic Framework Model for the Saturated Zone Site-Scale Flow and Transport Model* (SNL 2007 [DIRS 174109]).

In Section 6.3.1.6, the methodology for applying fixed-head lateral boundary conditions to the SZ site-scale flow model was described. With fixed-head boundary conditions, the flux through a boundary is a function of the permeabilities on that boundary. Flux targets were derived from the values simulated by the 2004 regional model (Appendix C). A comparison of the calibration target volumetric/mass flow rates and volumetric/mass flow rates derived from the calibrated SZ site-scale flow model is made in Table 6-11. The western boundary, for instance, has a total flux of 120.3 kg/s (3.8×10^6 m³/yr) across it for the target flux values and 101.0 kg/s (3.2×10^6 m³/yr) across it in the calibrated model. The difference in southern volumetric/mass flow rates, which is simply a sum of the other boundary volumetric/mass flow rates plus the recharge (528.1 kg/s), is a decrease of about 23%. The weighted RMSE for boundary volumetric/mass flow rates is 35.3 kg/s. It should be noted that in Table 6-11, the sum of all target boundary volumetric/mass flow rates (64.7 kg/s) is not equal to the sum of all volumetric/mass flow rates through the calibrated flow model (64.1 kg/s) because different infiltration boundary conditions were applied to each model (see Section 6.4.3.9 and Figure 6-14).

Factors that affect the flux match between the regional- and site-scale models include the horizontal and vertical resolution and the permeability distribution. The horizontal resolution of the site-scale flow model is 36 times finer than the regional model (250-m versus 1,500-m grid block size). The vertical resolution of the SZ site-scale flow model is about four times finer than the regional model (67 versus 16 layers). The increased resolution at the site scale means that, compared to the regional-scale model, volumetric/mass flow rates calculated by the SZ site-scale flow model may depend more strongly on a few units. Flux distribution in the regional model is also impacted by the use of permeability classes. In the regional model, permeabilities (actually hydraulic conductivities) associated with specific units are not defined. Rather, the permeabilities are grouped into classes, which are assigned to a particular grid block based on the percentages of the rock types contained in the grid block. Thus, although the regional-scale model was based on the same complex HFM used for the site-scale model, the regional model used only four permeability classes. Because of these fundamental differences, it is not possible to reproduce the distribution of volumetric/mass flow rates corresponding to the sides of the SZ site-scale flow model, when examined on a unit-by-unit basis. Nevertheless, the difference in the total flux across the southern boundary between the SZ site-scale flow model and the

regional model is within the range considered acceptable by the Expert Elicitation Panel (CRWMS M&O 1998 [DIRS 100353]).

Table 6-11. Comparison of Target and Site-Scale Volumetric/Mass Flow Rates

| Boundary Zone (Range in m) | Target Mass/Volume Flows | | Site-Scale Mass/Volume Flows | | Calibration Weight |
|---|--------------------------|---------------------------|------------------------------|--|--------------------|
| | Flow (kg/s) | Flow (m ³ /yr) | Flow (kg/s) ^a | Flow (m ³ /yr) ^a | |
| North (533,000–563,000) | -158.9 | -5.0 × 10 ⁶ | -57.1 | -1.8 × 10 ⁶ | 5 |
| West (4,046,500–4,091,500) | -120.3 | -3.8 × 10 ⁶ | -101.0 | -3.2 × 10 ⁶ | 5 |
| East ₁ (4,046,500–4,052,500) | -273.1 | -8.6 × 10 ⁶ | -232.1 | -7.3 × 10 ⁶ | 1 |
| East ₂ (4,052,501–4,058,500) | 33.3 | 1.0 × 10 ⁶ | -97.4 | -3.1 × 10 ⁶ | 1 |
| East ₃ (4,058,501–4,069,000) | -127.8 | -4.0 × 10 ⁶ | 260.9 | 8.2 × 10 ⁶ | 1 |
| East ₄ (4,069,001–4,079,500) | 30.2 | 9.5 × 10 ⁵ | -206.6 | 6.5 × 10 ⁶ | 1 |
| East ₅ (4,079,501–4,091,500) | -0.4 | -1.2 × 10 ⁴ | -30.7 | -9.7 × 10 ⁵ | 1 |
| South (533,000–563,000) | 681.9 | 2.2 × 10 ⁷ | 528.1 | 1.7 × 10 ⁷ | NA |

Source: Appendix D (qualified for one time use).

Output DTN: SN0612T0510106.004, sz06.pest.

NOTES: Negative values indicate flow into the model. South boundary volumetric/mass flow rates were not used as targets for the calibration of the SZ site-scale flow model; rather, they were calculated from the balance of infiltration and the volumetric/mass flow rates across north, west, and east boundaries.

^a Mass flows are approximate because of the technique FEHM uses in the *flxz* macro to sum and print boundary flows.

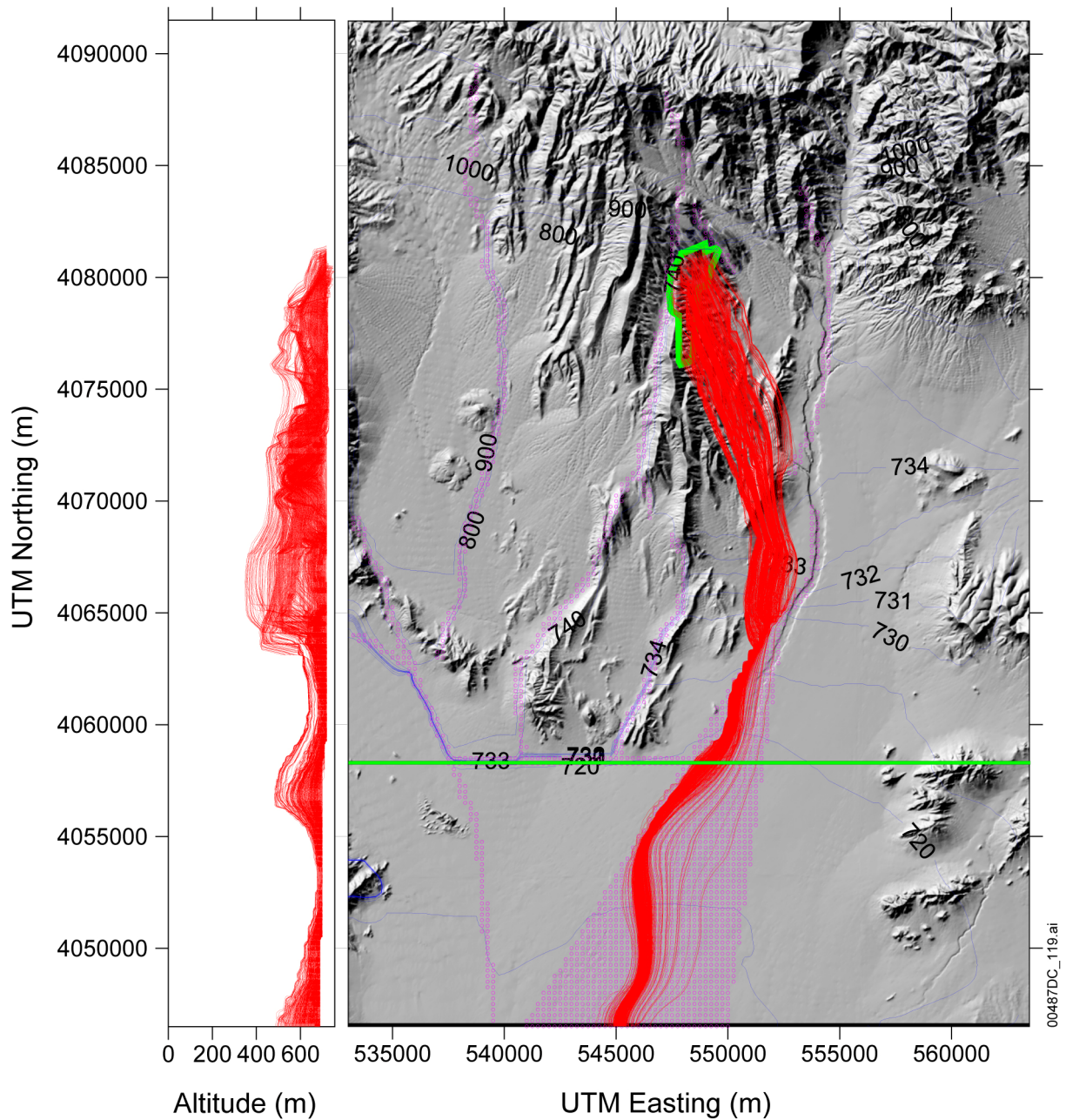
$$\text{Conversion factor: m}^3/\text{yr} = \frac{\text{m}^3}{1,000\text{kg}} \cdot \frac{86,400\text{s}}{\text{day}} \cdot \frac{365.25\text{day}}{\text{yr}} \cdot \frac{\text{kg}}{\text{s}}$$

6.5.2.3 Simulated Flow Paths

The particle-tracking capability of FEHM illustrates flow paths simulated by the calibrated SZ site-scale flow model. One hundred particles were distributed randomly over the area of the repository and allowed to migrate subject to advection only (non-dispersive) until they reached the model boundary (Figure 6-17). The pathways generally leave the repository and travel in a south-southeasterly direction to the 18-km compliance boundary. From the 18-km boundary to the end of the model, the flowpaths trend to the south-southwest and generally follow Fortymile Wash. Some of the pathways follow fault zones along Fortymile Wash (Zone 40 of Figure 6-12). The hydrogeologic units through which the flow below the repository passes consist of the Crater Flat group (Bullfrog, Tram, and Prow Pass) with most of the flow in the Bullfrog unit, the upper volcanic aquifer, the upper volcanic confining unit, the valley fill unit, and the undifferentiated valley-fill unit. Figure 6-17 includes a vertical cross section of the path lines. Evident in the figure is the shallow depth of the path lines along most of the pathways south of UTM Northing 4,065,000 m, which is consistent with data supporting an upward head gradient. In Section 7, the fluid pathways are compared with those inferred from geochemical data.

6.5.2.4 Specific Discharge

Using the calibrated SZ site-scale flow model, specific discharge was estimated as the average over 100 particles. These particles were randomly distributed below the repository and tracked until they traveled across UTM Northing 4,037,361 m (5 km south of the southern tip of the repository). Pathlength divided by travel time yields the specific discharge for a particle and the average across 100 particles was 0.36 m/yr (1.08 ft/yr) for the calibrated model. End members of the 100-particle plume had specific discharges of 0.11 and 0.66 m/yr. The Expert Elicitation Panel (CRWMS M&O 1998 [DIRS 100353], Figure 3-2e) estimated a median specific discharge of 0.6 m/yr (2.0 ft/yr) for the 5-km (3-mile) distance. Thus, reasonable agreement is found between the specific discharge simulated by the calibrated SZ site-scale flow model and that estimated by the Expert Elicitation Panel (CRWMS M&O 1998 [DIRS 100353]). Mass balance error for all runs was essentially zero.



Source: SNL 2007 [DIRS 179466] (Repository outline).

Output DTNs: SN0612T0510106.004 (water levels) and SN0704T0510106.008 (particle tracks).

NOTE: The contours represent the modeled potentiometric surface. Altitude is in meters above mean sea level. The green line across the model at UTM Northing equal to 4,058,256 m represents the 18-km compliance boundary. Pink represents special geologic features (see Table 6-7 and Figure 6-12). 1,000 particles are simulated to improve flowpath clarity.

UTM = Universal Transverse Mercator.

Figure 6-17. Flow Paths for Particles Released (uniformly but randomly distributed) below the Repository Area